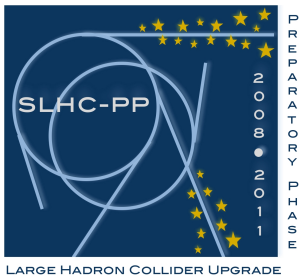

SLHC-PP

DELIVERABLE REPORT

EU DELIVERABLE: 7.2.2

Document identifier:	**SLHC-PP-7.2.2-1049283-v1.0**
Contractual Date of Delivery to the EC	**End of Month 27 (May 2010)**
Actual Date of Delivery to the EC	**15/04/2011**
Document date:	**15/04/2011**
Deliverable Title:	**Design of RF system architecture including modeling of RF components, simulation of the RF system and simulation of beam dynamics of the full LINAC; RF system and high power modulator specifications**
Work package:	**WP7: Development of critical components for the injectors**
Lead Beneficiary:	**CERN**
Authors:	**M. Hernandez, W. Hofle**
Document status:	**Version 1**
Document link:	https://edms.cern.ch/document/1049283/1

History of Changes

Version	Date	Comment	Authors
1.0	-	Final Version	-

The Preparatory Phase of the Large Hadron Collider upgrade (SLHC-PP) is a project co-funded by the European Commission in its 7th Framework Programme under the Grant Agreement n° 212114. SLHC-PP began in April 2008 and will run for 3 years.

TABLE OF CONTENTS

1. EXECUTIVE SUMMARY

The published report describes the achievement during the SLHC-PP project. It illustrates that a detailed modeling of the SPL RF system has been accomplished using the SIMULINK software. This model integrates the cavity characteristics measured on the RF test place at CEA (Saclay) for the multicell 704 MHz cavities built in the context of the HIPPI JRA (part of the CARE Integrated Activity supported within the FP6). It allows the analysis of the impact on the beam of different variants of the RF architecture (one klystron driving between 1 and 4 cavities). This modeling tool has already demonstrated that high power vector modulators are not necessary. It will now be extensively used to decide upon the specifications of the RF components.

2. REPORT

A full report on the design of the RF infrastructure for Linac4 and the SPL is given in [CERN sLHC-PROJECT-Report-0054].

[CERN sLHC-PROJECT-Report-0054] M. Hernandez and W Hofle, CERN-sLHC-PROJECT-Report-0054, http://cdsweb.cern.ch/record/1344800 .

EUROPEAN ORGANIZATION FOR NUCLEAR RESEARCH
European Laboratory for Particle Physics

sLHC Project

sLHC Project Report 0054

Progress Report on SIMULINK Modelling of RF Cavity Control for SPL Extension to LINAC4

Theory and Analysis behind Simulation Results of SPL Model Using I/Q Components in SIMULINK to Date, Including Lorentz Force Effects and Multiple Cavities Driven by Single Feedback Loop

Matias Hernandez
Wolfgang Höfle

Abstract

In the context of a luminosity upgrade for the LHC within the coming years, works have started on LINAC4 to provide an infrastructure for updating the LHC supplier chain. In order to achieve energy levels and particles per bunch necessary for the expected rate of events at LHC detectors and related experiments, a project proposal is underway for an appended Superconducting Proton LINAC (SPL) that will run from the normal conducting LINAC4 and LP-SPL onto the LHC supplier chain. Thus, the SPL will have two main functions: Firstly, to provide H- beam for injection into the PS2 which is compatible with LHC luminosity. For this purpose the SPL will accelerate the output beam of LINAC4 from 1GeV to 4GeV, removing, at the same time, the necessity for PSB operation in the LHC supply chain. Secondly, it will provide an infrastructure upgradeable to meet the needs of all potential high-power proton users at CERN (EURISOL) and possibly neutrino production facilities. For high-power applications of this nature the SPL will need to provide a 5GeV beam whose time-structure can be tailored to meet the specifications of each application. As of now, the design of the SPL is planned to make use of high-Q, 5-cell superconducting elliptical cavities pulsed at a resonant frequency of 704.4 MHz by multi-megawatt klystrons with a maximum repetition rate of 50 Hz, accelerating a 20/40 mA H⁻ beam with a maximum field of approximately 25 MV/m, depending on the output requirements of different applications. In the context of the development of a proposal for this conceptual design by mid-2011, this report consists on the progress to date of a SIMULINK model that follows the design specifications and will provide a useful means to foresee any issues that might arise with construction of the SPL, as well as a relatively precise feel for the costs involved in terms of power consumption and technology.

Acknowledgements:
CEA team, in particular O.Piquet (SIMULINK model)
W. Höfle, G. Kotzian, P. Posocco, J. Tuckmantel, D. Valuch.

Beams Department, Radio-Frequency Group
SPL : This project has received funding from the European Community's Seventh Framework Programme (FP7/2007-2013) under the Grant Agreement n° 212114

CERN
CH - 1211 Geneva 23
Switzerland
Geneva, April 2011

Contents

List of Figures

Chapter 1

Introduction

In conjunction with the restart of the Large Hadron Collider at CERN, studies on a luminosity upgrade for the machine started in April of 2008. The project, sLHC-PP, is aimed at gradually increasing the luminosity to reach levels up to ten times the original design specifications of the LHC, providing a smooth transition onto a higher discovery potential of the synchrotron [1]. In order to achieve these goals, technical improvements need to be deployed on several areas of the CERN complex, including new focusing magnets in LHC at the experiment regions. CMS and ATLAS, as general purpose detectors, will need to be prepared to record higher luminosity collisions, and finally, the LHC supplier chain will be updated. Construction has started on LINAC4 to cater for this need. The whole project has been divided into eight areas of interest referred to as Work Packages. WP1, 2, 3 and 4 are concerned with project management and the coordination of accelerator and detector upgrades. WP5 is investigating protection and safety issues related to the increased radiation due to higher luminosity, WP6 has been charged with developing the new focusing quadrupole magnets for the interaction areas of the LHC ring, WP7 is in charge of developing critical components for the injectors such as accelerating cavities and a hadron source, and finally, WP8 will develop the technology necessary for tracking detectors from the power distribution point of view. Within the scope of work package 7, Low-Level Radio Frequency (LLRF) simulations for a new generation of pulsed electric field superconducting LINAC have been commissioned. The idea is to provide a general idea of the possible setbacks that may arise during construction and operation, and their solutions. This report is a detailed description of the field stabilisation solutions when dealing with one or more superconducting cavities driven by a single pulsed klystron from the RF point of view.

Chapter 2

RF Cavity Theory

Particle physics arose only a few decades ago following the creation of a device capable of reaching far into the nucleus of an atom, and detectors equipped to observe matter constituting the building blocks of the building blocks of atoms. Particle accelerators have redefined particle physics and as they become increasingly more powerful, we are able to penetrate deeper into the standard model and possibly expand on it. The idea is to accelerate particles to imbue them with energies capable of separating matter, and then make them crash against each other in an infinitely precise point to observe with gigantic detectors what comes out of their collision. In order to achieve this, we insert particles into a vacuum tube, using magnets to ensure they stay within the vacuum, and accelerate them using electric fields contained within resonant cavities along the tube. From the point of view of RF power, we are interested in observing the effects of a time-varying electric field on a beam of particles travelling through a resonant cavity powered by a powerful generator (klystron). With this information, we can design the RF control system for a linear accelerator to suit a particular application.

2.1 Cavity Equivalent Circuit

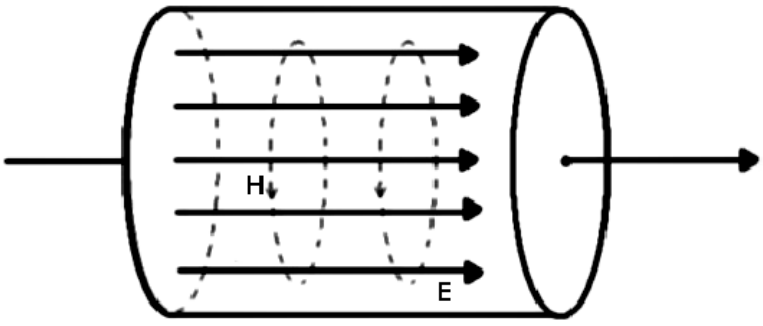

Figure 2.1: Pillbox cavity [2]

Resonant modes of electromagnetic (EM) waves in cavities can be described by

resonant R-C-L circuits. For the simplest case, we limit ourselves to the analysis of a single resonant cavity, which can be closely modelled via a pillbox with perfect electric conducting walls (a circular waveguide with closed ends). In an ideal case, only a finite number of propagating modes, corresponding to a finite number of frequencies will propagate within the pillbox, in the presence of losses, however, the delta function frequency response at different modes becomes a narrowband peak around the resonant frequency for that mode. A measure of the sharpness of this peak observed after an external excitation is the quality factor (Q) of that particular mode.
Q is defined as the ratio of the time-average of the energy W stored within the cavity walls to the energy loss per cycle.
$Q_0 = \frac{\omega W}{P_d}$ where P_d is the dissipated power in the cavity.

Ignoring the effects of losses due to vacuum impurities and surface irregularities (drift tubes), we calculate Q by integrating the power loss of wall currents over the cavity surface and the stored energy over the volume of the cavity

$$P_d = \int_{\delta V} P_d^{'} dA = \frac{1}{2} \int_{\delta V} \sqrt{\frac{\omega \mu}{2\kappa}} |H_{tan}|^2 dA \tag{2.1}$$

$$W = \int_V w dV = \frac{1}{2} \int_V \left(\frac{\varepsilon}{2} |\underline{\vec{E}}|^2 + \frac{\mu}{2} |\underline{\vec{H}}|^2 \right) dV = \frac{\varepsilon}{2} \int_V |\underline{\vec{E}}|^2 dV \tag{2.2}$$

where $P_d^{'}$ is the energy loss in the cavity walls per unit area due to surface currents, w is stored energy within the cavity, and κ is the conductivity of the material [3]. The Q factor as defined above is one of the main characteristics of an accelerator cavity, and together with the resonant frequency and shunt impedance, it is possible to describe the cavity completely from an electrodynamics point of view. The resonant frequency of a cavity depends mainly on its shape and it is thus too complex to calculate analytically for all but the simplest of shapes, thus it is found by numerical or experimental methods and usually quoted by designer or manufacturer. The shunt impedance of an accelerating cavity relates the voltage between two points in the cavity (e.g. between drift tubes) to the power dissipated in the cavity walls:

$$R_{sh} = \frac{U^2}{2P_d} (circuit) \tag{2.3}$$

For LINAC purposes, the shunt impedance definition is multiplied by a factor of two; therefore it is important when defining a shunt impedance to specify the convention applied. To calculate the shunt impedance, in any case we find the voltage between two points $U = |\int_{z_1}^{z_2} \underline{E}_z(z)|$.
This definition does not take into account the speed of the passing beam and its effect on the accelerating voltage. It is related to the effective shunt impedance by $R_{sh,eff} = R_{sh} T^2$, where the transit-time factor T is given by

$$T = \frac{|\int_{z_1}^{z_2} \underline{E}_z(z) e^{ik_z z} dz|}{|\int_{z_1}^{z_2} \underline{E}_z(z) dz|} \tag{2.4}$$

Here, $kz = \frac{2\pi}{\beta\lambda}$ is the wavenumber in the direction of acceleration and depends on the speed of the beam. This means that the shunt impedance is only meaningful when related to a certain beam speed.
$R_{sh,eff}$ is useful to define the characteristic impedance of a resonant cavity, which is defined as

$$\frac{R_{sh}(\beta_x)}{Q} = \frac{1}{2\omega W}\left|\int_{z_1}^{z_2} \underline{E}_z(z) e^{i\frac{2\pi}{\beta_x c}z} dz\right|^2 \tag{2.5}$$

For a beam of speed $v = \beta_x c$.
This is a very useful quantity as it depends only on the geometry of the cavity as energy scales with electric field. Going back to our R-C-L circuit, we know that when a cavity resonates on a certain mode, the time-average of the energy stored in the electric field equals that in the magnetic field. In an RF period, the energy oscillates between magnetic and electric field as is the case with an L-C pair. R was defined before and it models the effective shunt impedance due to energy dissipation of the cavity walls [2].

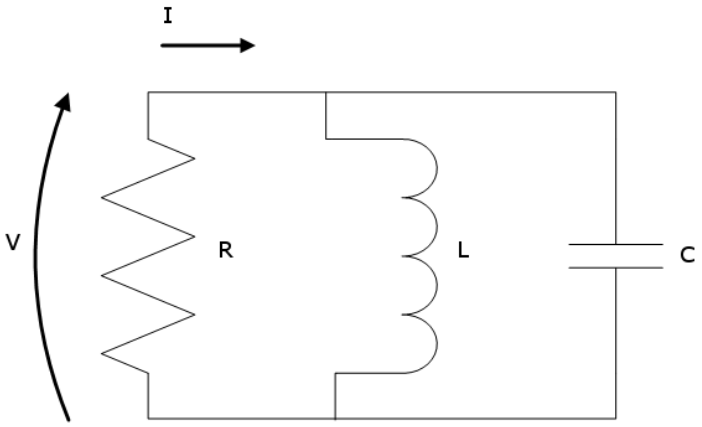

Figure 2.2: Cavity equivalent circuit

If we therefore think of the capacitance as the effect of the electric field on the cavity and the inductance as related to the magnetic field, we find that the average stored energy in the electric and magnetic fields respectively is given by

$$W_{sE} = \frac{1}{4}CV^2 \qquad W_{sM} = \frac{1}{4}LI^2 \tag{2.6}$$

where

$$\frac{\varepsilon}{4}\int_V |E|^2 dV = \frac{\mu}{4}\int_V |H|^2 dV$$

At resonance, the total average energy stored is then the addition of both the magnetic and electric:

$$W_s = W_{sE} + W_{sM} = 2W_{sE} = \frac{1}{2}CV^2 \tag{2.7}$$

If we take the power dissipated by the equivalent shunt resistance, bearing in mind $\omega_0 = \frac{1}{\sqrt{LC}}$ we find $P_d = \frac{1}{2}\frac{V^2}{R}$ and therefore (CIRCUIT) $Q_0 = \omega_0 RC$.

Thus, with the knowledge of the quality factor, resonant frequency and the shunt impedance, it is possible to construct an equivalent circuit for the resonant cavity.

2.2 Coupling Between RF Generator, Cavity and Beam

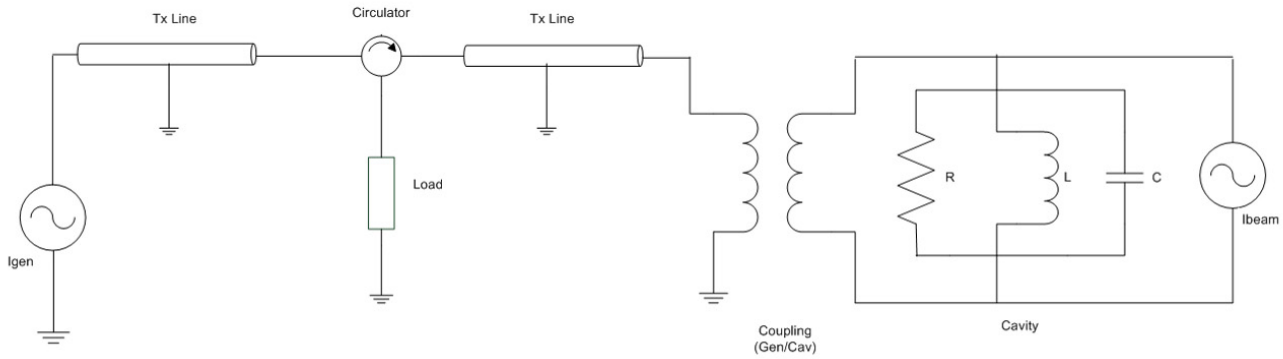

Figure 2.3: Cavity coupled to beam and generator [4]

Until now, we have concentrated on the behaviour of a resonant cavity obtained from a closed pillbox with perfectly conducting walls. We are now interested in the effects on the cavity of coupling to a generator and the passage of beam. We will now observe how the generator transmission line affects the quality factor of the cavity and how beam passage will induce a drop in the cavity voltage. Thus we introduce the concept of the cavity to generator coupling factor

$$\beta_0 = \frac{Q_0}{Q_{ext}} \tag{2.8}$$

which gives rise to the loaded quality factor Q_L

$$\frac{1}{Q_L} = \frac{1}{Q_0} + \frac{1}{Q_{ext}} \tag{2.9}$$

In superconducting cavities in particular, the loaded Q is virtually equal to the external Q as the unloaded Q is much greater than the external. This means the generator to cavity coupling will be of particular importance for the efficient performance of the system.

2.2.1 Steady-State Analysis

To start off, we assume steady-state voltages and currents. In figure 2.4, the beam is represented as a current source and the cavity, as previously shown, is equivalent to an L-C-R block, in this case coupled to a transmission line with complex impedance Z, with an incident current wave (towards the cavity) I_g and a reflected wave I_r [5].

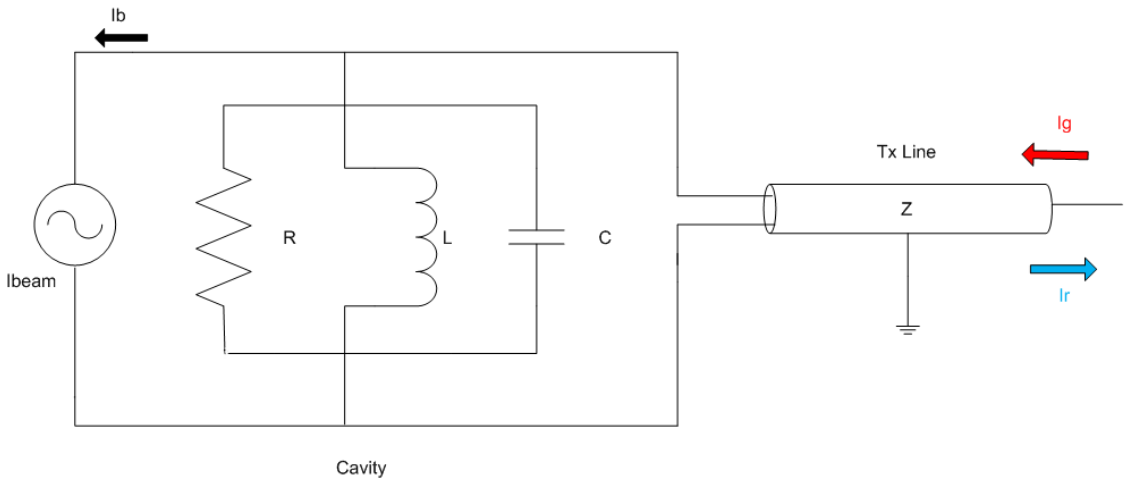

Figure 2.4: Steady-state cavity [5]

The generator emits a wave with frequency ω, which is not necessarily equal to the cavity resonant frequency ω_0. We assume all variables are proportional to $e^{i\omega t}$. In the case of imperfect tuning, the frequency difference between the resonant frequency and the generator frequency can be described as a mismatch between the generator and the cavity angle in phasor terms. We can define the tuning angle between the generator current and cavity voltage as

$$\tan\Psi = 2Q_L\frac{\Delta\omega}{\omega}$$

for small $\Delta\omega$.
From transmission line theory, we know $V = Z(I_g + I_r)$ and therefore $I_r = \frac{V}{Z} - I_g$.

From the circuit and the above equation, we get

$$I_{LCR} = I_g - I_r - I_{b,RF} = 2I_g - I_{b,RF} - \frac{V}{Z} \tag{2.10}$$

The current across the L-C-R block is also equal to the individual currents flowing through the passive components. So we can also say (j and i both refer to $\sqrt{-1}$)

$$I_{LCR} = I_C + I_L + I_R = V\left(\frac{1}{j\omega L} + j\omega C + \frac{1}{R}\right) \tag{2.11}$$

and equating both sides, we get

$$V\left(j\omega C\left(1 - \frac{1}{\omega^2 LC}\right) + \frac{1}{R} + \frac{1}{Z}\right) = 2I_g - I_{b,RF} \tag{2.12}$$

If $\Delta\omega = \omega_0 - \omega$ and $\Delta\omega \ll \omega$ and , we can say that , and the equation becomes

$$V\bigg(- i2\Delta\omega C + \frac{1}{R} + \frac{1}{Z}\bigg) = 2I_g - I_{b,RF} \tag{2.13}$$

where $\omega_0 = \frac{1}{\sqrt{LC}}$.
Now we want to express this in cavity parameters. To find expressions for C, R and Z, we use the capacitor voltage-capacitance relation, and the effect of a charge travelling through a resonant cavity (note that all parameters are specified in their LINAC definition):

$$\Delta V = \frac{q}{C} = \frac{q\omega}{2}\bigg(\frac{R}{Q}\bigg) \text{ (LINAC)} \tag{2.14}$$

$$C = \frac{2}{\omega(R/Q)} \text{ (LINAC)} \tag{2.15}$$

Using this and the equivalent cavity values for the shunt impedance R and the external impedance Z:

$$R = \frac{Q_0}{2}\bigg(\frac{R}{Q}\bigg) \text{ (LINAC)} \tag{2.16}$$

$$Z = \frac{Q_{ext}}{2}\bigg(\frac{R}{Q}\bigg) \text{ (LINAC)} \tag{2.17}$$

we find the circuit equation using cavity values to be given by the following equation:

$$V\bigg(- i\frac{2\Delta\omega}{\omega(R/Q)} + \frac{1}{(R/Q)}\bigg(\frac{1}{Q_0} + \frac{1}{Q_{ext}}\bigg)\bigg) = I_g - \frac{1}{2}I_{b,RF} \tag{2.18}$$

The RF beam current is a complex quantity, and as such can be expressed in terms of real and imaginary parts. For simplicity we can define the complex phase of all waves such that the cavity voltage V is always purely real (this is not the case for the model as shown later). Thus the cavity voltage is at the zero degree point in the complex plane. The synchronous angle ϕ_s is the angle of the RF voltage when the beam arrives. With LINAC machines, as is the case with electron synchrotrons, we generally operate close to maximum power transmission. This means that the synchronous angle is defined from the peak value of the RF voltage, i.e $\phi_{s,\,\text{LINAC}} = 0°$. when the cavity voltage and the beam pulse are in-phase, as opposed to the proton synchrotron case, in which the synchronous angle is taken with 90 degrees of difference. Using the LINAC convention:

$$I_{b,RF} = |I_{b,RF}|(\cos\phi_s - i\sin\phi_s) \tag{2.19}$$

The complex Fourier spectrum of a bunch train passing through the cavity is given by a frequency train which, in case of infinitely short bunches, has equal value for all frequencies $f = (-\infty, \infty)$. The corresponding real spectrum has no negative lines and corresponding frequencies add up, except for the DC term. Hence, the RF terms are twice the DC term, in the case of infinitely short bunches.

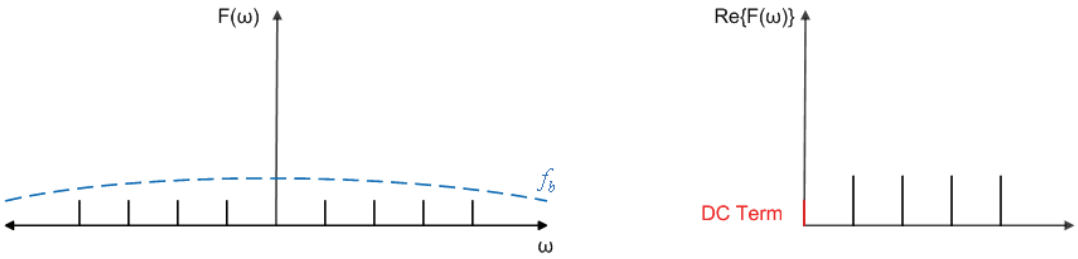

Figure 2.5: Fourier spectrum relation between RF and DC beam current

Thus $I_{b,RF} = 2I_{b,DC}$, except for finite bunches, in which case the factor 2 will become lower for higher frequency components. To take this effect into account we add a relative bunch factor f_b that is normalised to 1 for infinitely short bunches, so

$$I_{b,RF} = 2I_{b,DC} f_b(\cos\phi_s - i\sin\phi_s) \tag{2.20}$$

Substituting back into the previous equation, we find complex expressions for the generator and the reflected powers:

$$\begin{aligned} I_g = &\left[\frac{V}{(R/Q)Q_L} + I_{b,DC} f_b \cos\phi_{s,\,\mathrm{LINAC}}\right] \\ &-i\left[I_{b,DC} f_b \sin\phi_{s,\,\mathrm{LINAC}} + V\frac{2\Delta\omega}{\omega(R/Q)}\right] \end{aligned} \tag{2.21}$$

$$\begin{aligned} I_r = &\left[\frac{V}{(R/Q)}\left(\frac{1}{Q_{ext}} - \frac{1}{Q_0}\right) - I_{b,DC} f_b \cos\phi_{s,\,\mathrm{LINAC}}\right] \\ &+i\left[I_{b,DC} f_b \sin\phi_{s,\,\mathrm{LINAC}} + V\frac{2\Delta\omega}{\omega(R/Q)}\right] \end{aligned} \tag{2.22}$$

All equations above are defined using the LINAC convention for synchronous angle and R/Q. The LINAC definition for power, using peak values for current is

$$P_x = \frac{1}{4} R_{\mathrm{LINAC}} |I_x|^2$$

and therefore

$$P_{g,r} = \frac{1}{4}(R/Q)Q_{ext}|I_{g,r}|^2 \tag{2.23}$$

We can also find optimum detuning and loaded quality factor for the superconducting LINAC case using

$$\frac{\Delta\omega_{opt}}{\omega} = \frac{-I_{b,DC} f_b \sin\phi_s (R/Q)}{2V} \tag{2.24}$$

$$Q_{L,opt} = Q_{ext,opt} = \frac{V}{(R/Q) I_{b,DC} f_b \cos\phi_s} \tag{2.25}$$

The SPL design involves two types of superconducting cavities along the length of the LINAC. These are built for beams of $\beta = 0.65$ and $\beta = 1$. In practice, however, the (heavy) hydrogen ion beam gradually accelerates along the length of the accelerator. This means that the beam speed will be mismatched in the majority of cases with the cavity design. It is thus interesting to investigate the effects of different speed beamloading on the cavity voltage waveform.
For a certain field inside a resonant cavity, the accelerating voltage that the beam "sees" depends on the speed at which it is travelling. We want to see, thus, what the steady-state voltage of a cavity optimised for beam passage of a certain β_0 will be if we operate it with a beam of different speed β_x, in terms of the original steady-state voltage. We define the ratio:

$$\alpha_T = \frac{V_x}{V_o} = \frac{T(\beta_x)}{T(\beta_0)} \tag{2.26}$$

This ratio relates the accelerating voltage experienced by beams at different speeds for a given electric field within the cavity. If we recall

$$\frac{R_{sh}(\beta_x)}{Q} = \frac{V_x^2}{2\omega W}$$

we can say

$$\left(\frac{R}{Q}\right)_x = \alpha_T^2 \left(\frac{R}{Q}\right)_0$$

As we know, the forward and reflected currents interacting in a resonant cavity fed by constant generator power with constant beamloading are given by equations (2.21) and (2.22), where all voltages and currents are steady-state ($t \to \infty$). We assume that all cavities along the LINAC have been optimised for zero reactive beamloading. This means that the imaginary part of the equation vanishes always, and from now on we only deal with the real parts, thus the generator/reflected current equations become (for a superconducting LINAC):

$$I_g = \frac{V^{t\to\infty}}{(R/Q)Q_L} + I_{b,DC} f_b \cos\phi_s \tag{2.27}$$

$$I_r = \frac{V^{t\to\infty}}{(R/Q)Q_L} - I_{b,DC} f_b \cos\phi_s \tag{2.28}$$

Now, we optimise the coupling of the cavity for the design beam speed β_0 by choosing the external quality factor

$$Q_{ext,opt} = Q_{L,opt} = \frac{V_0^{t\to\infty}}{(R/Q)_0 I_{b,DC} f_b \cos\phi_s} \tag{2.29}$$

If we insert (2.29) into (2.27) and (2.28) the generator and reflected currents become

$$I_g^{(0)} = 2 I_{b,DC} f_b \cos\phi_s \qquad I_r^{(0)} = 0 \tag{2.30}$$

We now maintain the same forward power and operate the cavity with a different beam. If the forward power is equal for both cases and they are given by (LINAC)

$$\begin{aligned} P_g^{(0)} =& \frac{1}{4}(R/Q)_0 Q_L |I_g^{(0)}|^2 \\ P_g^{(x)} =& \frac{1}{4}(R/Q)_x Q_L |I_g^{(x)}|^2 \end{aligned} \tag{2.31}$$

then for $(R/Q)_x = \alpha_T^2 (R/Q)_0$, the forward current scales as $I_g^{(x)} = \frac{I_g^{(0)}}{\alpha_T}$ when Q_L is fixed. Bear in mind that all the values for current and voltage are virtual values dependent on the beam speed. The only absolute is the power.

The new current then is given by

$$I_g^{(x)} = \frac{I_g^{(0)}}{\alpha_T} = \frac{2 I_{b,DC} f_b \cos\phi_s}{\alpha_T}$$

and equating to (2.27) for a compensated cavity (no reactive beamloading)

$$\frac{2 I_{b,DC} f_b \cos\phi_s}{\alpha_T} = \frac{V_x^{t\to\infty}}{(R/Q)_x Q_L} + I_{b,DC} f_b \cos\phi_s$$

but the external coupling is optimised for the β_0 beam. If we insert our original equation for the optimal loaded quality factor in terms of β_0, we get

$$\frac{2 I_{b,DC} f_b \cos\phi_s}{\alpha_T} = \frac{V_x^{t\to\infty}(R/Q)_0}{V_0^{t\to\infty}(R/Q)_x} I_{b,DC} f_b \cos\phi_s + I_{b,DC} f_b \cos\phi_s$$

which means that the steady-state voltages for beams travelling through a resonant cavity fed by constant power at different speeds are related by:

$$V_x^{t\to\infty} = (2\alpha_T - \alpha_T^2) V_0^{t\to\infty} \tag{2.32}$$

where $\alpha_T = \frac{T(\beta_x)}{T(\beta_0)}$.

2.2.2 Transient Analysis

The superconducting proton LINAC will make use of pulsed generators, and so does the model developed for it. Hence, the scope of the project is not limited to steady-state analysis, and so it is that we now let go of our initial assumptions and plunge into the realm of transient analysis. We begin again from the externally driven L-C-R circuit. This time we include the external load in the loaded impedance [4].

$$R_L = R || Z_{ext} \tag{2.33}$$

Applying Kirchhoffs current rule

$$I_{cav} = I_{R_L} + I_C + I_L$$

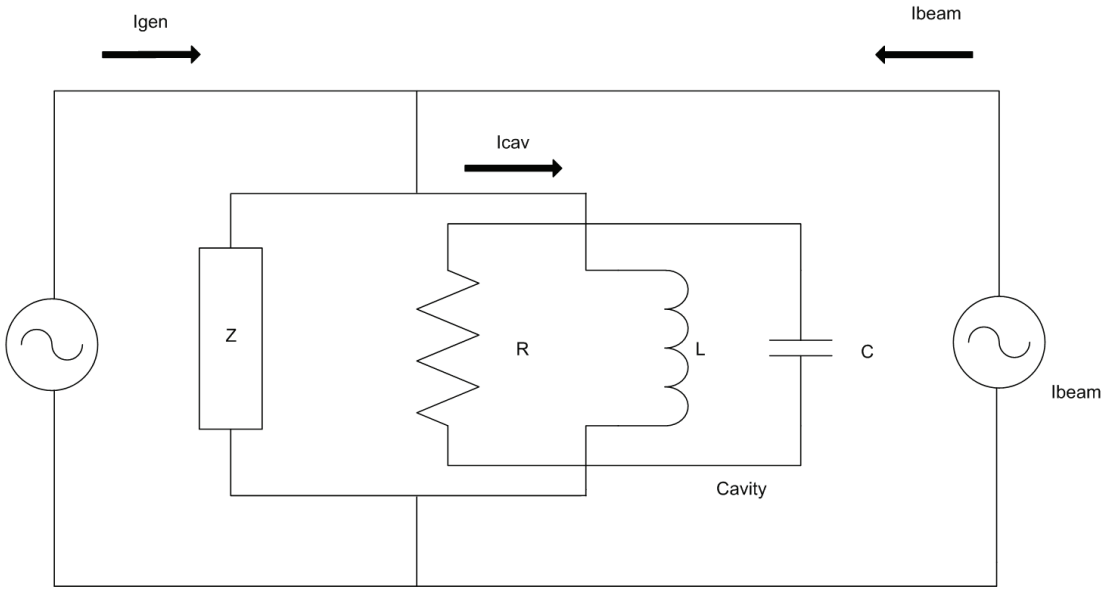

Figure 2.6: Cavity-beam interaction [4]

and the formulas

$$\dot{I_L} = V/L \qquad \dot{I_R} = 2\dot{V}/R_L \qquad \dot{I_C} = C\ddot{V}$$

and translating into cavity values

$$\frac{1}{R_L C} = \frac{\omega_0}{Q_L} \qquad \frac{1}{LC} = \omega_0^2$$

we find

$$\ddot{V}(t) + \frac{1}{R_L C}\dot{V}(t) + \frac{1}{LC}V(t) = \frac{1}{C}\dot{I}(t) \tag{2.34}$$

$$\ddot{V}(t) + \frac{\omega_0}{Q_L}\dot{V}(t) + \omega_0^2 V(t) = \frac{\omega_0 R_L}{Q_L}\dot{I}(t) \tag{2.35}$$

The driving current I_g and the Fourier component of the pulsed beam $I_{b,RF}$ are harmonic with $e^{i\omega t}$. We now separate fast RF oscillation from the slowly changing amplitudes and phases of real and imaginary (I/Q) components of the field vector:

$$\begin{aligned} V(t) &= (V_r(t) + iV_i(t))e^{i\omega t} \\ I(t) &= (I_r(t) + iI_i(t))e^{i\omega t} \end{aligned} \tag{2.36}$$

We insert this into the differential equation 2.28 and we end with the result

$$\begin{aligned} \dot{V_{RE}} + \omega_{1/2}V_{RE} + \Delta\omega V_{IM} &= R_L\omega_{1/2}I_{RE} \\ \dot{V_{IM}} + \omega_{1/2}V_{IM} - \Delta\omega V_{RE} &= R_L\omega_{1/2}I_{IM} \end{aligned} \tag{2.37}$$

Where $\omega_{1/2} = \frac{\omega_0}{2Q_L}$ is the half bandwidth of the cavity. The driving current in steady-state is given by $I = 2I_g + I_{b,RF}$. In the case of on-crest acceleration (zero synchronous angle) for a train of infinitely short bunches passing through a cavity on resonance, we can approximate the resonant frequency component of the beam current to twice its DC value $I = 2(I_g - I_{b,DC})$, bearing in mind the 180 phase shift of the beam. Filling a cavity with constant power results in an exponential increase of the cavity voltage

$$V_g = R_L I_g \left(1 - e^{\frac{-t}{\tau}}\right)$$

where V_g represents the generator-induced cavity voltage and the LINAC convention is taken for the loaded impedance. Similarly, a beam current injected at time t_{inj} results in an opposite voltage gradient within the cavity

$$V_b = -R_L I_{b,DC} \left(1 - e^{-\frac{1}{\tau}(t - t_{inj})}\right)$$

where V_b represents the beam-induced cavity voltage and $\tau = \frac{1}{\omega_{1/2}} = \frac{2Q_L}{\omega_0}$ is the filling constant of the cavity.
The total cavity voltage is a superposition of the beam-induced and generator-induced voltages.

$$V_{cav}(t) = R_L I_g \left(1 - e^{\frac{-t}{\tau}}\right) \quad \text{for } t < t_{inj} \tag{2.38}$$

$$V_{cav}(t) = R_L I_g \left(1 - e^{\frac{-t}{\tau}}\right) - R_L I_{b,DC} \left(1 - e^{\frac{-(t - t_{inj})}{\tau}}\right) \quad \text{for} \quad t_{inj} < t < t_{OFF} \tag{2.39}$$

In the case of superconducting cavities, the generator power is almost entirely transferred to the beam. The injection time can then be chosen to arrive at an immediate steady-state condition. In other words, if we time the beam in such a way that the positive voltage gradient induced by the generator is equal to the negative voltage gradient induced by the beam on the cavity, the cavity voltage will remain constant during beam loading. This can be achieved, for optimal matching and $I_g = \alpha I_{b,DC}$, when the cavity field has reached $1 - \frac{1}{\alpha}$ of its maximum:

$$t_{inj} = \ln \alpha \times \tau \tag{2.40}$$

$$\begin{aligned} V_{cav}(t) &= R_L I_g \left(1 - e^{-\frac{t}{\tau}}\right) - R_L I_{b,DC} \left(1 - \alpha e^{-\frac{t}{\tau}}\right) \\ V_{cav}(t) &= R_L I_g \left(1 - e^{-\frac{t}{\tau}}\right) - \frac{R_L I_g}{\alpha} \left(1 - \alpha e^{-\frac{t}{\tau}}\right) \end{aligned} \tag{2.41}$$

$V_{cav} = V_{max} \left(1 - \frac{1}{\alpha}\right)$, where $V_{max} = R_L I_g$ (LINAC)
Figure 2.7 shows the effect on the cavity voltage of an infinitely short bunch train, with an average current $I_{b,DC}$ passing through a cavity at the right injection time

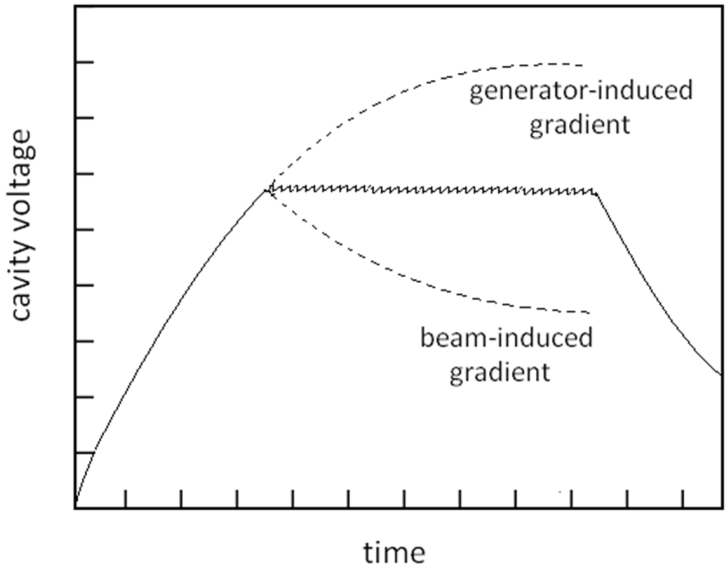

Figure 2.7: Cavity voltage gradients induced by generator and beam

t_{inj} such that the generator-induced gradient is cancelled by that induced by the beam.

Each infinitely short bunch is seen as an instant drop in the cavity voltage, while the generator-induced voltage has a continuous effect on the cavity. When both the beam and generator are OFF, the cavity voltage decays exponentially.

In the last section, we arrived at the conclusion that the beamloading effects in terms of cavity voltage and beam acceleration differ depending on the speed of the beam traversing a resonant cavity with a given electric field. As explained before, the accelerating voltage that a beam "sees" when passing through the resonant cavity will depend on its relativistic β factor, as it will experience a number of cycles of the RF power. This means, when operating close to relativistic speeds, that beamloading will be weaker for a slower beam than a faster one. For example, a beam travelling at the speed of light will absorb more RF power from the cavity than a slower one. This will result in a higher beam-induced voltage on the cavity and the steady-state equilibrium voltage inside the cavity will be lower for a given coupling, forward power, and beam current.

The cavity voltage envelope waveform needs to be specified for a certain beam speed in order to have meaning. Until now, we have assumed a fixed geometric factor (R/Q), which is expressed for the design beam speed of the cavity. Now, it is interesting to investigate the transient effects during filling, injection and decay time of the cavity with different beam speed. We assume again that the aforementioned voltage envelope is actually the accelerating voltage that a beam travelling with a β_0 speed would experience when passing through the cavity. What happens if a different beam of speed β_x is present at injection?

Before beamloading, the voltage within the cavity can be expressed in terms of any beam. Thus, if we know the behaviour of $V_0(t)$ for a β_0 beam during filling, $V_x(t)$

is merely given by $\alpha_T V_0(t)$, where $\alpha_T = \frac{T_x}{T_0}$ (T is the transit-time factor). In other words

$$V(\beta_x, t) = \alpha_T V(\beta_0, t) \tag{2.42}$$

If the cavity is loaded up to the β_0 steady-state voltage, at injection

$$V(\beta_x, t_{inj}) = \alpha_T V_0^{t\to\infty} \tag{2.43}$$

The voltage will remain constant during beamloading (flat-top) for the β_0 beam. For a different beam, a new equilibrium will be reached. The cavity voltage will tend towards the steady-state voltage for the new beam, and the voltage swing between injection and the new steady-state will be given by $V_x^{t\to\infty} - \alpha_T V_0^{t\to\infty}$ as seen by the β_x beam. If the new equilibrium voltage $V_x^{t\to\infty} = (2\alpha_T - \alpha_T^2)V_0^{t\to\infty}$, then the voltage swing during beamloading is

$$\Delta V_x = V_x^{t\to\infty} - V_x(t_{inj}) = (2\alpha_T - \alpha_T^2 - \alpha_T)V_0^{t\to\infty} \tag{2.44}$$

Therefore, the complete voltage envelope as seen by the new beam becomes

$$V_x(t < t_{inj}) = \alpha_T V^{\infty}\Big(1 - e^{\frac{-t}{\tau}}\Big) \tag{2.45}$$

$$V_x(t > t_{inj}) = \alpha_T V_0^{t\to\infty}\left[1 + (1 - \alpha_T)\Big(1 - e^{\frac{-(t-t_{inj})}{\tau}}\Big)\right] \tag{2.46}$$

where $V^{\infty} = R_{L0} I_g$ is the steady-state voltage without beam as would be seen by the β_0 beam, and $V_0^{t\to\infty}$ is the design accelerating voltage as seen by the β_0 beam.

It is important to note that the above description is somewhat different in the case of out of phase beam loading. It is important to bear in mind that when the beam arrives with a certain synchronous angle, the beam current is expressed by

$$I_{b,RF} = |I_{b,RF}|(\cos\phi_s - i\sin\phi_s) \tag{2.47}$$

and similarly, the generator current is given by

$$\begin{aligned} I_g = &\left[\frac{V}{(R/Q)Q_L} + I_{b,DC} f_b \cos\phi_{s,\,\mathrm{LINAC}}\right] \\ &-i\left[I_{b,DC} f_b \sin\phi_{s,\,\mathrm{LINAC}} + V\frac{2\Delta\omega}{\omega(R/Q)}\right] \end{aligned} \tag{2.48}$$

This means that the relationship between Ig and Ib becomes

$$\underline{I}_g = \underline{\alpha}\ \underline{I}_{b,DC}$$

where the underlining represents complex quantities. This means that the injection time would have to be complex in order to obtain flat-top operation, which is, of course, physically impossible. In practice this means that the cavity voltage flat-top operation can be optimised with respect to the real part by means of optimal

coupling and with respect to the imaginary part by detuning the cavity. For the purpose of our analysis, the focus is on the real part and thus the effects of flat-top drift during beam loading due to reactive effects are in practice curbed by a fast feedback loop in both magnitude and phase, though other methods life pre-detuning or half-detuning have proven successful in the past.

2.3 Beam loading Theorem

Until now, the passage of the beam through a resonant cavity has been represented by a DC current source pulled from the cavity. This is a good approximation and works well to observe the beam effect on the magnitude of the cavity voltage. In reality, however, beam loading consists on the effects of several single bunches (modelled with infinitely small width) accelerated by a resonant cavity. These bunches not only have an effect in the cavity voltage magnitude, but also its phase. When a beam is perfectly in-phase with the RF voltage in a tuned cavity, the cavity voltage will stay in tune during beam passage, while its amplitude decays, however, the transient effects of a detuned cavity and the beam synchronous angle remain to be discussed. As we will see during the course of this paper in both theory and practice, a beam that arrives at the cavity with a synchronous angle ϕ_s will asymptotically pull the cavity voltage towards this angle (note that we use the LINAC definition for ϕ_s). After the passing of a point charge through a resonant cavity, an induced voltage V_{bn} remains in each resonant mode (for simplicity we will consider the main mode only). What fraction of V_{bn} does the charge "see"? We will prove this to be $\frac{1}{2}V_{bn}$. This result is called the fundamental theorem of beam loading [6]. The fundamental theorem of beam loading relates the energy loss by a charge crossing the cavity to the electromagnetic properties of resonant modes in the cavity computed in the absence of field. By superposition, the beam-induced voltage in a resonant cavity is the same whether or not there is a generator-induced voltage already present. We observe the effect of a charge passing through a cavity, being accelerated by generator-induced field present within said cavity. A single bunch passing through a cavity excites a field within it. Taking into account the fundamental resonant mode only, the excited field can be expressed as an exponentially decaying sine wave oscillating with the cavity's resonant frequency ω_0. In vector terms, the power delivered to the beam by the RF, taking into account the beam-induced cavity voltage is given by

$$P_{b,eff} = -(\vec{V_g} + \vec{V_b}) \bullet \vec{I}_{b,RF}$$

where the generator-induced voltage is not necessarily in-phase with the beam current component at the resonant frequency of the cavity. V_b represents the effective beam-induced voltage seen by the beam. To find this voltage, the cavity gap impedance (in transient mode) can be represented by a single capacitor

$$\frac{1}{C} = \frac{R_{sh}}{Q_0}\omega_0$$

and so the bunch-induced voltage in the cavity is given by

$$V_{bunch} = \frac{q_b}{C} = \frac{q_b}{2} \times \left(\frac{R}{Q}\right)(\text{LINAC}) \times \omega_0 \tag{2.49}$$

The energy lost by the bunch and stored in the cavity (Capacitor) is then

$$W = \frac{1}{2}CV_{bunch}^2 = \frac{1}{2}q_b V_{bunch} \tag{2.50}$$

The power received by the beam is then the vector sum of the generator-induced power and the beam self-induced power.

$$P_{b,eff} = -\vec{V}_g \bullet \vec{I}_{b,RF} - \frac{1}{2}\vec{I}_{b,RF} \bullet \vec{V}_{bunch} = -(\vec{V}_g + \frac{1}{2}\vec{V}_{bunch}) \bullet \vec{I}_{b,RF} \tag{2.51}$$

and so, returning to our original result for the power delivered to the beam, it is clear that

$$\vec{V}_b = \frac{1}{2}\vec{V}_{bunch} \tag{2.52}$$

The beam only "sees" half of its own induced voltage in the cavity [7].

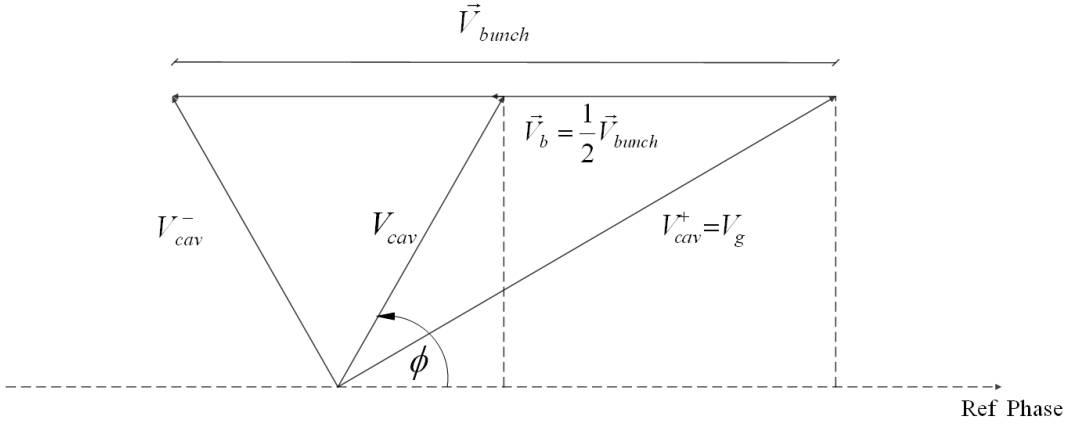

Figure 2.8: Effect of single bunch passage on cavity voltage [6]. V_{cav}^+ and V_{cav}^- refer to cavity voltage before and after bunch passage respectively.

Now we are interested in computing the transient variation of the cavity voltage due to the passing of a periodic bunch train (with infinitely small bunches). Consider first an undriven cavity with resonant frequency ω_0 and a filling time constant τ. Suppose the cavity is initially charged to $V_{cav}(0)$, and this voltage then decays exponentially with the filling constant, while rotating at the RF frequency ω, which is not necessarily the resonant frequency, i.e. the reference frame for the phasor diagram is chosen as the RF driving frequency.
The time variation in magnitude and phase of the cavity voltage is given by

$$V_{cav}(t) = V_{cav}(0)e^{\frac{-t}{\tau}}e^{jt\Delta\omega}$$

where $\Delta\omega = \omega_0 - \omega$,and the tuning angle is the angle between the generator current and the cavity voltage and related to the frequency detuning by

$$\tan\Psi = \tau\Delta\omega$$

These equations, in essence, explain that the RF field within an undriven cavity with a resonant frequency that differs from the RF frequency will rotate in phase as it decays exponentially. Furthermore, the rotation in time will be proportional to the frequency detuning (between RF and resonant frequencies). This effect is shown in figure 2.9.

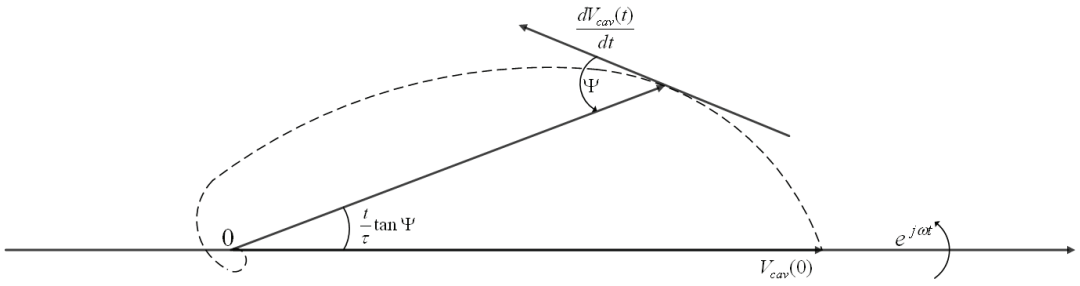

Figure 2.9: Voltage decay in detuned cavity [6]

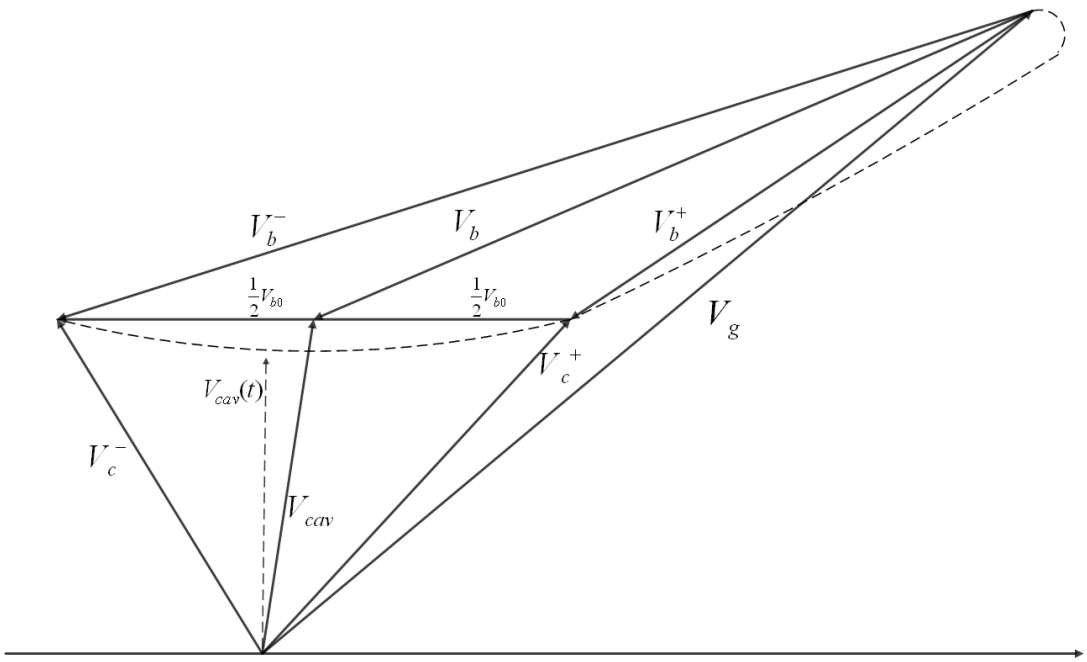

Figure 2.10: Overall effect of beam loading on detuned cavity [6]

If we now include the effect of several bunches and the generator voltage, note that the zero degree phase is set as the positive direction of the bunch-induced voltage, we

observe the effect of both the frequency detuning and the synchronous angle.If the cavity voltage starts in-phase with the generator voltage, we can see how each bunch passage pulls the cavity voltage towards the synchronous angle (shown in figure 2.11 with the zero phase angle set for the generator current). The spiral path in the figure 2.10 shows the cavity voltage driven by the generator. The cavity voltage tends asymptotically towards the generator voltage, but the beam passage opposes this effect, creating flat-top operation if timed right. The path is not straight, as shown in figure 2.9 due to the mismatch between cavity resonant frequency and RF generator frequency. Interestingly enough, the synchronous angle and the tuning angle can be such that their combined effects are somewhat cancelled, depending on the magnitude of the bunch-induced voltage in the cavity and the frequency of bunch passage in regards to the generator-induced voltage and the filling time constant of the cavity. In the case above, the time between bunch passages is such that $V_c(t)$ returns to V_c^- after each bunch passage. If the tuning angle is zero, and the injection time is such that the magnitude of the beam-induced cavity voltage is equal to that of the generator-induced voltage, the phase change of the total cavity voltage will be driven by the beam current, as we will observe in the results section.

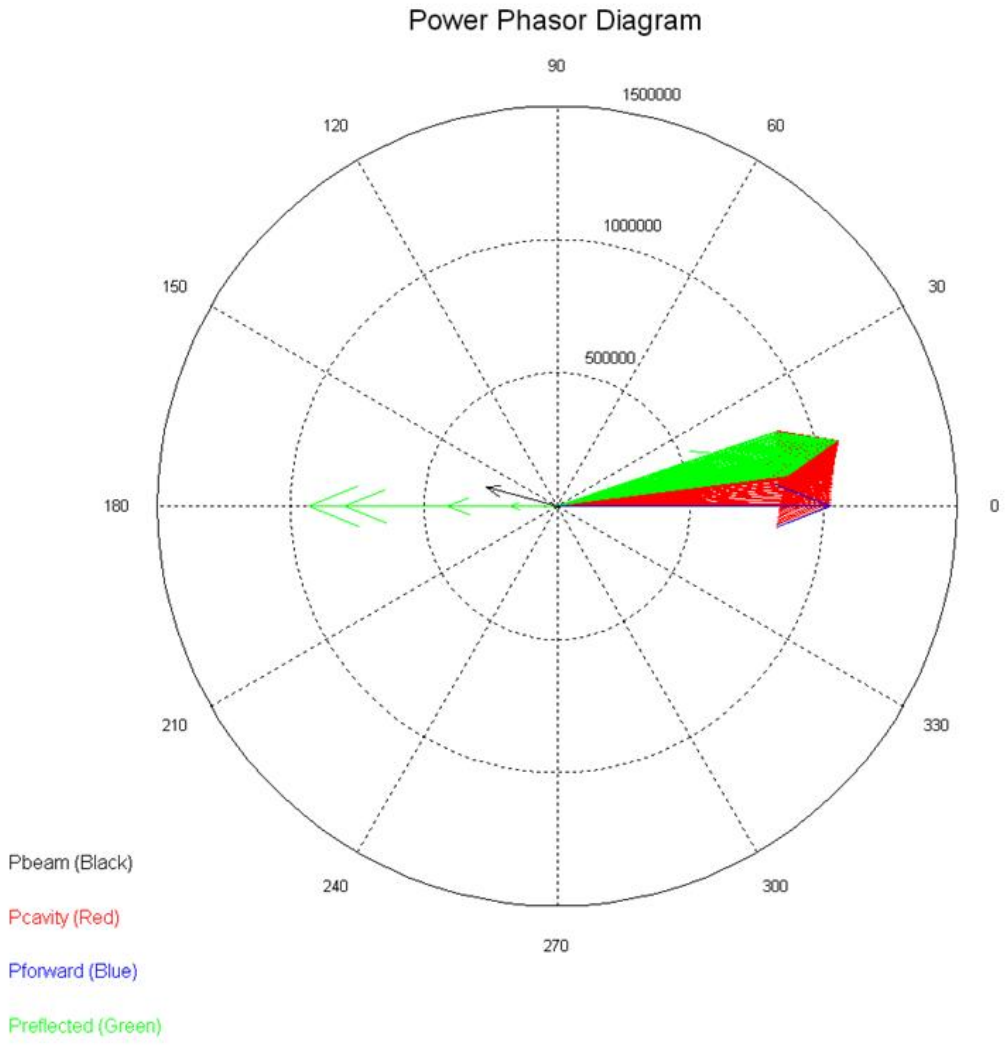

Figure 2.11: Generator-beam power interaction in tuned cavity

Chapter 3

RF Control of a 5-Cell 704.4 MHz Resonant Cavity

3.1 SPL Design and Modes of Operation

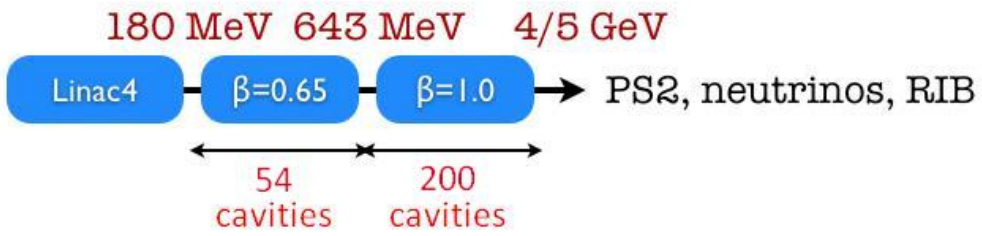

Figure 3.1: General SPL Design [8]

LINAC4 and the SPL are being developed as a possible generic solution to many of CERNs needs in terms of high-power beam experiments. Perhaps one of the most important features of the SPL, in order to meet these needs, is its flexibility. The SPL is planned to accelerate H^- ions firstly for the purpose of injecting to the LHC supplier chain, that will include an upgrade to the proton synchrotron and the proton-synchrotron booster referred to as PS2. The second goal of the SPL is to create a beam that is upgradeable to feed all of CERNs high power proton users or neutrino-production facilities. The SPL, as of now, is planned to accelerate a 40mA beam pulse lasting 0.4 ms with a repetition rate of 50 Hz at high current operation, and a 20 mA beam lasting 0.8 ms at low current. The couplers from the RF generator to the resonant cavity will be optimised for 40 mA, where a movable-coupler scheme has been dismissed after budget considerations to favour a slight increase in 20 mA operation power to compensate for the power reflection due to the transmission line mismatch.
In order to effectively accelerate the hydrogen ion beam over the energy range specified for the SPL, its full design, from the RF point of view, consists of 254 resonant cavities operating at superconducting temperatures, spread along a beam pipe measuring about 550 meters in length. The RF accelerating effort is separated into two

sections dictated by the speed of the beam as it accelerates. The 54 cavities along the slower section are optimised for a beam travelling with a speed of $\beta = 0.65$ relative to the speed of light, while 200 cavities along the faster section are optimised for $\beta = 1$. Of course, as the beam accelerates continuously, most cavities will not operate with optimum beam loading. This is further analyzed in section 5.

General linac parameters

Parameter	Unit	HP-SPL	LP-SPL	Timestamp
Energy	[GeV]	5	4	15 August 2007
Beam power	[MW]	>4.0	0.192	31 March 2008
Repetition rate	[Hz]	50	2	15 August 2007
Average pulse current	[mA]	20/40	0-20	28 November 2008
Peak pulse current	[mA]	32/64	32	15 August 2007
Source current	[mA]	40/80	40	21 April 2008
Chopping ratio	[%]	62	62	21 November 2008
Beam pulse length	[ms]	0.4[(1)] - 0.8[(2)]	0.9	2010-04-13
Number of klystrons (704 MHz, 5 MW)		tbd	tbd	15 August 2007
Geometric cavity beta		0.65/1.0	0.65/1.0	24 April 2009
Number of cavities		60/184	60/144	2009-10-06
Additional cavities for debunching		0/16	0/16	2009-10-06
Cavities/klystron		tbd	tbd	22 April 2008
Cavities/cryostat		3/8	3/8	2010-05-04
Max. power/cavity	[MW]	1	0.5	21 April 2008
Length[(3)]	[m]	525	450	2009-11-09

[(1)] high-current operation
[(2)] low-current operation
[(3)] excluding Linac4, including 16 debuncher cavities at linac end, including extraction to ISOLDE and EURISOL

Figure 3.2: General SPL parameters [9]

3.2 Power Requirements

The beam is expected to travel with a varying synchronous angle of around 15 degrees with respect to the cavity voltage (LINAC convention). This implies that not all of the power delivered to the cavities will be absorbed by the beam, even in the case of a matched coupler. The RF power will thus need to be raised above 1 MW to operate the higher gradient cavities. The 20 mA case has a similar result due to both coupling mismatch and beam synchronous angle effects. The maximum accelerating field is of around 19 MV/m for the low-speed section of the LINAC, and 25 MV/m at the high-speed end. These correspond to accelerating voltages of

Cryo design parameters

Parameter	Unit	low-beta	high-beta	Timestamp
*	*	nominal/ultimate	nominal/ultimate	*
Cavity bath temperature	[K]	2.0	2.0	2010-05-11
Beam loss	[W/m]	1.0	1.0	2010-05-11
Static loss along cryo-modules at 2 K	[W/m]	?	?	2010-05-11
Static loss at 5-280 K	[W/m]	?	?	2010-05-11
Accelerating gradient	[MV/m]	19.3	25	2010-05-11
Quality factor	10^9	6/3	10/5	2010-05-11
R/Q value (linac def.)	[Ohm]	290	570	2010-05-11
Cryogenic duty cycle	[%]	4.09/8.17	4.11/8.22	2010-05-11
Coupler loss at 2.0 K	[W]	<0.2/0.2	<0.2/0.2	2010-05-11
HOM loss at 2.0 K in cavity	[W]	<1/<3	<1/<3	2010-05-11
HOM coupler loss at 2.0 K (per coupler)	[W]	<0.2 /0.2	<0.2/0.2	2010-05-11
HOM & Coupler loss 5-280 K	[g/s]	0.05	0.05	2010-05-11
Tunnel slope	[%]	1.7%	1.7%	2010-05-11
Magnet operating temperature	[K]	ambient	ambient	2010-05-11
No of cavities		60	200	2010-05-11
No of cryostats		20	25	2010-05-11
Cavities per cryostat		3	8	2010-05-11
Dynamic heat load p. cavity	[W]	4.2/16.8	5.1/20.4	2010-05-25

Figure 3.3: General cryogenics parameters [9]

13.3 MV and 26.6 MV respectively. In order to maintain flat-top operation at these voltages, the injection time for 20/40 mA operation needs to be calculated as shown below. The total power needed for each scenario can then be specified to match the voltage required at the calculated injection time [10].

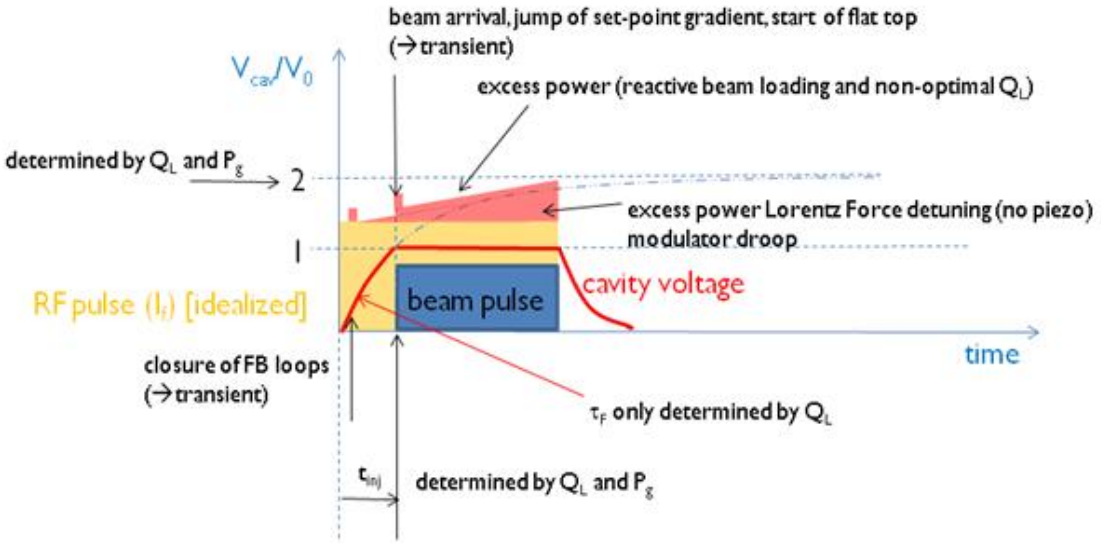

Figure 3.4: Transient power in resonant cavity (figure taken from presentation by Wolfgang Hofle at CERN) [10]

The low-speed and high-speed sections of the SPL have slightly different parameters. The following calculations correspond to the maximum accelerating fields for each of the two speed-sections of the LINAC. The geometric factors are specified for a beam travelling at the cavity design speed.
For 40 mA operation, the following parameters apply:

$f_{RF} = 704.4$ MHz

$I_{b,DC} \simeq 40$ mA

$\phi_s = 15°$ (LINAC)

$E_{acc} = 25$ MV/m

$\text{length}_{cav} = \beta \times \frac{\lambda_{RF}}{2} \times 5$ (5 cell, π mode) $= 1.064$ m

$V_{acc} = E_{acc} \times \text{length}_{cav} = 26.6$ MV

$P_b = V_{acc} \times I_{b,DC} \times \cos\phi_s = 1.0285$ MW

$\frac{R}{Q} = 570\Omega$ (LINAC)

$Q_L = \frac{V_{acc}}{\frac{R}{Q} \times I_{b,DC} \times \cos\phi_s} = 1.2078 \times 10^6$

$R_L = Q_L \frac{R}{Q} = 688$ MΩ (LINAC)

$I_g = \frac{V_{acc}}{R_L} + I_{b,DC} \cos\phi_s = 77.3$ mA

$\alpha = \frac{I_g}{I_{b,DC}\cos\phi_s} = 2$

$\tau_{fill} = \frac{2Q_L}{\omega_{RF}} = 0.5458$ ms

$t_{inj} = \tau_{fill}\ln\alpha = 0.3783$ ms

$t_{pulse} = 0.4$ ms

With a power consumption given by $P_{fwd} = \frac{1}{4}R_L|I_g|^2 = 1.0286$ MW.

Now, if we recall the general equation for the generator current from the steady-state analysis of the theory, we find

$$\begin{aligned} I_g = &\left[\frac{V}{(R/Q)Q_L} + I_{b,DC} f_b \cos\phi_{s,\,\mathrm{LINAC}}\right] \\ &-i\left[I_{b,DC} f_b \sin\phi_{s,\,\mathrm{LINAC}} + V\frac{2\Delta\omega}{\omega(R/Q)}\right] \end{aligned} \tag{3.1}$$

It is thus possible to compensate for reactive beam loading

$$P_{reactive\_BL} = \frac{1}{4}|I_b \sin\phi_s|^2 \tag{3.2}$$

This value can be added on the power budget or corrected by detuning the cavity as we can see from the equation above, otherwise the feedback loop will have to compensate for its effects. In these cases, it is also possible to use a half-detuning method, which means the cavity is detuned in between the optimum tuning for filling and beam loading. This will result in compensation being necessary during both filling and beam loading, but at a lower power level.
For the 20 mA case, the same reasoning applies. For the matched case, power consumption is halved while the optimum loaded quality factor and injection and filling times double. This would imply, however, that the loaded quality factor needs to vary between 40 mA and 20 mA operation, which involves using variable coupling between generator and resonant cavity. In practice, this is bulky and very expensive. It is more viable to slightly increase the generator power requirements during mismatched operation. So, if the loaded quality factor is matched for 40 mA operation, the operating values are as follows:

$I_{b,DC} \simeq 20$ mA

$P_b = V_{acc} \times I_{b,DC} \times \cos\phi_s = 514$ kW

$Q_L = 1.2085 \times 10^6$

$I_g = \frac{V_{acc}}{R_L} + I_{b,DC}\cos\phi_s = 58$ mA

$\alpha = \frac{I_g}{I_{b,DC}\cos\phi_s} = 3$

$\tau_{fill} = \frac{2Q_L}{\omega_{RF}} = 0.5458$ ms

$t_{inj} = \tau_{fill}\ln\alpha = 0.5996$ ms

$I_{ref} = \frac{Vacc}{\frac{R}{Q}Q_{ext}} - I_{b,DC}\cos\phi_s = 19.3$ mA

$P_{ref} = \frac{1}{4}R_L|I_{ref}|^2 = 64$ kW

If we now compare the power requirements with matched operation, for one cavity with 40 mA beam and for two cavities with 20 mA beam respectively, the powers are

$$P_{40\text{ mA}} = 1.029\text{ MW}$$
$$P_{2\times 20\text{ mA}} = 1.156\text{ MW}$$

This entails a 12.3% power increase for the mismatched case.

The power requirements for the $\beta = 0.65$ section of the LINAC are evaluated using the same method. When using 40 mA of current:

$I_{b,DC} \simeq 40$ mA

$E_{acc} = 19.3$ MV/m

$\text{length}_{cav} = \beta \times \frac{\lambda_{RF}}{2} \times 5$ (5 cell, π mode) $= 0.6916$ m

$V_{acc} = E_{acc} \times \text{length}_{cav} = 13.348$ MV

$P_b = V_{acc} \times I_{b,DC} \times \cos\phi_s = 516$ kW

$Q_L = 1.1913 \times 10^6$

$I_g = \frac{V_{acc}}{R_L} + I_{b,DC}\cos\phi_s = 77.3$ mA

$\alpha = \frac{I_g}{I_{b,DC}\cos\phi_s} = 2$

$\tau_{fill} = \frac{2Q_L}{\omega_{RF}} = 0.5383$ ms

$t_{inj} = \tau_{fill}\ln\alpha = 0.3731$ ms

And for the mismatched beam current case:

$I_{b,DC} \simeq 20$ mA

$P_b = V_{acc} \times I_{b,DC} \times \cos\phi_s = 258$ kW

$Q_L = 1.1913 \times 10^6$

$I_g = \frac{V_{acc}}{R_L} + I_{b,DC} \cos \phi_s = 58$ mA

$\alpha = \frac{I_g}{I_{b,DC} \cos \phi_s} = 3$

$\tau_{fill} = \frac{2Q_L}{\omega_{RF}} = 0.5383$ ms

$t_{inj} = \tau_{fill} \ln \alpha = 0.5914$ ms

$I_{ref} = \frac{Vacc}{\frac{R}{Q} Q_{ext}} - I_{b,DC} \cos \phi_s = 19.3$ mA

$P_{ref} = \frac{1}{4} R_L |I_{ref}|^2 = 32.2$ kW

The power difference is both modes of operation is given by:

$$P_{40 \text{ mA}} = 516 \text{ kW}$$
$$P_{2\times 20 \text{ mA}} = 580 \text{ kW}$$

This is a 12.4% power increase for mismatched operation.

3.3 Sources of Perturbation

Due to injection tolerances and stability requirements for the SPL injection onto the LHC supplier chain and other high-energy proton users at CERN, the cavity voltage magnitude and phase have been specified to very accurate values. According to SPL design, the voltage magnitude deviation must be below 0.5% of the total value and its phase deviation must not exceed 0.5 degrees. This is clearly a challenge as the constraints are quite restrictive. It is therefore important to anticipate and analyze the main possible sources of perturbation and their effects on the overall performance of the system. In this way, two main error causes have been identified; namely Microphonics and Lorentz Force Detuning. Superconducting cavities are made of a thin niobium wall and are therefore subject to mechanical deformations due to various external factors. One such factor is the pressure of the liquid helium bath. Other factors can include structural resonances or even external conditions such as outside temperature or ground movement. The overall effect is not easily modelled due to the many possible environmental factors that cause cavity deformations. The effects of this deformation due to liquid helium bath pressure are usually referred to as microphonics [11]. The detuning may be mathematically described as a sum of slowly modulated harmonic oscillations:

$$\Delta\omega_\mu(t) = \sum_i^N \Delta\bar{\omega}_i(t) \sin(\omega_i t + \phi_i) \tag{3.3}$$

Perhaps a more important source of frequency detuning arises when resonant cavities are filled with powerful electric and magnetic fields. When a resonant cavity,

made of thin niobium is filled with a high-power electric field and its magnetic counterpart, the fields exert a pressure on the cavity walls that can result in mechanic deformation. This is known as Lorentz Force Detuning. In mathematical terms, the wall pressure due to electric and magnetic fields within the cavity is given by

$$P_{\vec{E},\vec{H}} = \frac{1}{4}\left(\mu_0|\vec{H}|^2 + \varepsilon_0|\vec{E}|^2\right) \tag{3.4}$$

This gives rise to a change in volume, and thus a change in resonant frequency of the cavity given by

$$\frac{\omega_0 - \omega}{\omega_0} = \frac{\int_{\Delta V}\left(\varepsilon_0|\vec{E}|^2 - \mu_0|\vec{H}|^2\right)}{\int_V\left(\varepsilon_0|\vec{E}|^2 + \mu_0|\vec{H}|^2\right)} \tag{3.5}$$

the integral of the change in volume over the total volume [4].
In the case of a pillbox-like cavity, the pressure is concentrated in regions with high field. In this way, the electric field close to the irises (drift tubes) contracts the cavity, while the magnetic fields along the equator expand it. This results in a more disk-like cavity which results in a negative frequency change. Thus the frequency deviation is found to be proportional to the negative square of the accelerating field: $\Delta f_0 = -K \times E_{acc}^2$, where K is referred to as the Lorentz detuning factor in Hz/(MV/m)². Since the electric field varies and the cavity walls have an inertial mass, Lorentz detuning has a transient variation that can be seen as low frequency damped oscillations with the cavity's mechanical resonant modes. If we now take into account the main mechanical mode, we arrive at a 1st order differential equation:

$$\tau_m \Delta\dot{\omega}(t) = -(\Delta\omega(t) - \Delta\omega_T) + 2\pi K \cdot E_{acc}^2(t) \tag{3.6}$$

This equation describes the time-variation of the frequency deviation with time. τ_m is the mechanical damping time constant and $\Delta\omega_T$ is a frequency shit due to an external mechanical excitation (such as a piezo-electric tuner).

3.4 Feedback and Feed-Forward Control

Until now, the sources of error have been identified and the need for a stable cavity voltage in terms of both magnitude and phase has been stressed. In order to effectively control a resonant cavity to meet the necessary specifications, it is necessary to predict errors using mathematical descriptions for the sources identified, and also develop an automated system that can deal with unforeseen variations. The most widely used control technique and one that applies to our necessities is that of negative feedback. The idea is to control a system‘s output by comparing it to a desired setpoint and feeding the error back to the input dynamically.
The solution used in this particular implementation of the cavity control is done using I/Q components of the signal (refer to chapter 4). The advantage of this is that phase and magnitude can be controlled simultaneously using a setpoint in I/Q description. Common feedback controllers use mathematical information of the error

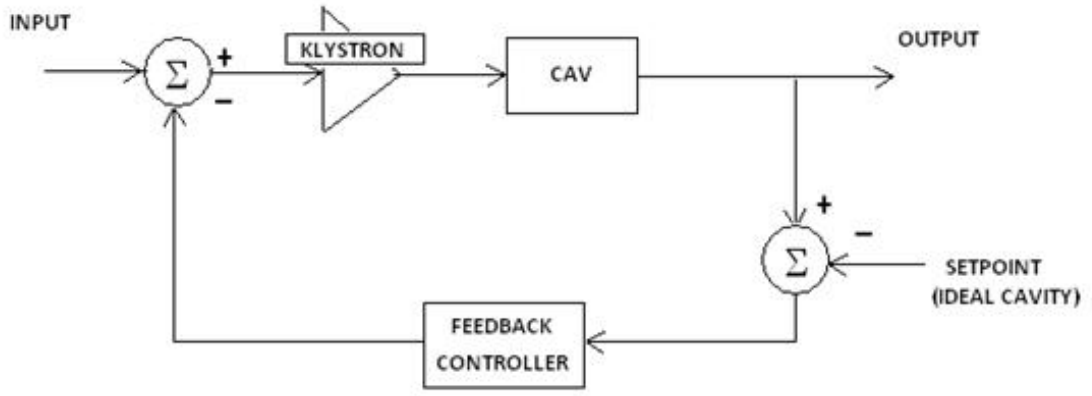

Figure 3.5: Negative feedback operation

signal $e(t)$ to determine a signal to be fed to the system input. In the context of this report, PID feedback is of interest. PID feedback stands for Proportional-Integral-Derivative Feedback. This means that not only a fraction of the error signal is fed back to the input, but also of its derivative and integral. The proportional value determines a reaction to the current error, the integral value determines a reaction to the cumulative error, and the derivative term determines a reaction based on the rate at which the error is changing. Together, they form a very powerful means for controlling the output of a system [12] [13]:

$$\text{Out}_{FB} = K_p e(t) + K_i \int_0^t e(\tau)d\tau + K_d \frac{d}{dt} e(t) \tag{3.7}$$

A high proportional gain K_p results in a large change in the output for a given input change. If the proportional gain is too high, the system can become unstable. In contrast, too small a gain can result in poor control effort with respect to the output changes. Pure proportional control, furthermore, will not settle to the setpoint value, but it will retain a steady-state error that depends on the proportional gain and the system (cavity) gain. It is the proportional term that usually contributes the bulk of the control effort. The control contribution from the integral term is proportional to both the magnitude and the duration of the error. Summing the instantaneous error corrects the accumulated offset that results from pure proportional gain. The integral gain K_i accelerates the process towards the setpoint and eliminates the steady-state error. However, a high integral gain can cause the present value to overshoot responding to accumulated errors from the past. The rate of change of the system output error is calculated by determining its slope over time. The derivative term's effect is most noticeable close to the controller setpoint, as the rate of change varies the most. Derivative control is used to reduce the magnitude of integral overshoot and improve closed-loop stability. Too much differential gain K_d, however, can result in amplification of noise and instability. The overall effect on a step-change in the output can be observed in figure 3.6 [13].

Feed-forward is the opposite of feedback, as you might suspect from its name. The

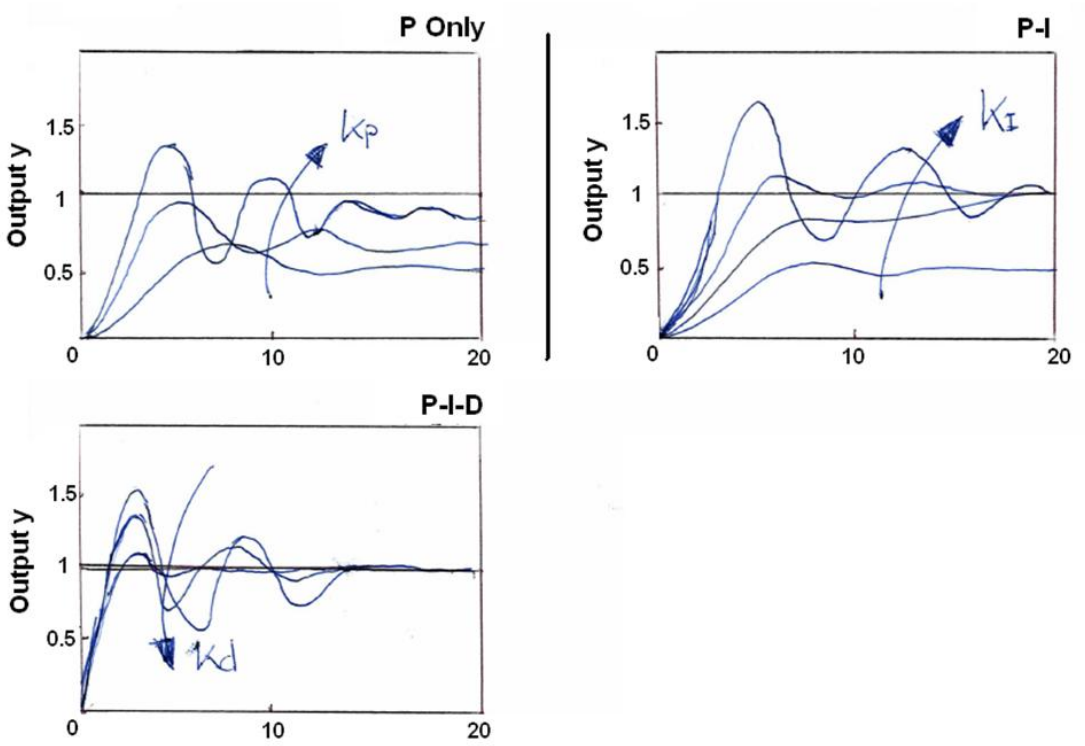

Figure 3.6: Effects of PID gain on output control performance [13]

idea is to prevent a foreseen error. To do this, the opposite effect is purposely fed to the system to counteract the known error at the time it arises. Combined feedback and feed-forward control can significantly improve performance over simple feedback architectures when there is a major disturbance to the system that can be measured beforehand [14].
To eliminate the effect of the measured disturbance, we need to choose Q_{ff} so that $P_d - PQ_{ff} = 0$, where P is the effect of the klystron and the cavity on the system. We can do this directly or by using an adaptive scheme.
On top of feedback and feed-forward applied to the Klystron modulator as control means, a piezo-electronic system is embedded onto the resonant cavities being developed specifically for use on the SPL. The idea is to be able to control the actual shape of the resonant cavities within certain boundaries, which will give the user a little big of wiggle room in terms of the cavity‘s resonant frequency, and can be a solution to the Lorentz deformation and its resulting detuning of the cavity. This can work as an adaptive feed-forward scheme by measuring the cavity‘s detuning during a beam pulse, and acting on the next beam pulse to counter-act the measured effect. The resulting (corrected) detuning will then be measured and added to the last control effort, resulting in an adaptive scheme that optimises the overall effect to a minimal detuning after a few beam pulses.
To measure the Lorentz detuning of a cavity containing high electric fields, we use information from the forward and cavity antenna voltages using a directional coupler and a cavity pickup respectively. The frequency deviation is then given by:

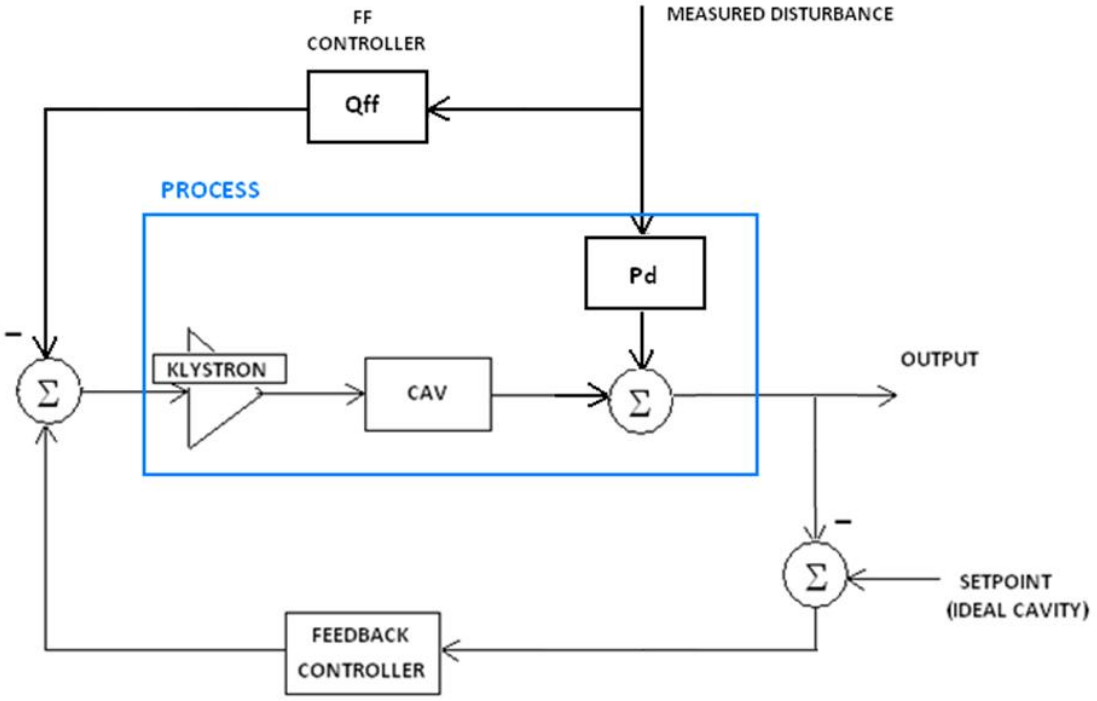

Figure 3.7: Feedback and feed-forward complementary control

$$\Delta\omega = \frac{d\phi_{\mathrm{ANT}}}{dt} - \omega_{1/2}\frac{V_{\mathrm{FWD}}}{V_{\mathrm{ANT}}}\sin(\phi_{\mathrm{FWD}} - \phi_{\mathrm{ANT}}) \tag{3.8}$$

The signal obtained in this way will then be recursively added to its last pulse measurement and filtered to avoid high frequency error accumulation. The overall piezo-system is shown in figure 3.8.

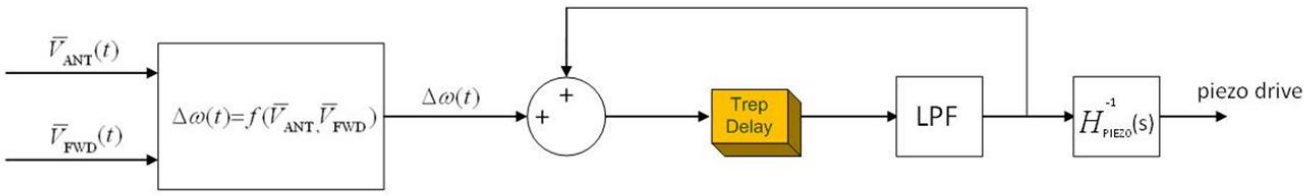

Figure 3.8: Diagram of piezo-electric tuner control

3.5 Kalman Filtering

When the need arises for adaptive feed-forward, it is interesting to develop a practically viable scheme to achieve the best possible efficiency and accuracy. The Kalman filter, in the presence of noisy measurements of a known system, is an ideal optimiser with respect to most criteria in advanced signal processing, and introduces almost no delay in the system as it implements a recursive algorithm. In the context of SPL resonant cavity control, it can be a possible means for measuring with optimal accuracy any critical signal within the system (e.g. cavity antenna voltage). The Kalman filter finds the best possible fit out of a noisy measurement of a known system. This means we can estimate with the minimum possible error the real output of a system from which we have a noisy measurement. The idea is to characterise the system using previous knowledge of its dynamics and compare an estimate given from that model to a real (noisy) measurement taken from the real process. Provided we have an appropriate model for the estimating part of the filter and the statistical description of the system and measurement noises, we can fit the best estimate of the real output using our model, the noise corrupted measurement, and, of course, some very clever mathematics. Now, it is possible to write whole books on the underlying processes of Kalman filtering and its applications, but we will concentrate on the applications that are relevant to our needs, namely adaptive feed-forward. The secret to Kalman filtering stems from the power of iteration; it is possible to asymptotically reach a best fit by perpetuating trials towards a given value, propagating the probability density function of the estimate, which narrows with each trial [15]. The Kalman filter works with systems that fulfill the following assumptions:

1. Noise is white Gaussian.

2. System is linear.

It might seem like an overly restrictive set of assumptions, but in signal processing, the fact is this is usually the case. Linear systems are common for many real applications, and when a nonlinear system is more appropriate, the standard approach is to linearize about a certain point of interest. White noise has equal power across its whole frequency spectrum, which makes it of infinite power. However, bandpass characteristic of all real systems will limit the noise power, and even when the noise is not equal for all spectra, we can use a shaping filter to "whiten" the noise, adding the shaping filter's characteristics to our system model within the Kalman filter. The Gaussian noise assumption can be defended using the central limit theorem. In many applications, measurement and process noise comes from a variety of sources, making their overall effect close to that of Gaussian noise. This means the mode, median and mean of the noise probability density function are all the same value and thus the Kalman algorithm optimises with respect to all three [16]. Consider a system governed by the linear stochastic differential equation

$$\dot{x}(t) = F(t)x(t) + B(t)u(t) + G(t)w(t) \tag{3.9}$$

from which we take a measurement at time t

$$z(t) = H(t)x(t) + v(t) \tag{3.10}$$

With:

$x(t)$ = system state vector (output).
$u(t)$ = control functions vector.
$w(t)$ = white Gaussian model noise vector with zero mean and variance Q.
$F(t)$ = continuous system dynamics matrix.
$B(t)$ = control input matrix (system dynamics).
$G(t)$ = noise input matrix, equal to 1 for our purposes.
$z(t)$ = measured output vector.
$H(t)$ = measured output matrix, equal to 1 for our purposes.
$v(t)$ = measurement noise vector with zero mean and variance R.

The Kalman filter, for our particular application, is defined a discrete-time optimal estimator. In order to characterise the hardware necessary to build the filter, it is necessary to investigate the discrete-time **difference equation** of the system. The solution for this differential equation at time t is given by:

$$x(t) = \Phi(t, t_0)x_0 + \int_{t_0}^{t} \Phi(t, \tau)B(\tau)u(t_0)d\tau + \int_{t_0}^{t} \Phi(t, \tau)G(\tau)d\beta(\tau) \tag{3.11}$$

With:

$x(t_0) = x_0$.
$\beta(\tau)$ = Brownian motion process [17].
$d\beta(\tau) = w(\tau)d\tau$.
$\Phi(t, t_0)$ = state forward transition matrix.

$\Phi(t, t_0)$ satisfies the differential equation,

$$\begin{aligned} &\frac{d\big(\Phi(t, t_0)\big)}{dt} = F(t)\Phi(t, t_0) \\ &\Phi(t_0, t_0) = I \end{aligned} \tag{3.12}$$

For a certain sampling time Δt, we can rewrite the process and measurement equations as:

$$\begin{aligned} x(t_{k+1}) &= \Phi(\Delta t)x(t_k) + B_d(t_k)u(t_k) + w_d(t_k) \\ z(t_{k+1}) &= H(t_{k+1})x(t_{k+1}) + v_d(t_{k+1}) \end{aligned} \tag{3.13}$$

With:

$B_d(t_i) = \int_{t_i}^{t_{i+1}} \Phi(t_{i+1}, \tau) B(\tau) d\tau$ is the discrete control input matrix.
$w_d(t_i)$ = discrete process noise vector, with mean and variance given by:

$E\{w_d(t_i)\} = 0$
$E\{w_d(t_i) w_d(t_i)^T\} = Q_d(t_i) = \int_{t_i}^{t_{i+1}} \Phi(t_{i+1}, \tau) G(\tau) Q G^T(\tau) \Phi^T(t_{i+1}, \tau) d\tau$

$v_d(t_i)$ = discrete measurement noise vector, with mean and variance given by:

$E\{v_d(t_i)\} = 0$
$E\{v_d(t_i) v_d(t_i)^T\} = R_d(t_i)$

In practice, Q and R are the tuning parameters of the Kalman filter and are often set experimentally by trial and error.
The expressions for the forward transition, control input, and noise matrices can be further simplified using the following expressions:

$\Phi(t_{i+1}, t_i) \simeq I + F(t_i)(t_{i+1} - t_i)$
$B_d(t_i) \simeq B(t_i) dt$

This analysis tells us that all that is necessary to model a system for Kalman filtering applications is:

- A linear system corrupted with white Gaussian noise or the best approximation.
- A differential equation relating the measurable variable or state of interest to its derivative.
- Knowledge of the initial conditions of the system.

Now we can concentrate on the Kalman filtering part of Kalman filtering. For the scope of this project, it is unnecessary, as mentioned previously, to look into the exhaustive proof of the Kalman algorithm. For a more complete explanation of the Kalman filter, refer to [16] [17].
The process of estimation of a particular state can be separated into two steps; the time update and the measurement update [18]. During the time update stage, a "prediction" of the next value is calculated using our knowledge of the system and the previous outputs. The information of the last outputs propagates through an error covariance matrix that contains information about the innovation or amount of new (unpredicted) data of each new value. In other words, error equals innovation.

$$\begin{aligned} E\{x_k\} &= \hat{x}_k \\ E\{x_k - \hat{x}_k\} &= P_k \end{aligned} \tag{3.14}$$

P_k is the expected value of the innovation; it contains information about how far from the real value the prediction $\hat{x}_k$ is at time/sample k.

The measurement update stage incorporates the information given by the noisy measurement of the system of interest, weighting it more or less heavily depending on its accuracy. In order to do this, a matrix known as the "Kalman Gain" becomes a part of the algorithm. The Kalman gain (K) is the main feature of the filter; it decides what factor of information to take from the real measurements as opposed to the model prediction. Once the Kalman gain is calculated, the new (measured) value is incorporated to the prediction to create an estimate of the actual output. Finally, a new (a posteriori) error covariance matrix is calculated from the old (a priori) matrix. Just to be clear, a priori and a posterior refer to before and after receiving information from the actual (noisy) measurement.

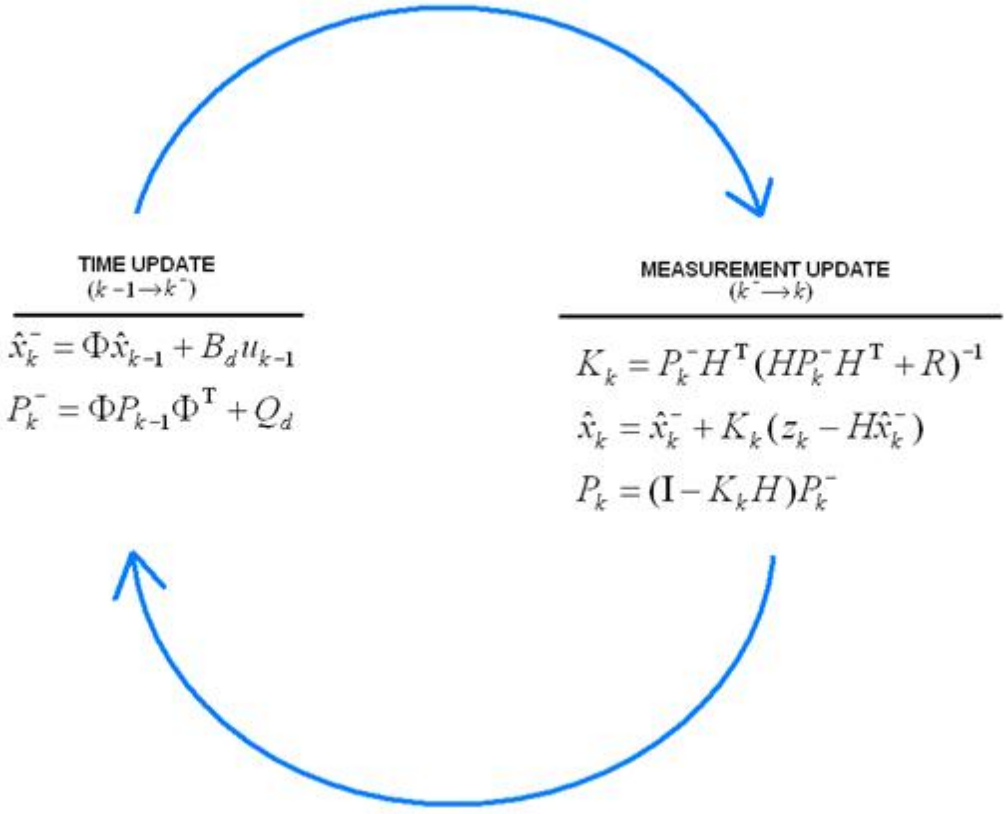

Figure 3.9: Kalman filtering operation [18]

For the SPL case, we want to measure the frequency detuning of the resonant cavity due to Lorentz force effects, using a noisy measurement of the time-varying cavity voltage. To do this, we measure and model the cavity voltage using a vector state-space with the in-phase and quadrature components of the voltage and their respective differential equations. If we recall the cavity voltage I/Q relationship to the generator current pulse:

$$\begin{bmatrix} \dot{V_{re}}(t) \\ V_{im}(t) \end{bmatrix} = \begin{bmatrix} \frac{-\omega_0}{2Q_L} & -\omega(t) \\ \omega(t) & \frac{-\omega_0}{2Q_L} \end{bmatrix} \begin{bmatrix} V_{re}(t) \\ V_{im}(t) \end{bmatrix} \begin{bmatrix} \frac{-\omega_0}{2}\frac{R}{Q} & 0 \\ 0 & \frac{-\omega_0}{2}\frac{R}{Q} \end{bmatrix} \begin{bmatrix} I_{re}(t) \\ I_{im}(t) \end{bmatrix} \tag{3.15}$$

If we recall the state transition equation, we can distinguish clearly the Kalman filter parameters:

$$\begin{aligned} x(t) &= \begin{bmatrix} V_{re}(t) \\ V_{im}(t) \end{bmatrix} \\ u(t) &= \begin{bmatrix} I_{re}(t) \\ I_{im}(t) \end{bmatrix} \\ F(t) &= \begin{bmatrix} \frac{-\omega_0}{2Q_L} & -\omega(t) \\ \omega(t) & \frac{-\omega_0}{2Q_L} \end{bmatrix} \\ B &= \begin{bmatrix} \frac{-\omega_0}{2}\frac{R}{Q} & 0 \\ 0 & \frac{-\omega_0}{2}\frac{R}{Q} \end{bmatrix} \end{aligned} \tag{3.16}$$

The tuning parameters of the filter will be the process and measurement noise variances; this means that if the process noise adequately follows our models shortcomings, and the filter measurement noise is close to the actual noise, the output of the filter will closely follow the real signal even in very poor SNR conditions. Refer to section 4.4 for detailed schematics of the filter implementation.

Chapter 4

SIMULINK I-Q Model for SPL RF Components

Developing a project of great magnitude such as a high-power linear accelerator is a staggering task and demands careful consideration of all elements involved, such as power budget, technology requirements and space and time necessary. In order to foresee difficulties and answer some of the many questions that arise from these considerations, it is useful to develop a virtual model of what we hope to achieve. This section describes the design of a model that hopes to achieve flexibility of design as well as accuracy of results and strives to follow reality as closely and as reliably as possible. The SPL model described in this section (see overleaf) consists of a Generator (Klystron) coupled via a circulator and transmission line to 1, 2 or more resonant cavities, taking into account the effects of beam loading and Lorentz force detuning. The output is controlled by means of PID feedback and complementary feed-forward. The model also includes a versatile GUI (graphical user interface) which will be described further within this chapter. With this layout, it is possible to observe many characteristics of the RF system. The outputs, in addition to the cavity voltage amplitude and phase, include forward and reflected power (to and from cavity) with and without feedback and the additional power due to the feedback loop, all displayed as a function of time. These results can be observed in open and closed loop operation for varying component values, in the presence or absence of Lorentz detuning and source current fluctuation, and for different beam speeds at low and high energy sections of the SPL. A phasor diagram of beam, cavity, forward and reflected powers is also available. In addition, for the multiple-cavity cases, the individual cavity waveforms are displayed, with the option of Lorentz detuning correction using dedicated piezo-electric tuners. All calculations are done in baseband using Inphase and Quadrature components of complex signals. A band limited signal centered at a carrier frequency ω_0 can be represented using slow-varying components in-phase $I(t)$, named as such because they are 0° or cosine components and in-quadrature $Q(t)$, which are the 90° or sine components of the signal [19].
In this section the modelling of each block is explained.

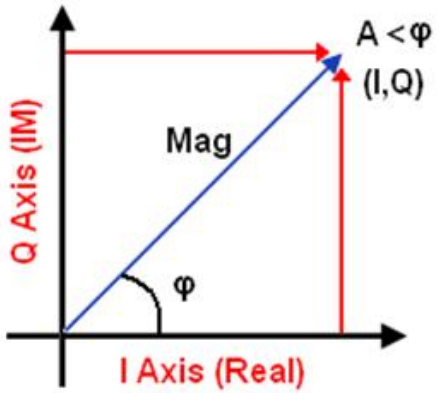

$$x(t) = A(t)\cos(2\pi\omega_o t + \varphi(t)) = I(t)\cos(2\pi\omega_o t) - Q(t)\sin(2\pi\omega_o t)$$
$$Q(t) = A(t)\cos(\varphi(t))$$
$$I(t) = A(t)\sin(\varphi(t))$$

Figure 4.1: I/Q equivalence [19]

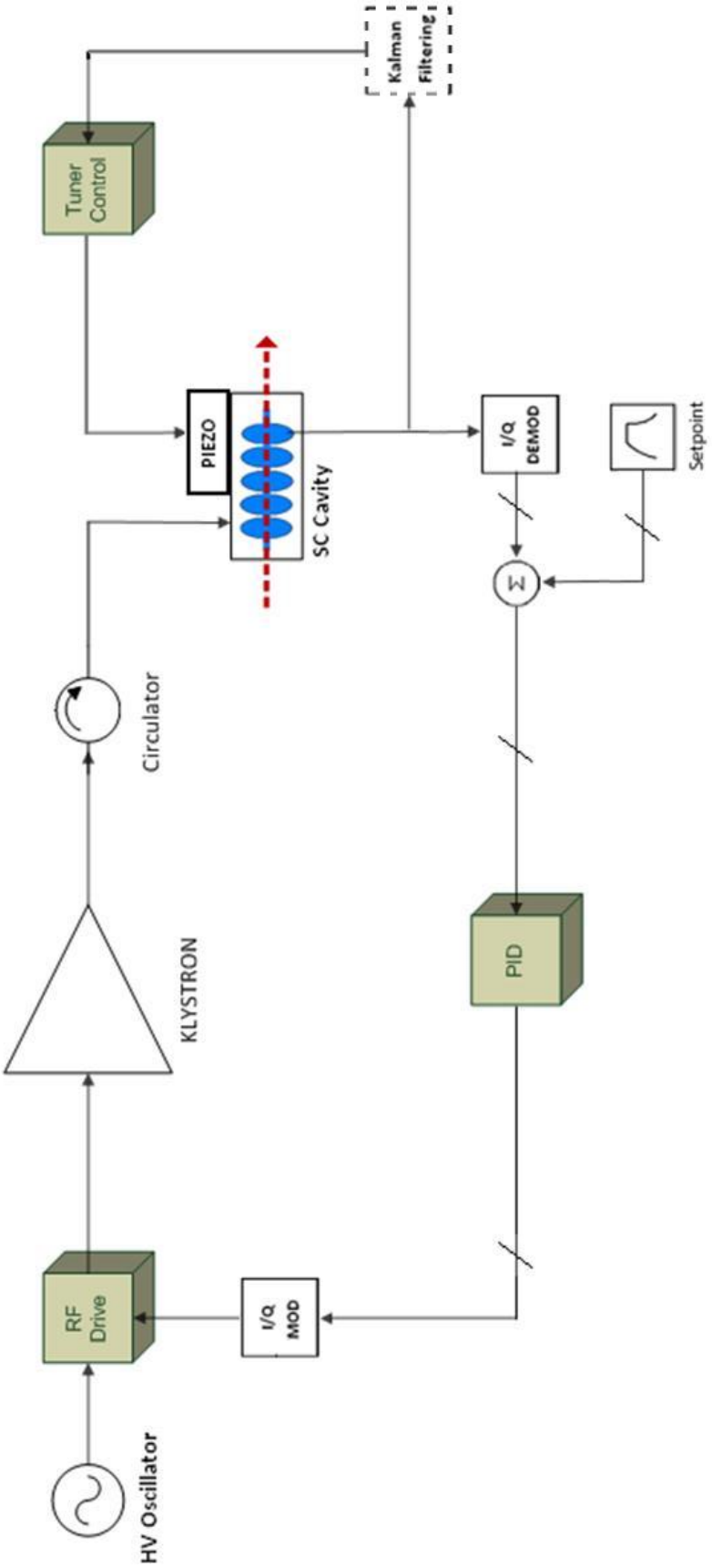

Figure 4.2: SPL 1 cavity control high level diagram

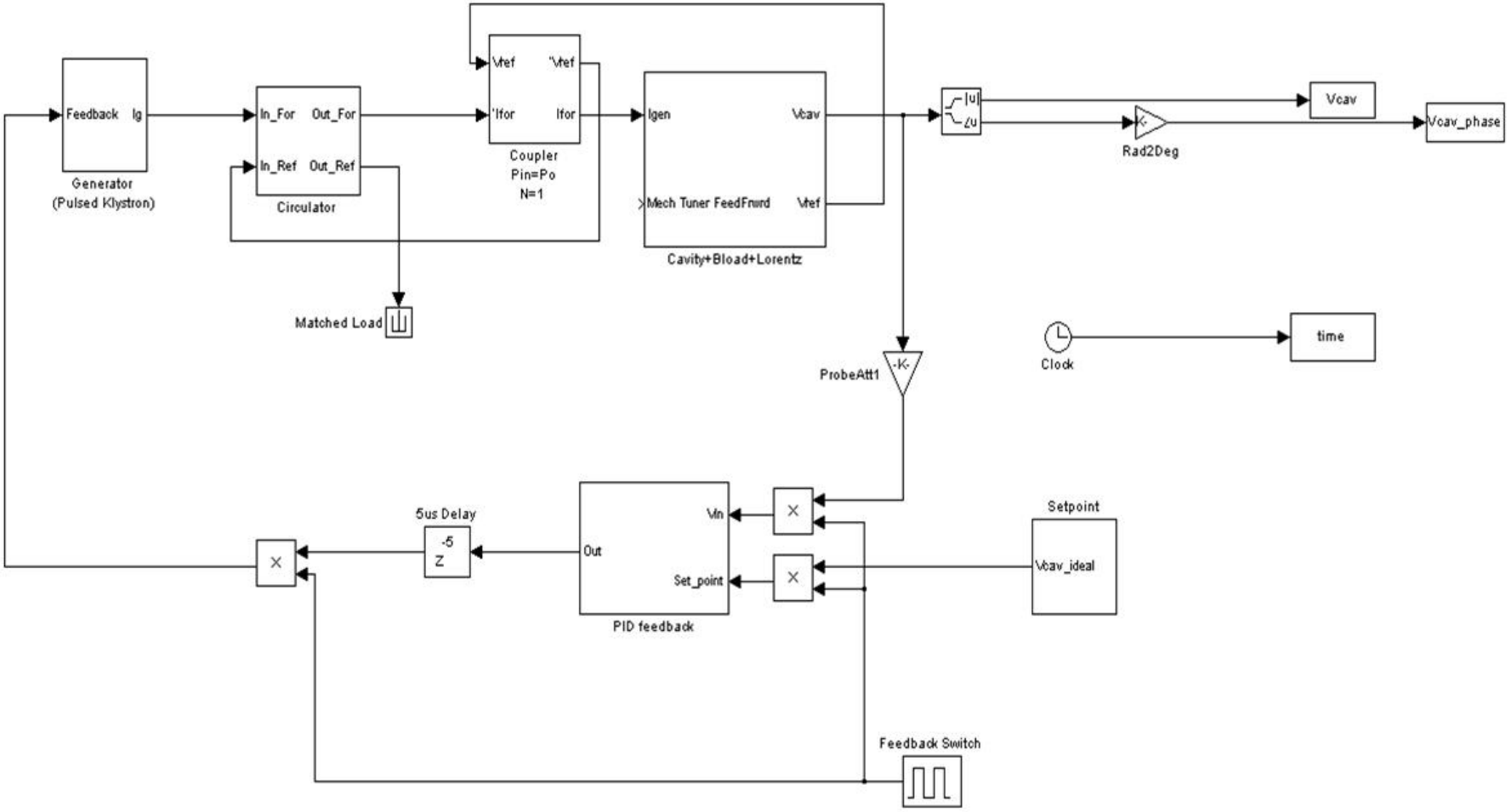

Figure 4.3: SPL single-cavity control SIMULINK model overview

4.1 Generator, Generator-Cavity Coupling

The generator is modelled as a square wave current source that emits a current pulse that lasts until cavity filling and beam loading have occurred, the frequency response of the Klystron is modelled as a low pass filter with 1 MHz bandwidth (as we are using I-Q components we work in baseband); this bandwidth is considered high compared to the rest of the system so stability will not be affected by the Klystron bandwidth. The generator angle is set to zero and this is used as the reference angle for the cavity and beam phases. We can also observe the feedback I-Q components adding to the input, all tags (goto) are used to display results. The coupling from the generator to the cavity is set to 1:1 ratio with no circulator loss for present calculations. The diagram for the generator is shown in figures 4.6 and 4.7.

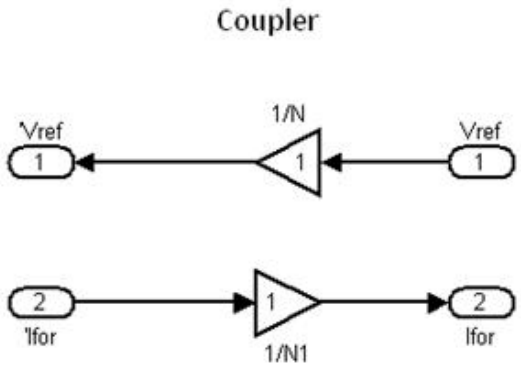

Figure 4.4: Coupler SIMULINK model (1/N)

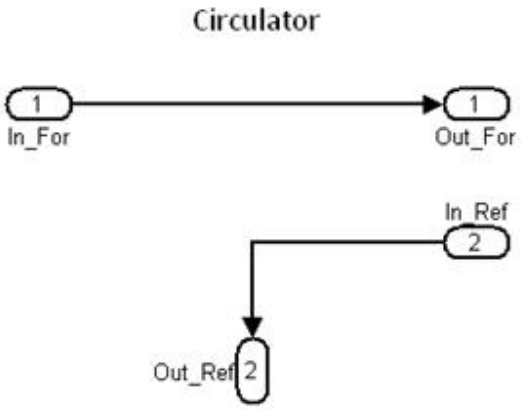

Figure 4.5: Circulator SIMULINK model

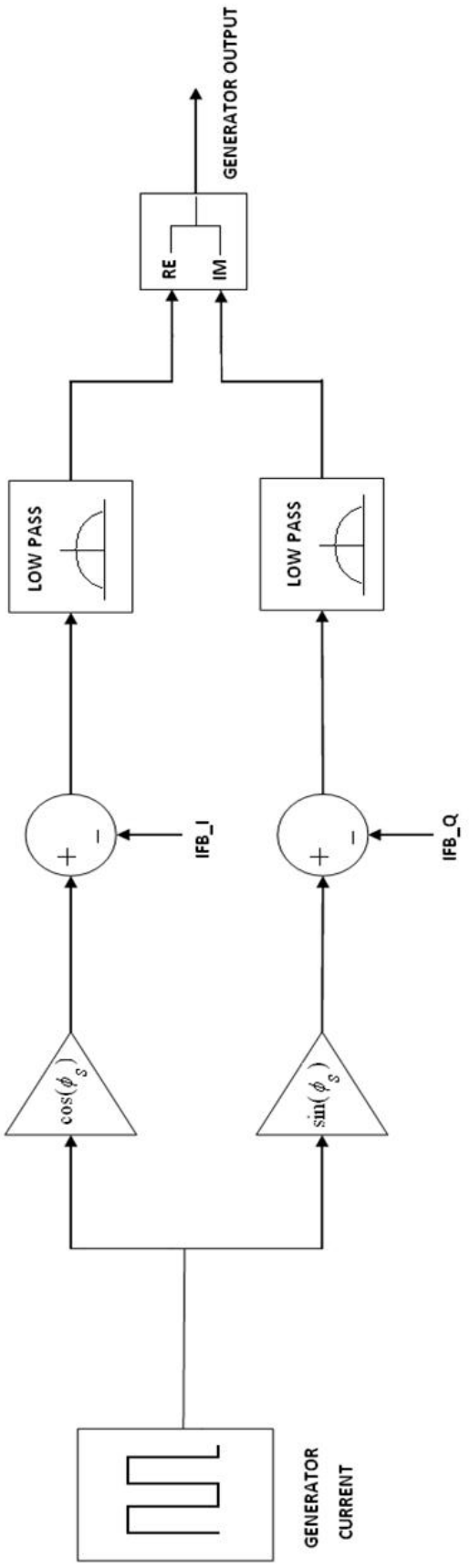

Figure 4.6: RF generator high level diagram

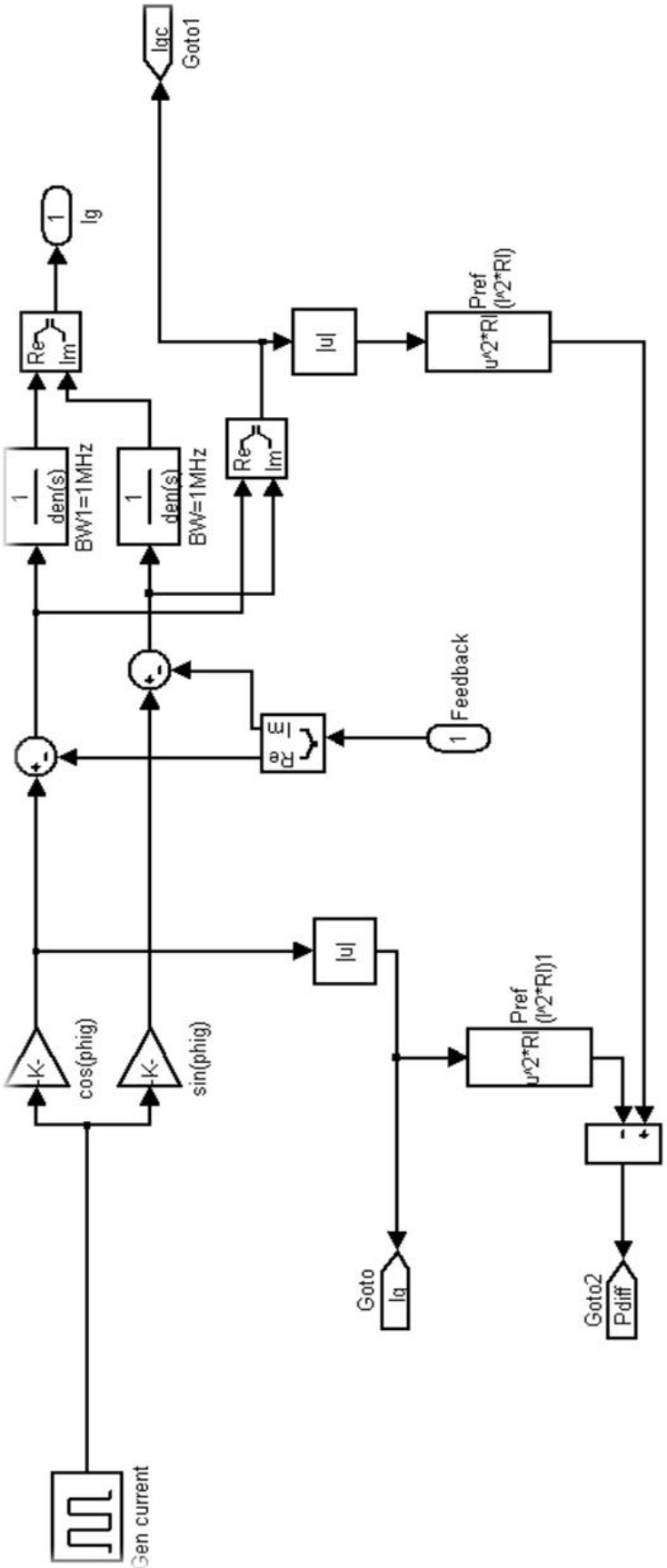

Figure 4.7: RF generator SIMULINK model

4.2 Resonant Cavity Model

The resonant cavity is the most important and complex part of the entire model. It contains physical and mathematical descriptions on cavity performance as well as beam loading effects and Lorentz force detuning due to physical deformation at high voltages. In I-Q description, the cavity output behaves like coupled first order differential equations driven by the generator current I-Q components.

$$\begin{aligned} R_L(2I_g + I_b)_{inphase} &= \tau\frac{dV_{inphase}}{dt} + V_{inphase} - yV_{quad} \\ R_L(2I_g + I_b)_{quad} &= \tau\frac{dV_{quad}}{dt} + V_{quad} + yV_{inphase} \end{aligned} \tag{4.1}$$

Where $y = -\tan\Psi = 2Q_L\frac{\Delta\omega}{\omega_0}$ is the detuning caused by a frequency mismatch, and $\tau = \frac{2Q_L}{\omega_0}$ is the cavity filling time. Beam loading can be viewed as a train of instantaneous voltage drops in the cavity voltage corresponding to infinitely narrow bunches passing every 2.8 nanoseconds. The voltage drop due to each bunch is given by [11] [7]:

$$V_{cav\_bunch} = \omega_{RF} \times \frac{R}{Q}(\text{circuit}) \times q_b \tag{4.2}$$

Where the synchronous angle ϕ_s is given by its LINAC definition, which means the beam loading occurs with a phase shift of ϕ_s degrees before the positive maximum value of the RF field in the cavity. The injection-time parameter is chosen at a point in the cavity filling time such that the negative gradient induced by the beam on the cavity voltage is equal to the positive gradient induced by the generator, and so we observe flat-top operation during the beam pulse. After the beam has been accelerated, the generator is switched off until the next period of operation.

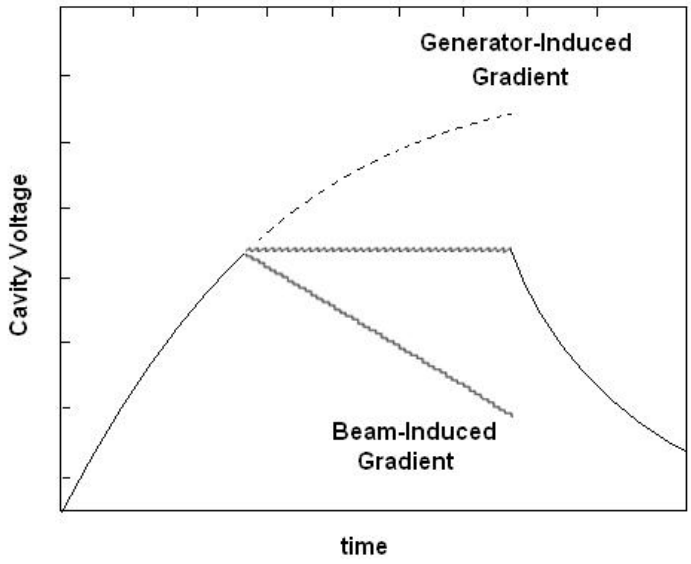

Figure 4.8: Beam and generator-induced voltage gradients in cavity

In I/Q representation, however, the current is modelled simply as a DC driving term to the cavity differential equations. In this way, we are able to observe the envelope of the full effect. For a complete description of the beam effects it is therefore best to investigate the characteristics of the cavity voltage signal and the phasor diagram of the generator-beam-cavity interaction available from the simulation results. The model also includes the effects of variations in the DC current of the beam source during beamloading. Lorentz force effects are added to the tuning angle of the system as an extra shift in the cavity resonant frequency with respect to the generator centre frequency. Lorentz detuning is modelled, as of now, as a 1^{st} order differential equation driven by the square of the accelerating field [4].

$$\frac{d\Delta\omega(t)}{dt} = \frac{1}{\tau}\big(- \Delta\omega(t) + \Delta\omega_T + 2\pi K E_{acc}^2\big) \tag{4.3}$$

Where K is known as the Lorentz detuning factor and relates the frequency shift to the square of the electric field inside the cavity, its units being $\mathrm{Hz/(MV/m)^2}$.

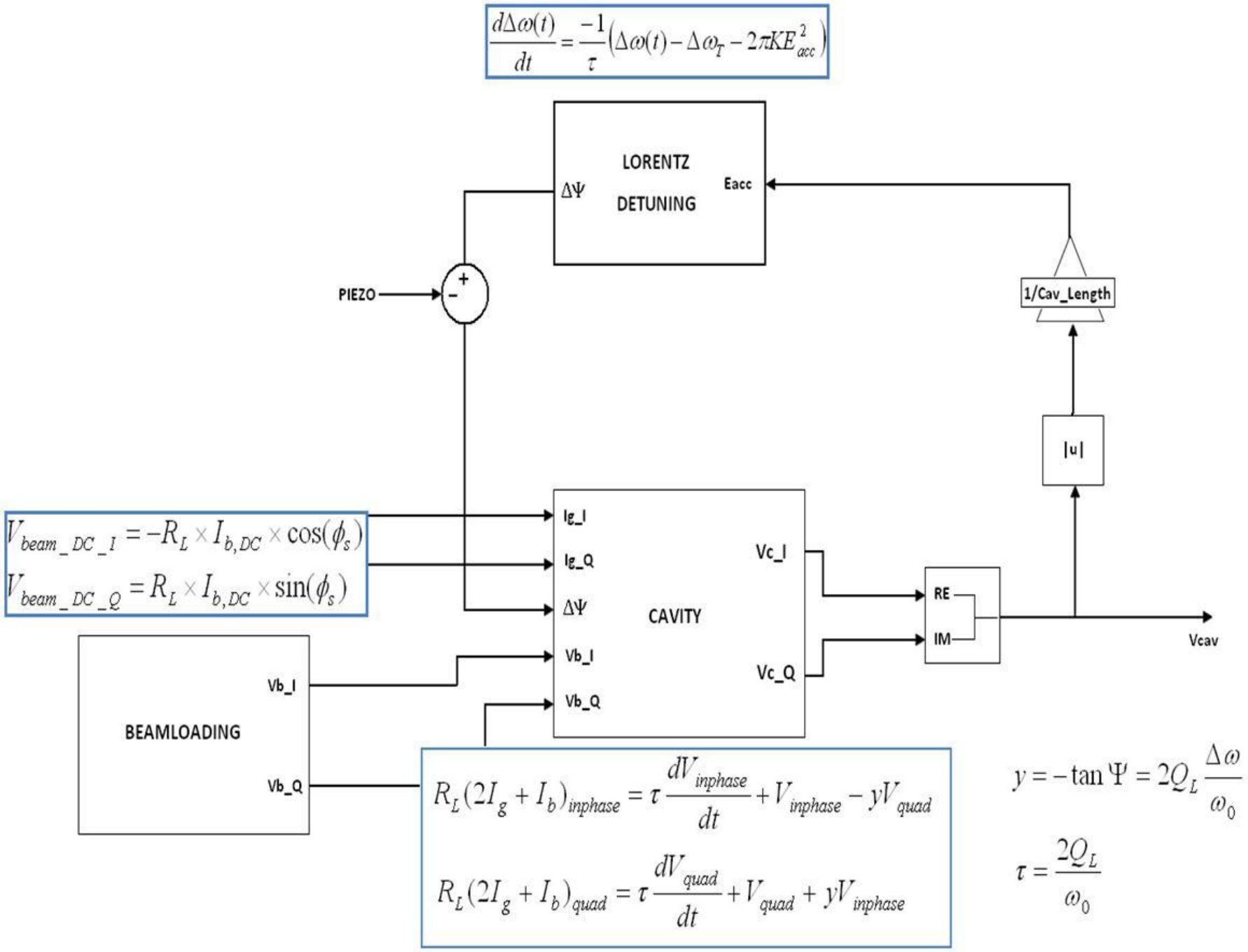

Figure 4.9: Cavity high level diagram with beam loading and Lorentz detuning

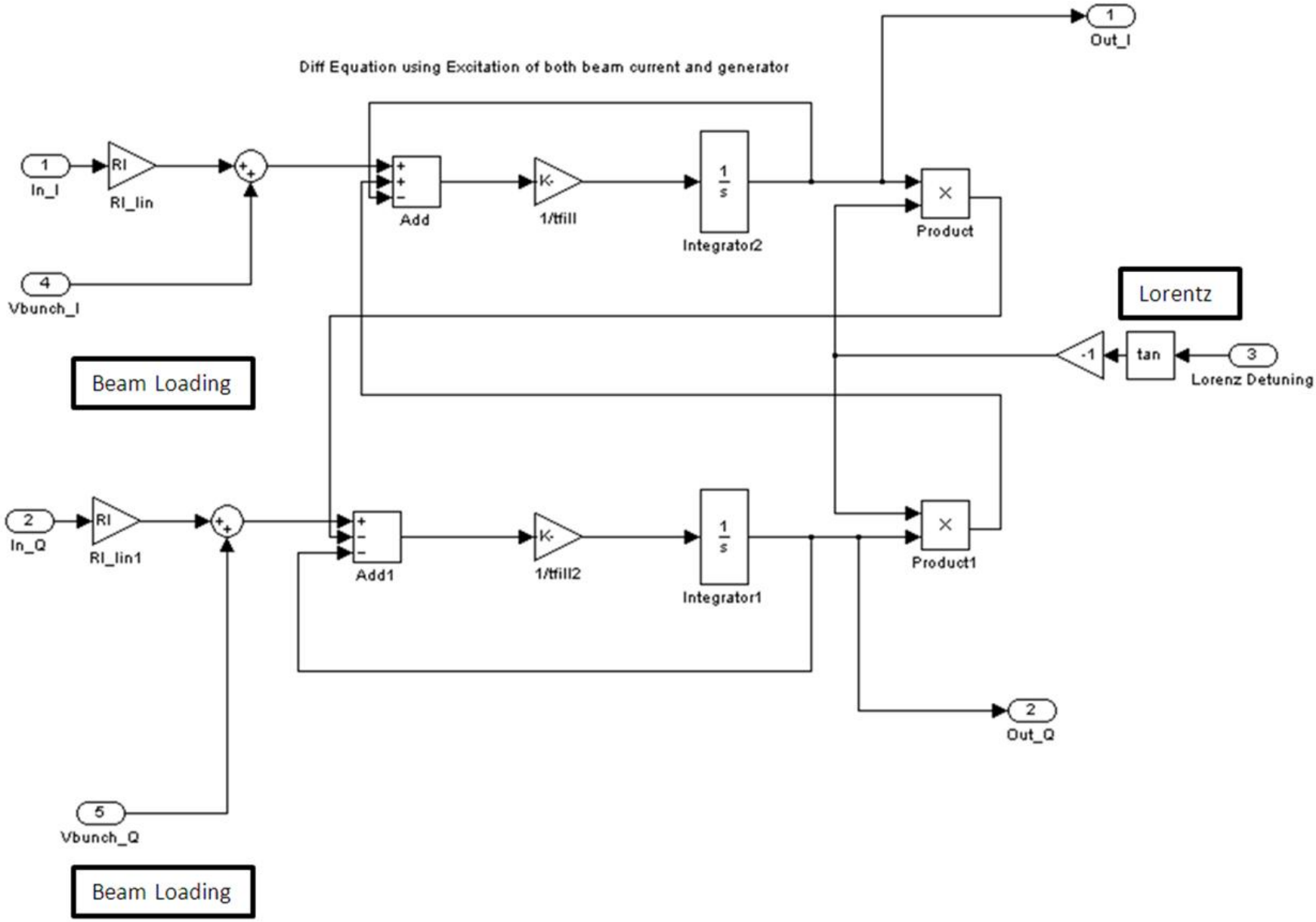

Figure 4.10: Cavity SIMULINK model with beam loading and Lorentz detuning

4.3 RF Feedback Loop

The goal of the model for both singular and multiple-cavity cases is to maintain the cavity voltage during beam loading within certain amplitude and phase values. As the output is affected by Lorentz detuning and synchronous angle mismatches as well as microphonics effects and external conditions, a feedback loop is necessary to maintain the output of our system within the specified parameters. In order to achieve this, a PID feedback model was used. The proportional gain was set using stability considerations, taking into account a feedback loop with a 5 microsecond delay and a bandwidth of 100 kHz. The integral and differential gains were found by trial and error to produce stable results shown in section 5. The integral gain was added to suppress any DC offset introduced between the setpoint and the output by the proportional gain and the differential gain results in a smoother operation (less oscillation). The SIMULINK model schematic for this block is shown in figure 4.12.

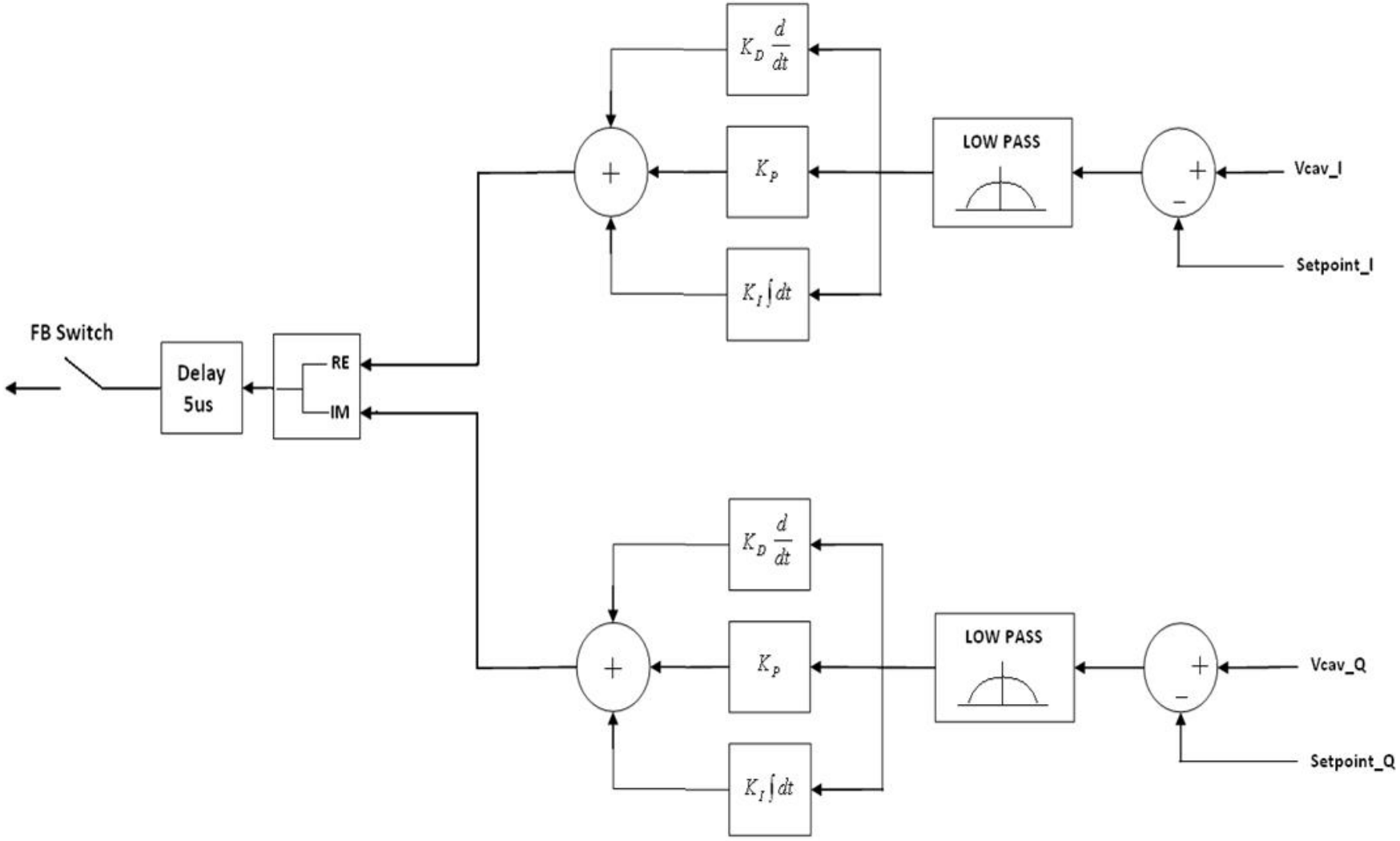

Figure 4.11: PID feedback loop high-level diagram

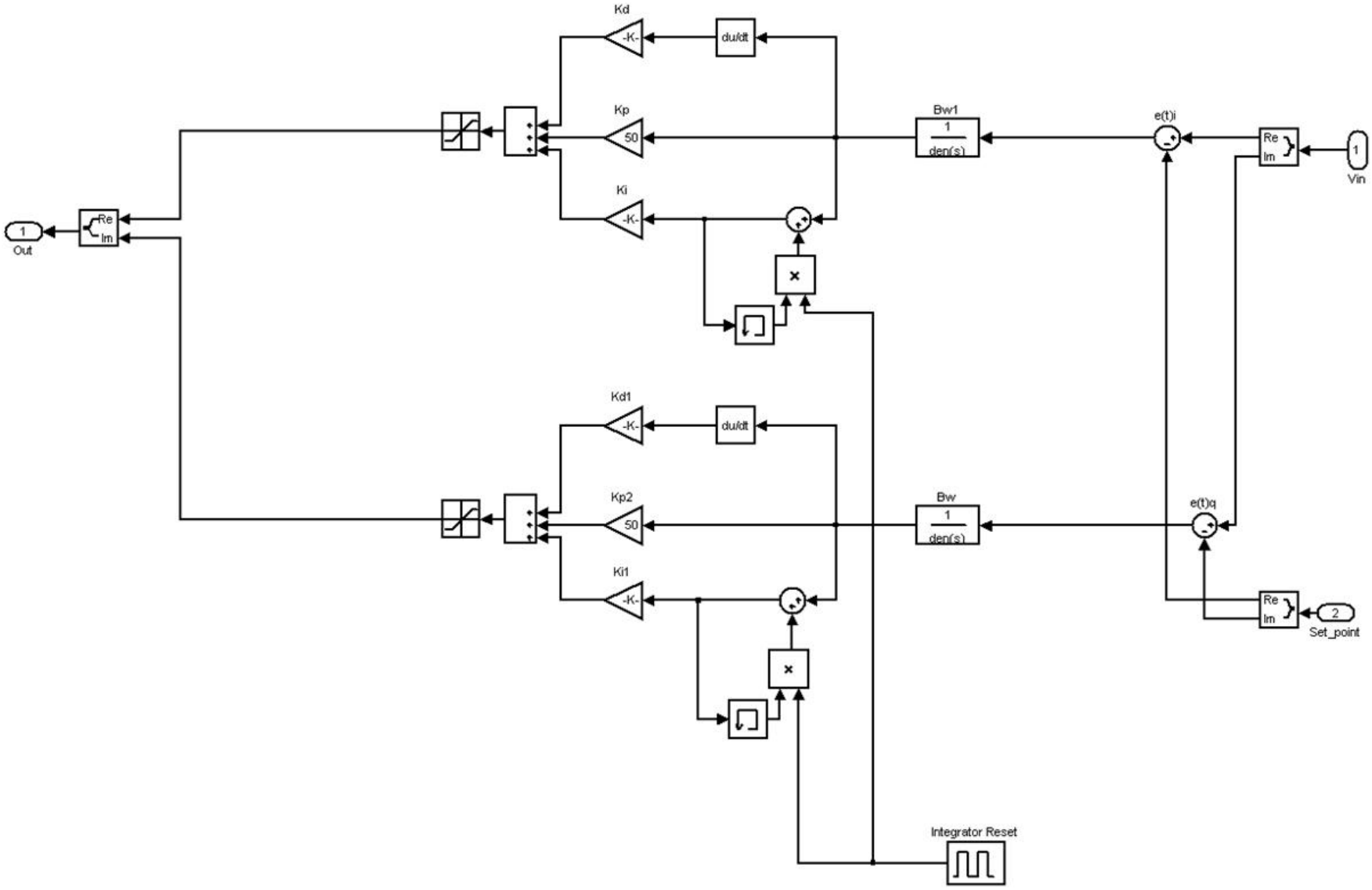

Figure 4.12: PID feedback SIMULINK model

4.4 Dual Cavity Model

Figures 4.14 and 4.15 show the layout for the two-cavity case. Both cavities are identically modelled but some of their values can vary slightly to observe the effects of a slight mismatch between the cavities in the actual SPL design. The real addition in this model is the feed-forward scheme using the piezo tuners and the possibility of Kalman filtering to optimize accuracy. Figures 4.16 and 4.17 show the Kalman filter model and its operation. Figures 4.18 and 4.19 are diagrams that explain the operation of the piezo tuner control. The feedback loop works on the vector average of the outputs from the individual cavities (figure 4.13).

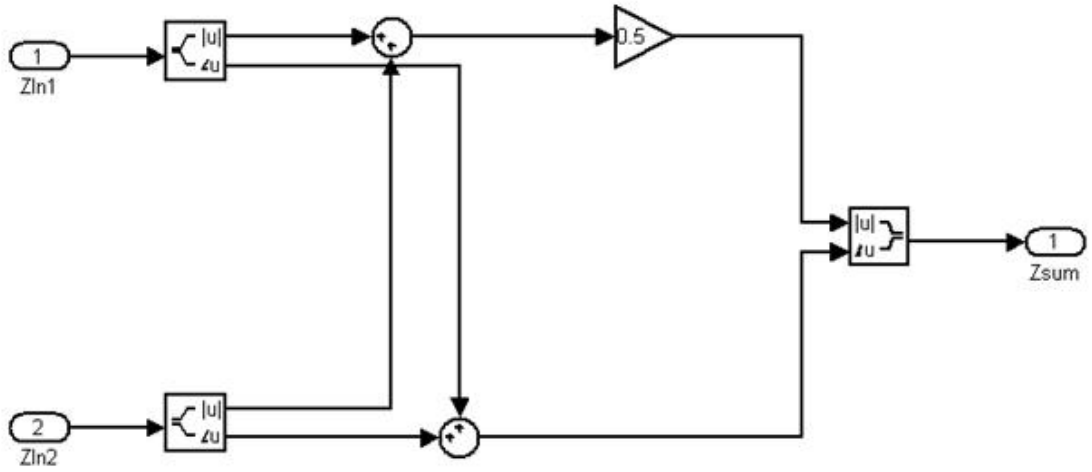

Figure 4.13: Vector average block

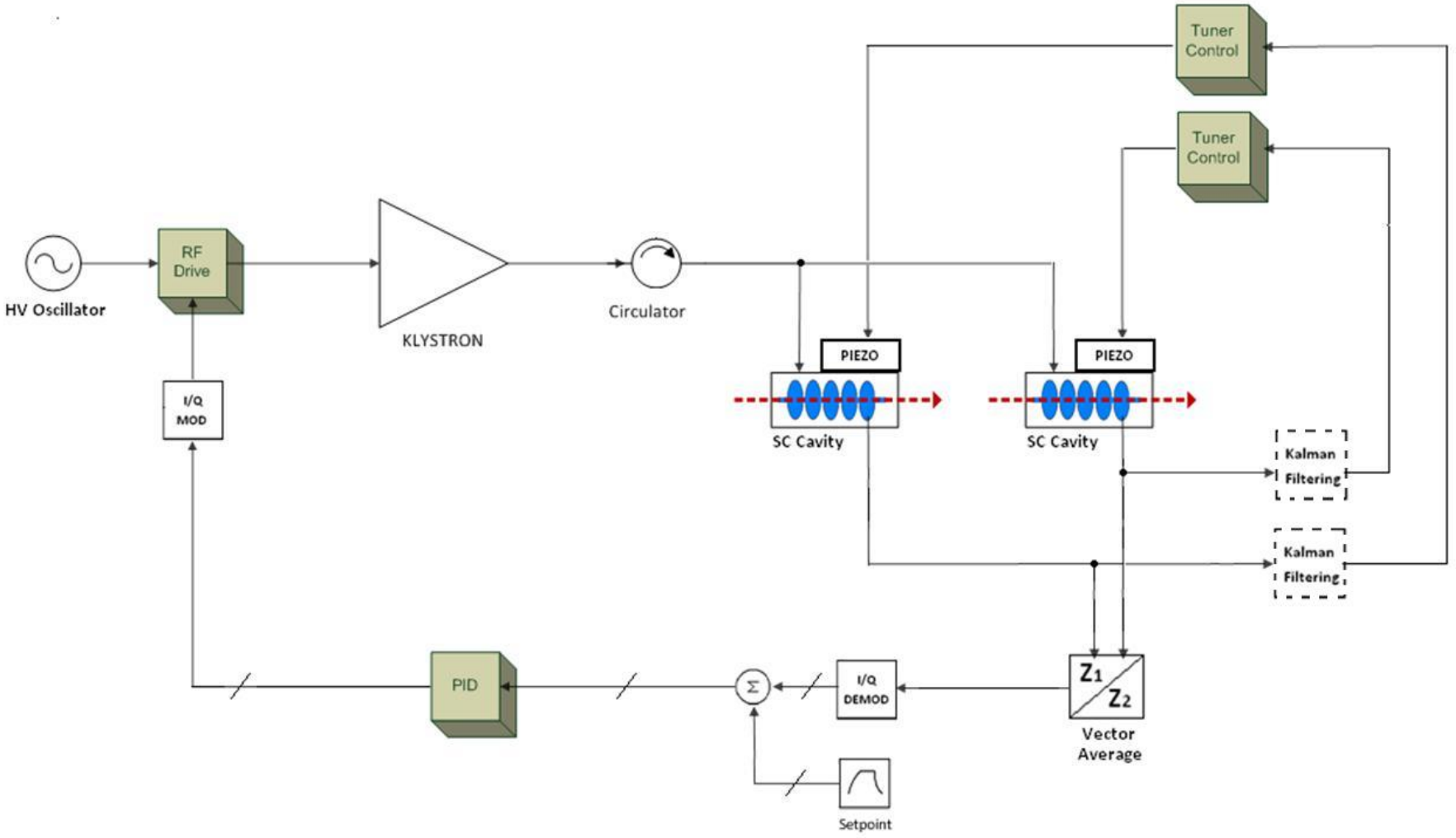

Figure 4.14: PID feedback loop high-level diagram

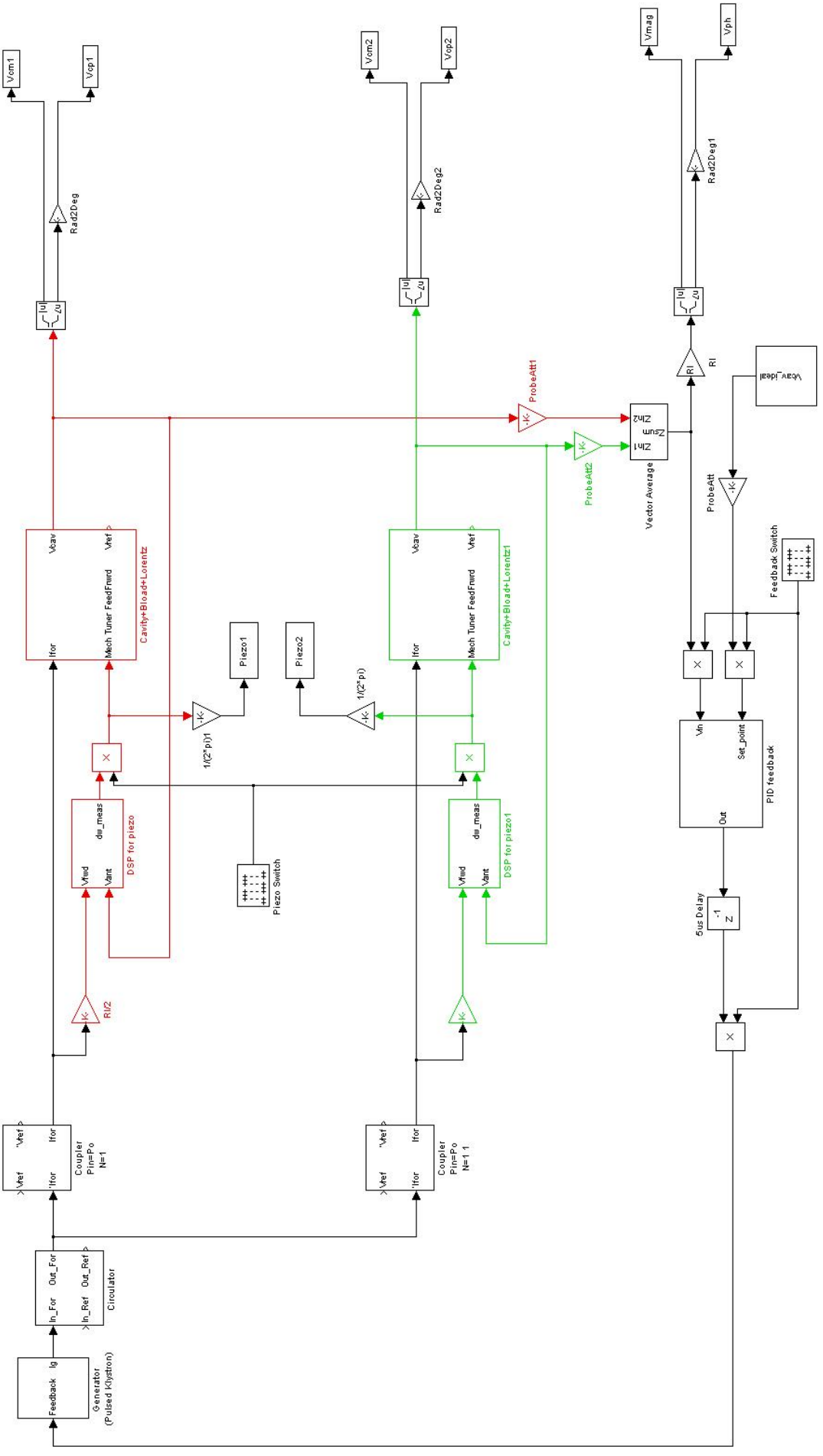

Figure 4.15: PID feedback SIMULINK model

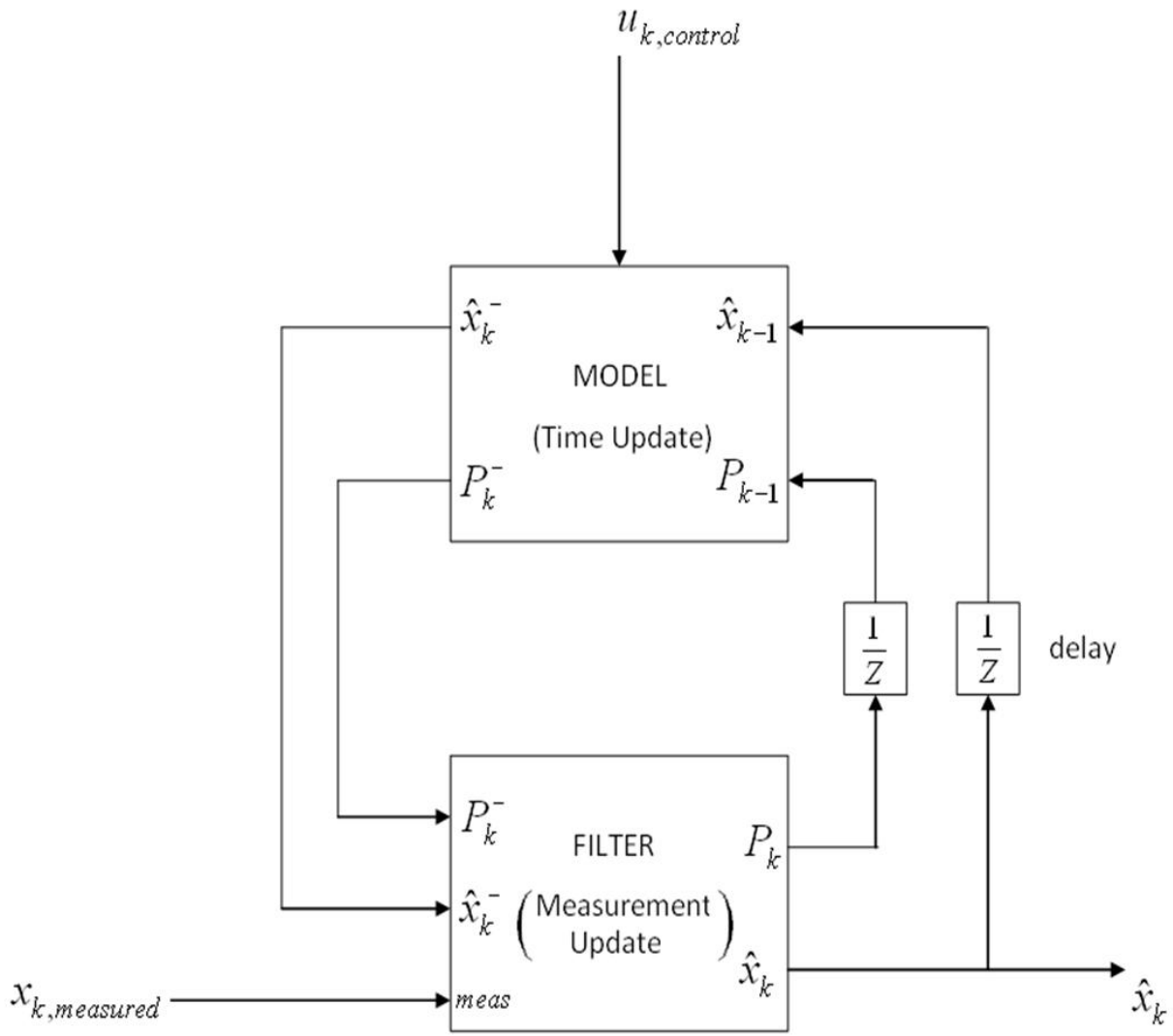

Figure 4.16: Kalman filter high-level diagram

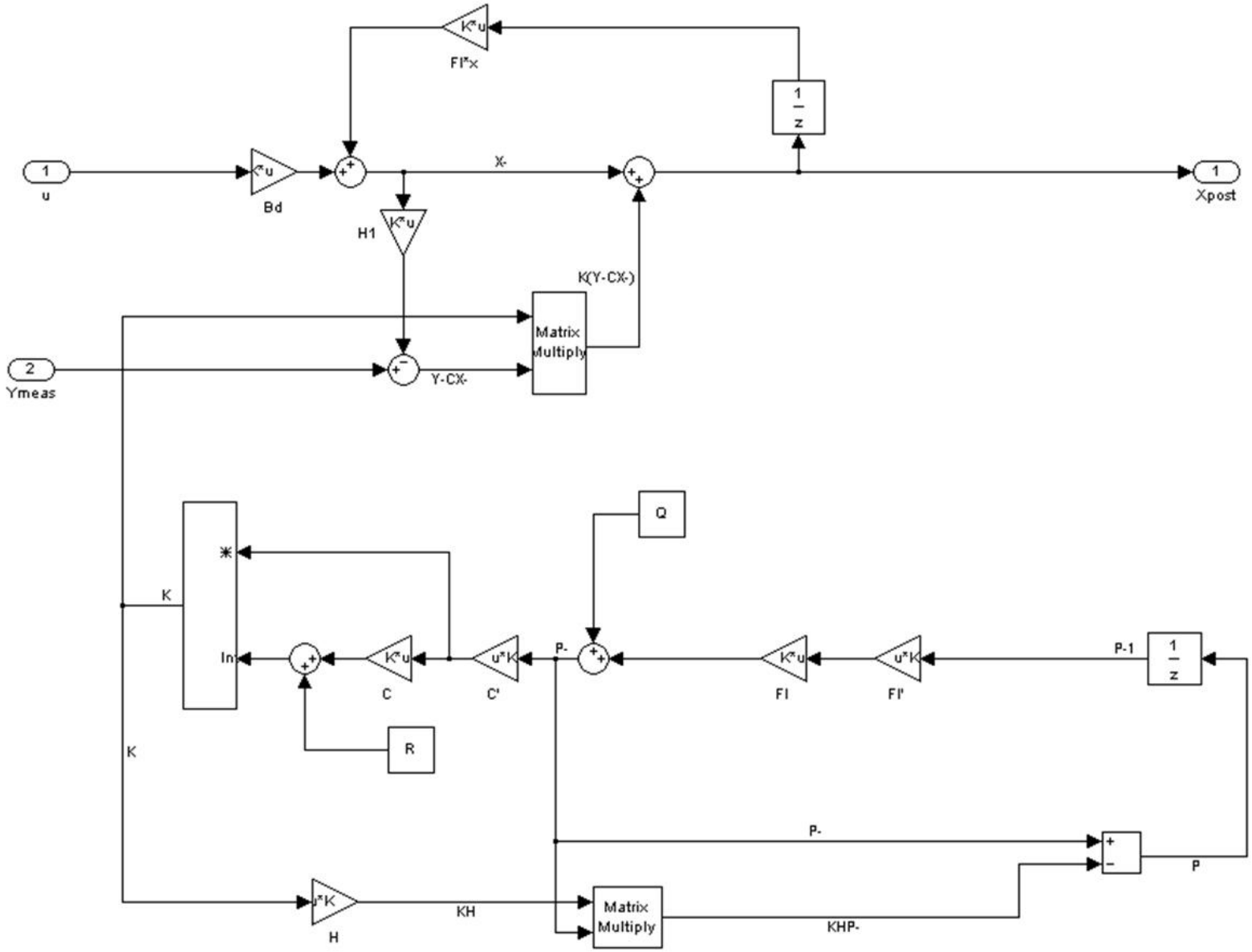

Figure 4.17: Kalman filter SIMULINK model

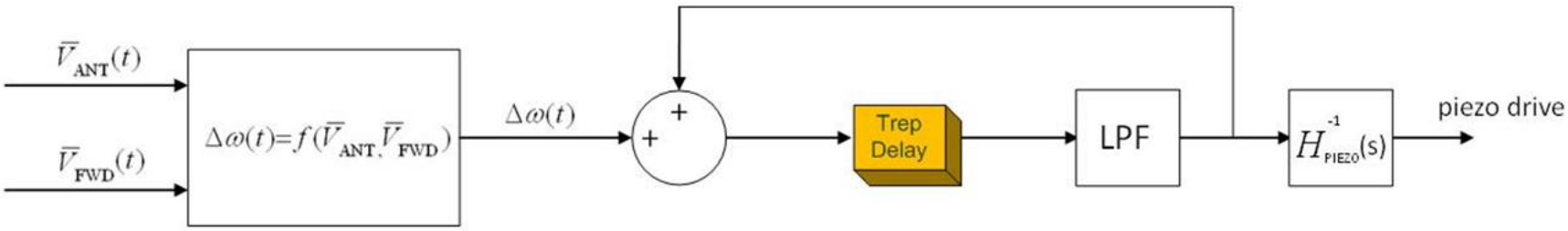

Figure 4.18: High-level diagram of piezo-electric tuner control

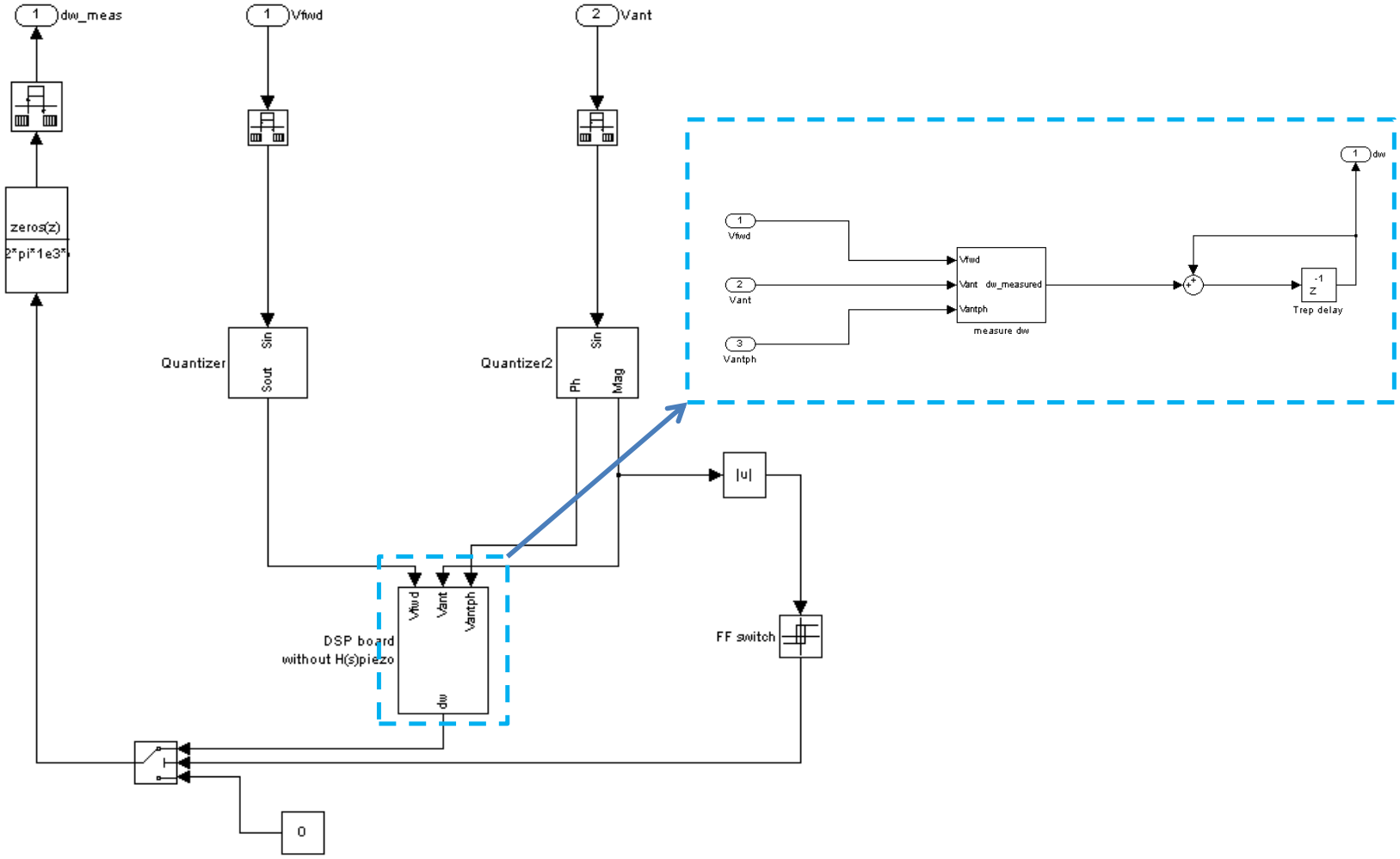

Figure 4.19: SIMULINK diagram of piezo-electric tuner control

4.5 Graphical User Interface (GUI)

In order to be able to display results quickly and conveniently, add versatility to the model and shield the user from the low-level design of the project, a GUI has been designed, striving to be a user-friendly tool for the interpretation of data derived from the model. The GUI, at its present state, can analyze the behaviour of single, double and quad-cavity operation with control loops in many different scenarios, depending on user inputs and display choices. A .exe file was also created in MATLAB for portability. It is, thus, not necessary to have MATLAB installed in the machine to operate the GUI. The GUI is displayed in figures 4.20, 4.21 and 4.22; following is an explanation of its main features:

- **Start Simulation:** the button group labelled as such allows choosing between single, double and quad-cavity operation in closed-loop and open-loop, as well as possible feed-forward in all cases. Piezo feed-forward refers to Lorentz force effects correction using a piezo-electric tuner, while $\beta_0 \neq \beta_x$ refers to suboptimal beam speed beamloading. Simulation begins when the Simulate button is activated.

- **Operating Parameters:** within this box, the user can specify cavity, generator and beam parameters to match their application. The loaded quality factor can be specified as fixed or left blank, in which case the program will calculate the optimum for simulation. The Simulate button in the Start Simulation button group will not be enabled until numerical inputs for these values are added. Inputs that are not critical are set to zero without user input.

- **Progress Bar:** As it is impossible to maintain processing speed and output data from SIMULINK while a simulation is running, the progress bar does not show the time left for the simulation to finish, but notifies the user when it has, and shows the time elapsed during the last simulation.

- **Axis Control**: Both axes in the GUI behave in exactly the same way. There are two for the purpose of visually comparing graphs and result displays. Using the pop-up menu on the right, the user can choose to display different results for interpretation. These include cavity voltage amplitude and phase, forward and reflected power, power consumed by feedback loop, frequency shift with Lorentz detuning, piezo tuner outputs, and a phasor diagram of the effects of beam loading with synchronous angle ϕ_s. Most graphs can also be zoomed to view critical areas in more detail. In addition, the plot to figure button can be chosen to plot outside the GUI, for saving or manipulating the graphs further.

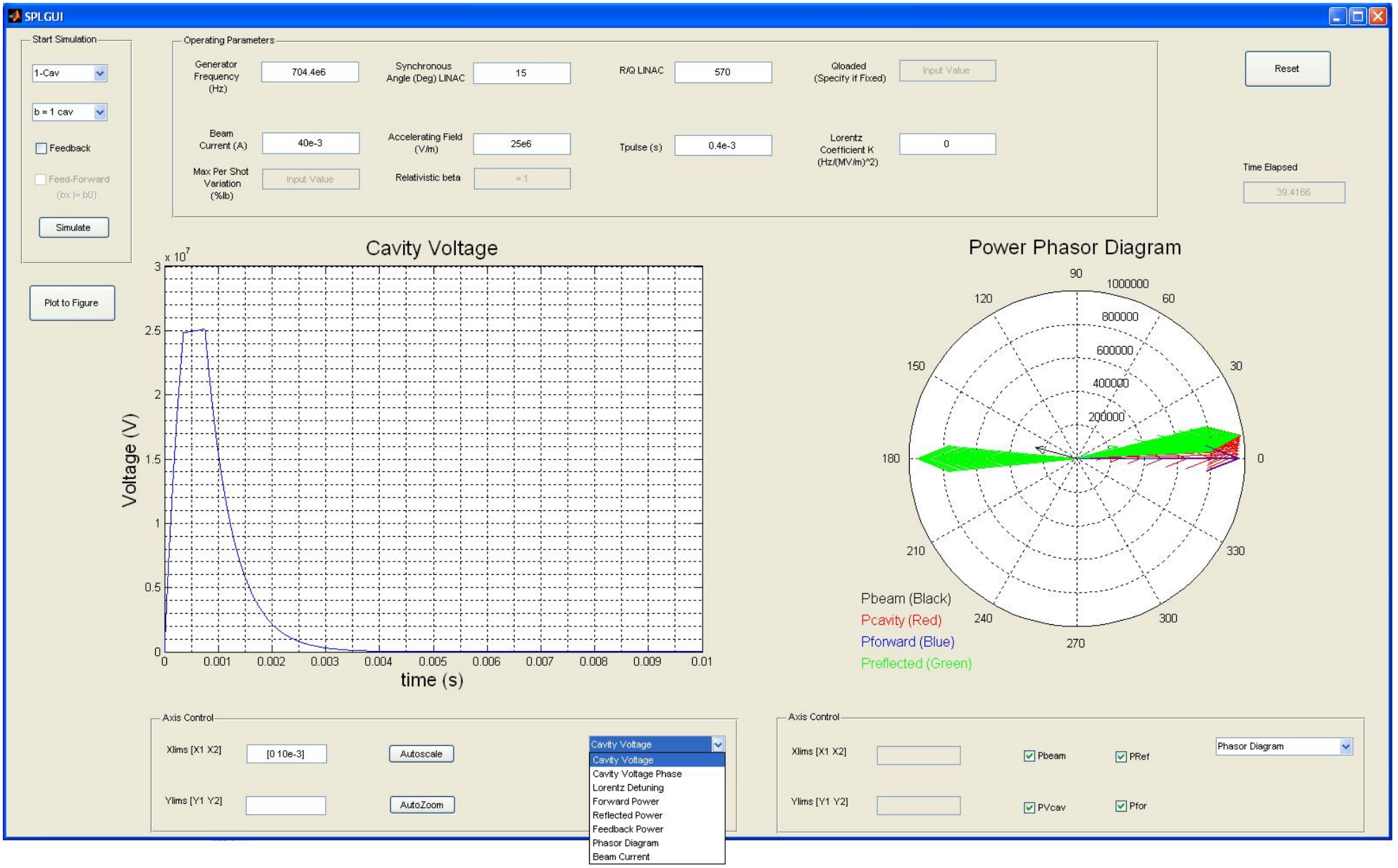

Figure 4.20: Graphical user interface (1-Cavity)

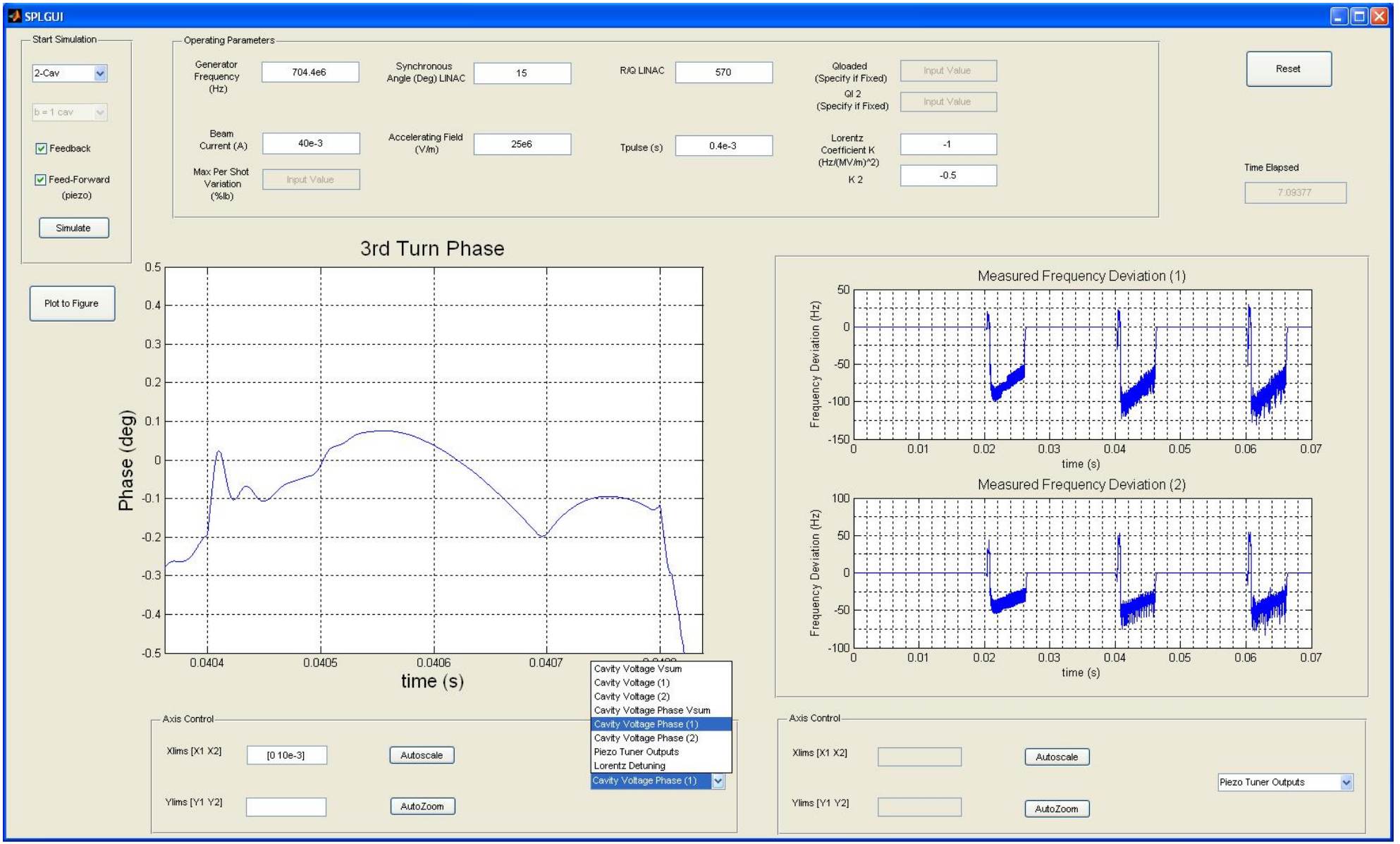

Figure 4.21: Graphical user interface (2-cavities)

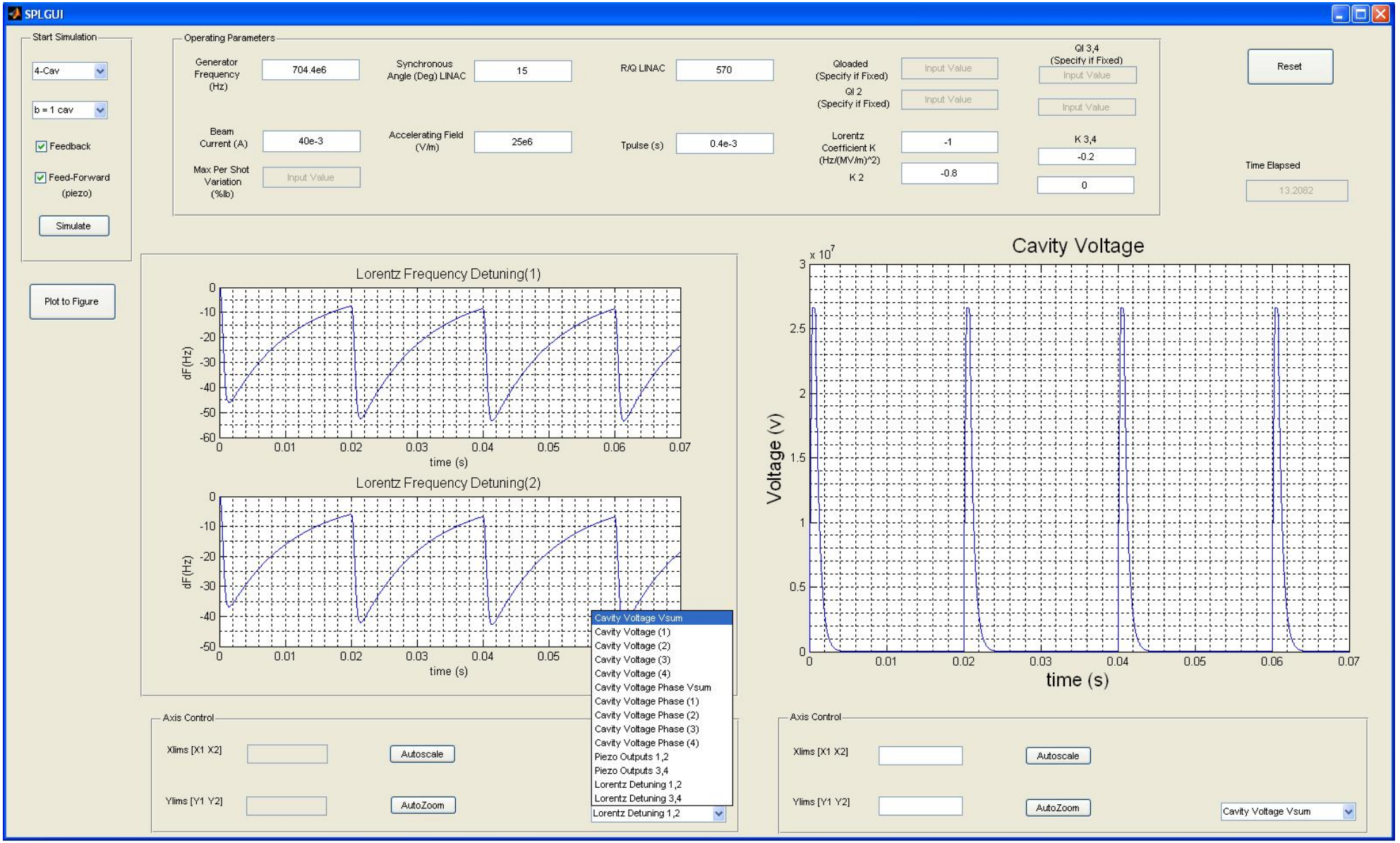

Figure 4.22: Graphical user interface (4-cavities)

4.6 Full SPL

In addition to the single cavity and dual cavity investigation with respect to the fields within the resonant cavities, a rough model focusing on the full effect of the 254 cavities along the SPL on a beam of charged particles was developed. The idea is to observe the extent of the damage by the feedback loop transients at the head of each beam pulse, especially those of the cavity voltage phase. If we observe the results from the next section, all of them have something in common: there is always a spike in the cavity at the beginning of beamloading of around 0.3 degrees. This leads to believe that it can become a cumulative effect throughout the LINAC that can result in an unacceptable deterioration of the beam pulse head with respect to the rest of the beam.
The following model was developed to check the difference in ultimate energy (including rest energy) of the particles and the time they take to traverse the full beam pipe between a beam accelerated with nominal voltage as opposed to that accelerated with an accumulated 0.3 degree error in the synchronous phase.

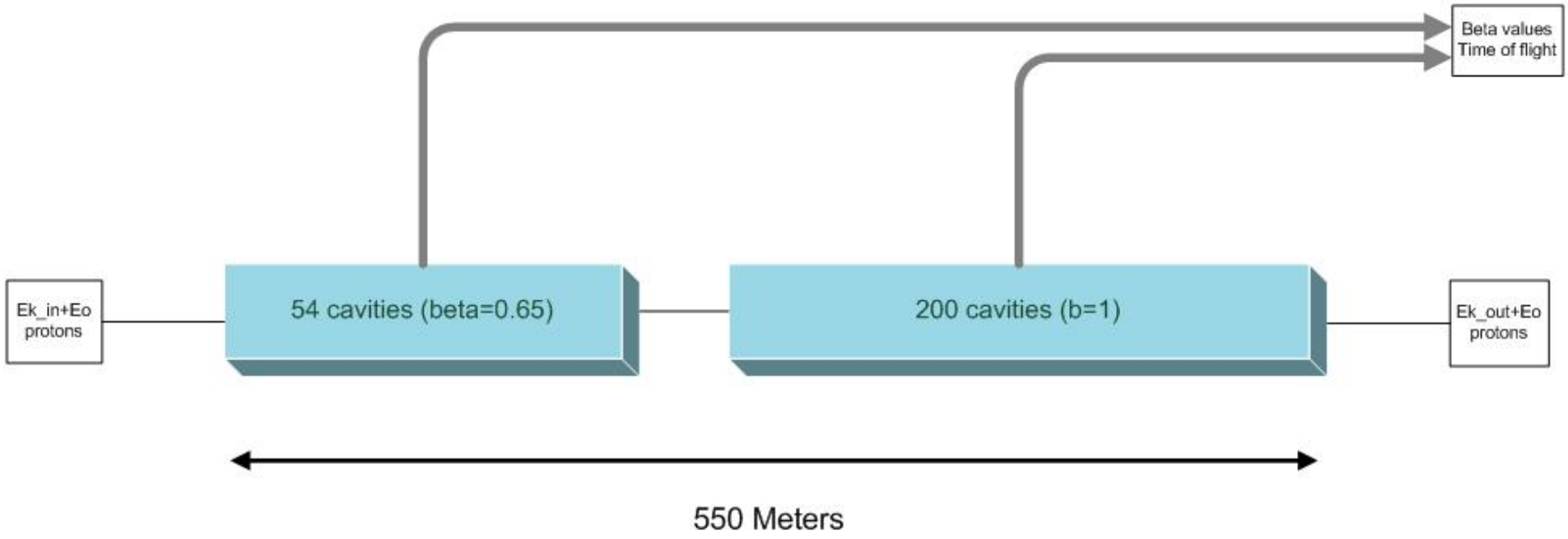

Figure 4.23: Full SPL high-level diagram

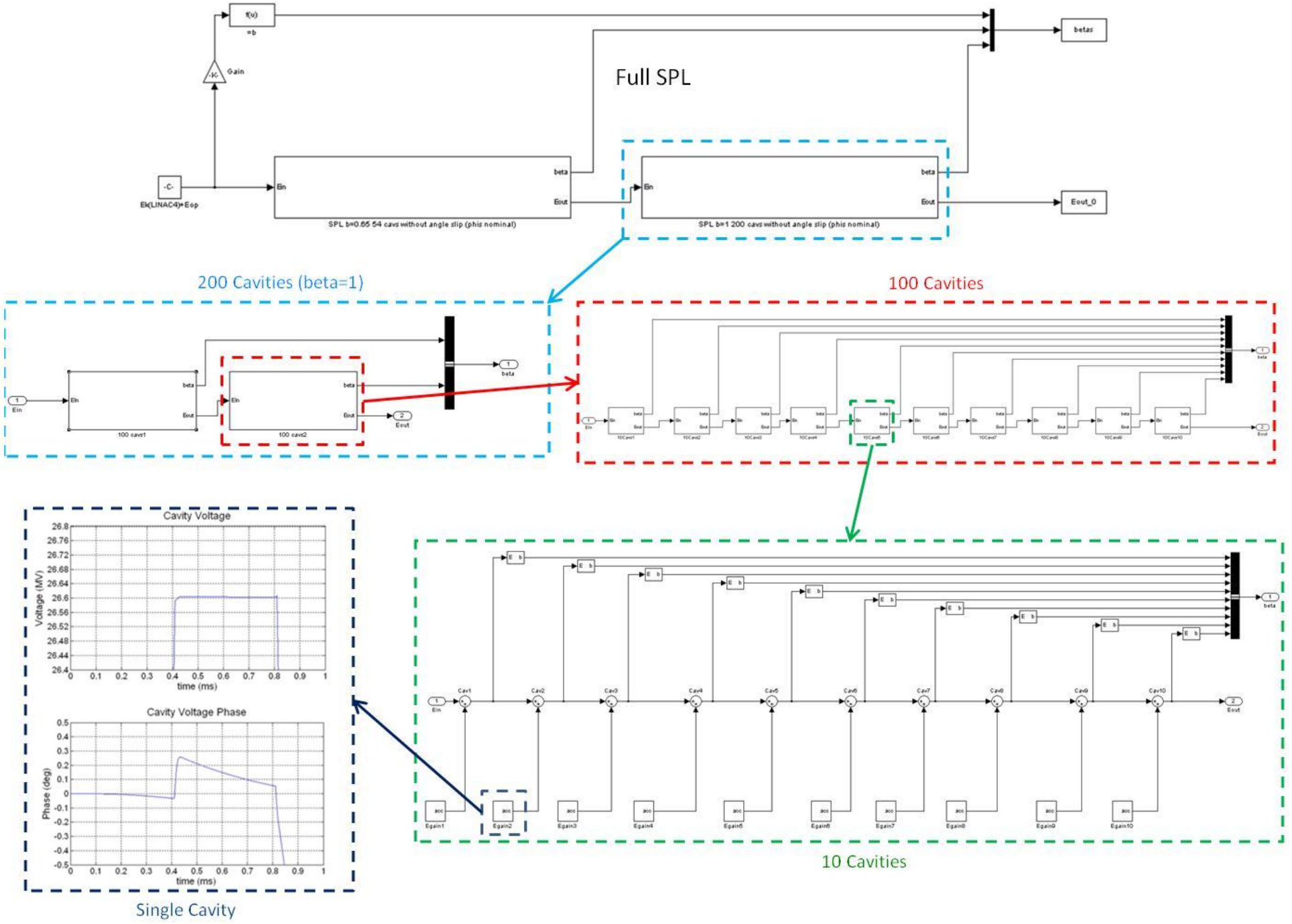

Figure 4.24: Full SPL SIMULINK implementation diagram

Chapter 5

Results of Model Analysis

In this section, modelling results are portrayed in a gradual fashion. The single cavity case is observed for the ideal case, in the presence of Lorentz detuning, source fluctuations, beam speed mismatches, etc. and finally results are shown for the dual-cavity scheme. Bear in mind that all angles in the phase of the cavity voltage are those of the cavity with respect to the generator. The results given focus on the cavities optimised for $\beta = 1$ beam speed operation as their parameters are more restrictive. All results, thus, refer to these cavities unless otherwise specified in sections 5.3 and 5.5, where the $\beta = 0.65$ section of the LINAC is investigated with relation to mismatch in actual beam speed during beamloading and full SPL effect on the beam.

5.1 Single Cavity (β=1) in the Absence of Lorentz Detuning

5.1.1 Open Loop

We start off with the simplest case, a single cavity with a matched loaded quality factor to beam current. At the time of injection, given by

$$t_{inj} = \ln 2 \times \tau_{fill}$$

the beam arrives with a phase shift given by the synchronous angle. This explains the fact that the power delivered by the generator is not entirely absorbed by the beam and the cavity voltage increases with time. As the cavity is uncompensated, the unsynchronised beam causes the voltage amplitude to rise above the 0.5% tolerance level and detunes the cavity phase with respect to the generator (0 degree) phase towards 15 degrees. This also means that some reflected power is observed during beam loading.

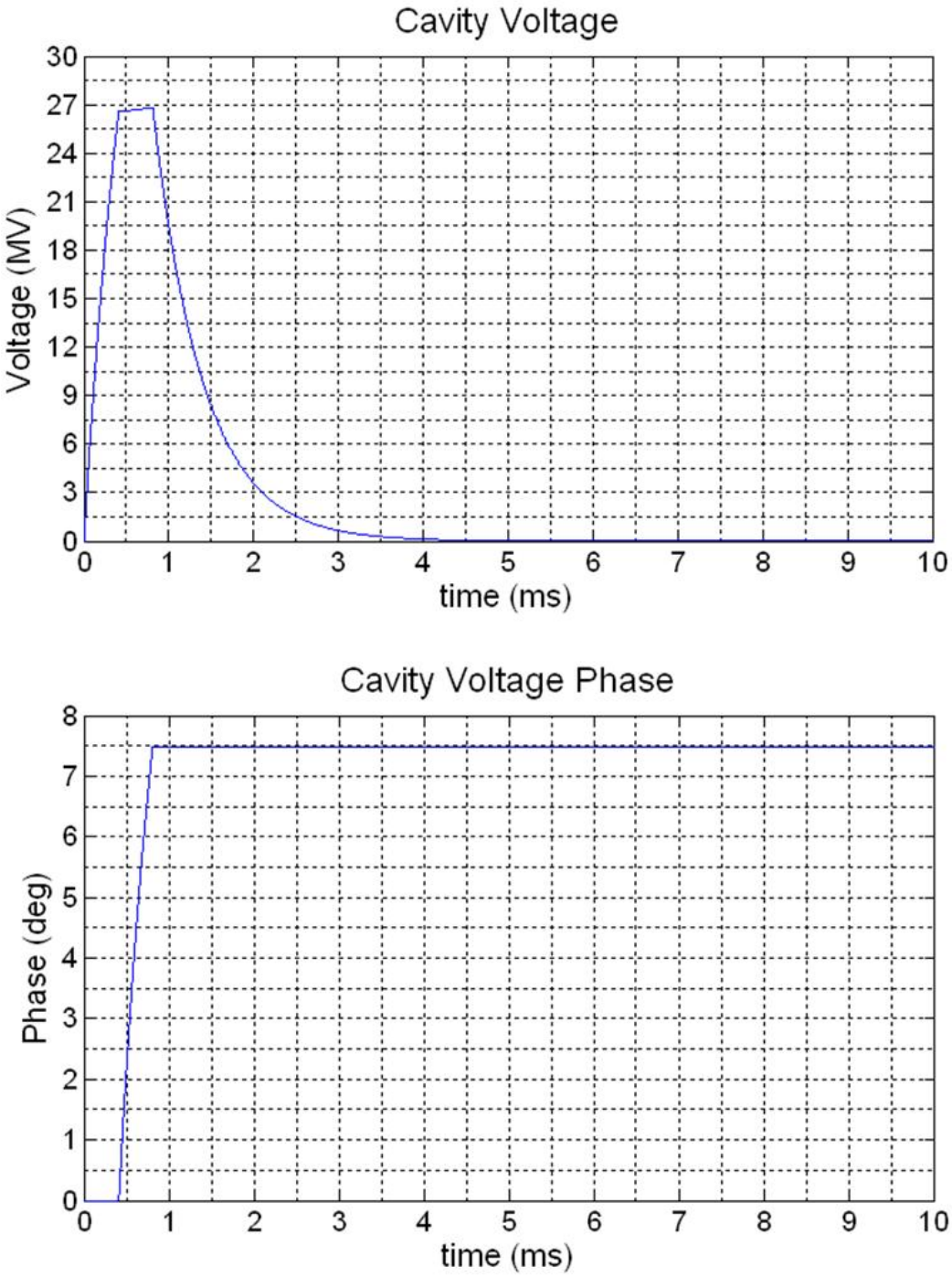

Figure 5.1: Cavity voltage magnitude and phase in the absence of Lorentz detuning (open loop)

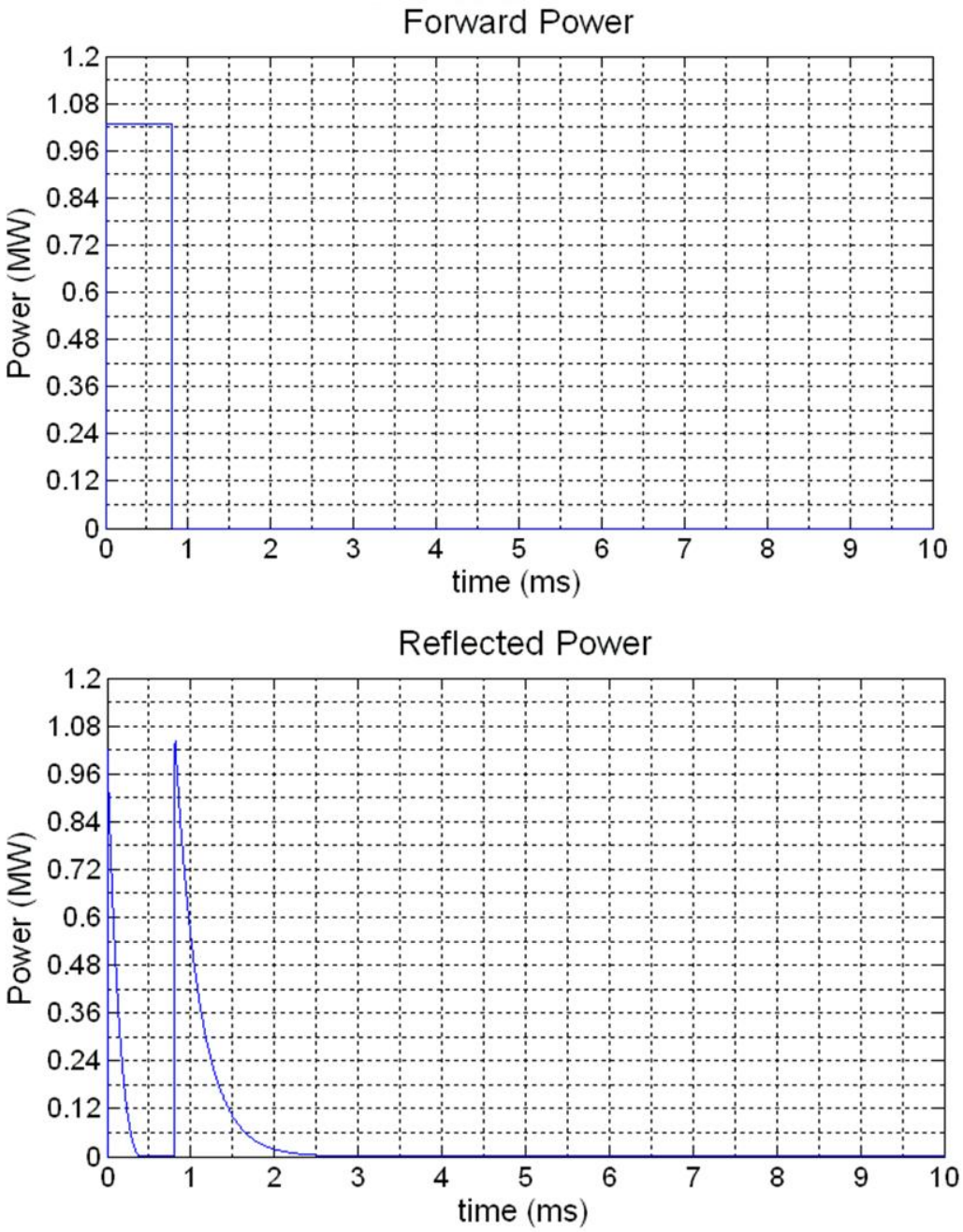

Figure 5.2: Forward and reflected power in the absence of Lorentz detuning (open loop)

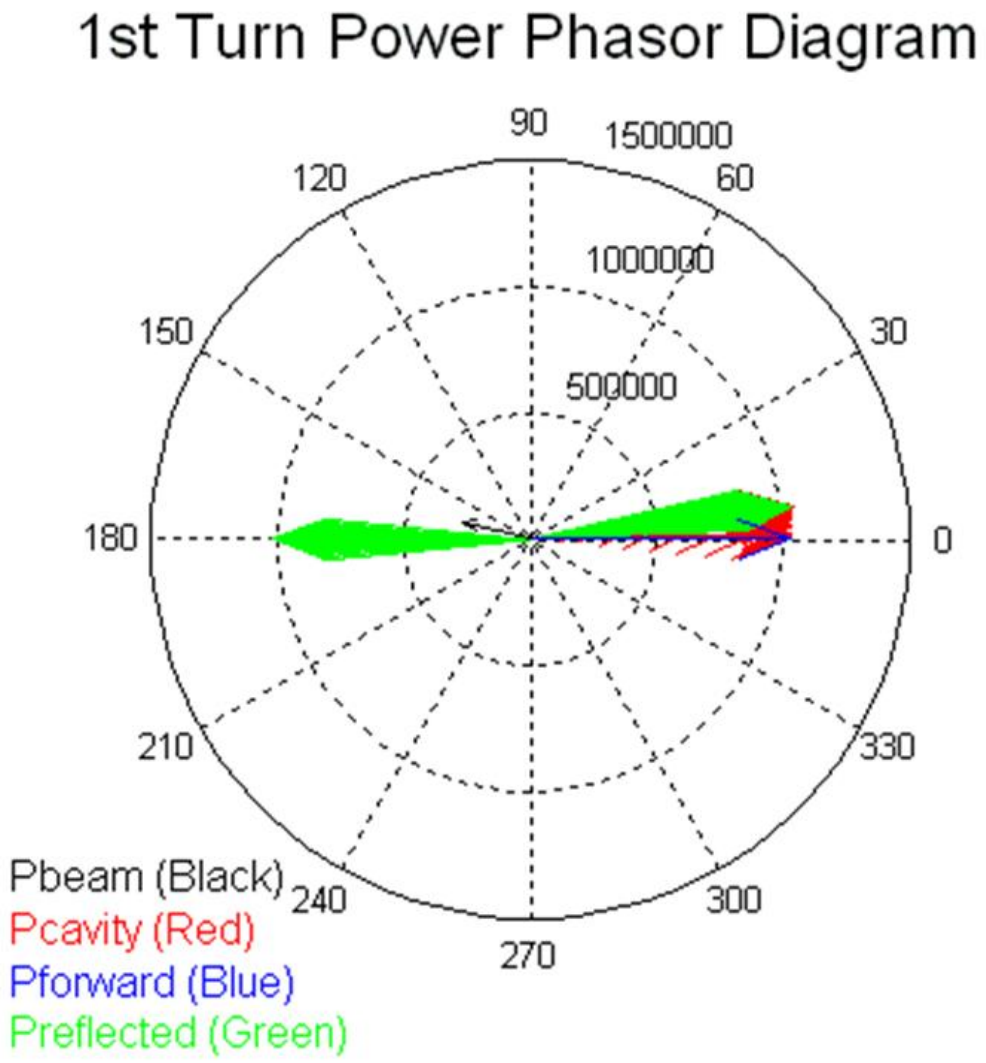

Figure 5.3: Power phasor diagram for open loop system

5.1.2 Closed Loop

It is clear from the results in the previous sub-section that feedback is necessary for the correct operation of the system output. The following results were obtained by adding PID feedback with an ideal cavity output as a setpoint. The proportional gain was set by stability considerations, assuming a feedback loop delay of 5 microseconds. The integral and differential gains were set by trial and error. Both the cavity magnitude and phase are now within the design specifications, as shown by figure 5.4. The feedback loop is closed (ON) right after the generator pulse begins, which means it is already ON when the beam arrives. Right after the beam has passed, the feedback loop is turned OFF to save power, leaving the cavity detuned at a constant value depending on the oscillations resulting from the end of beam loading. The forward and reflected powers are as before, with the addition of the feedback compensation. The power consumed by the feedback peaks at around 23 kW at the moment of beam injection.

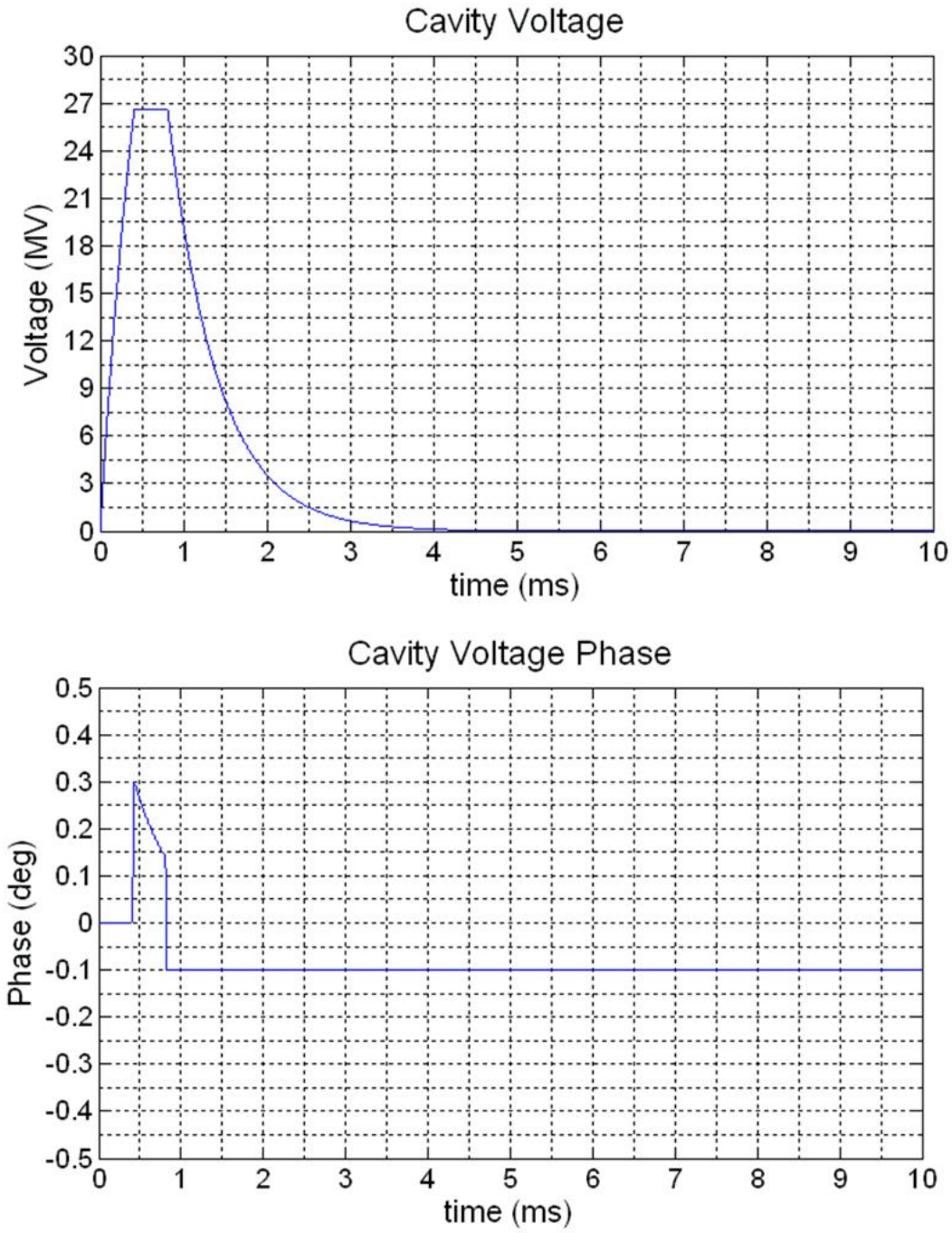

Figure 5.4: Cavity voltage magnitude and phase in the absence of Lorentz detuning (closed loop)

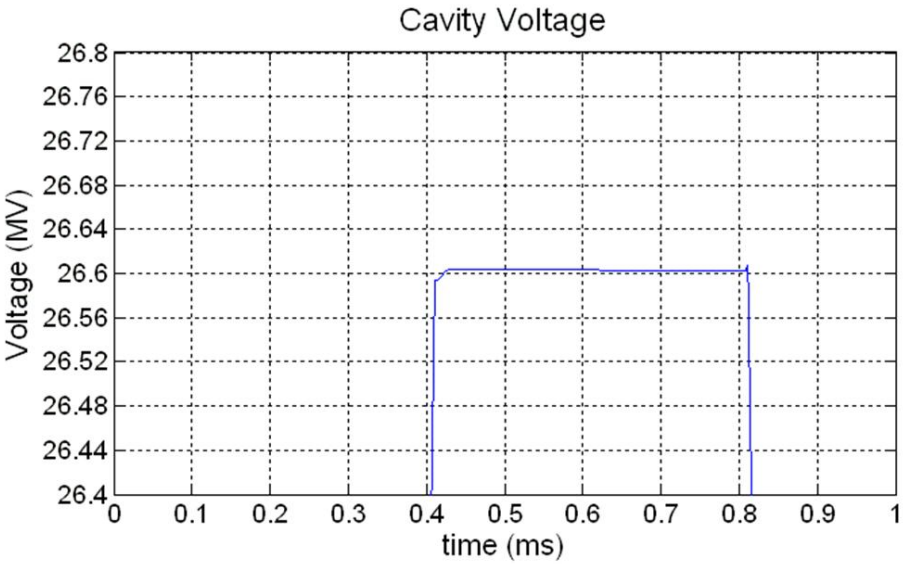

Figure 5.5: Cavity voltage magnitude detail

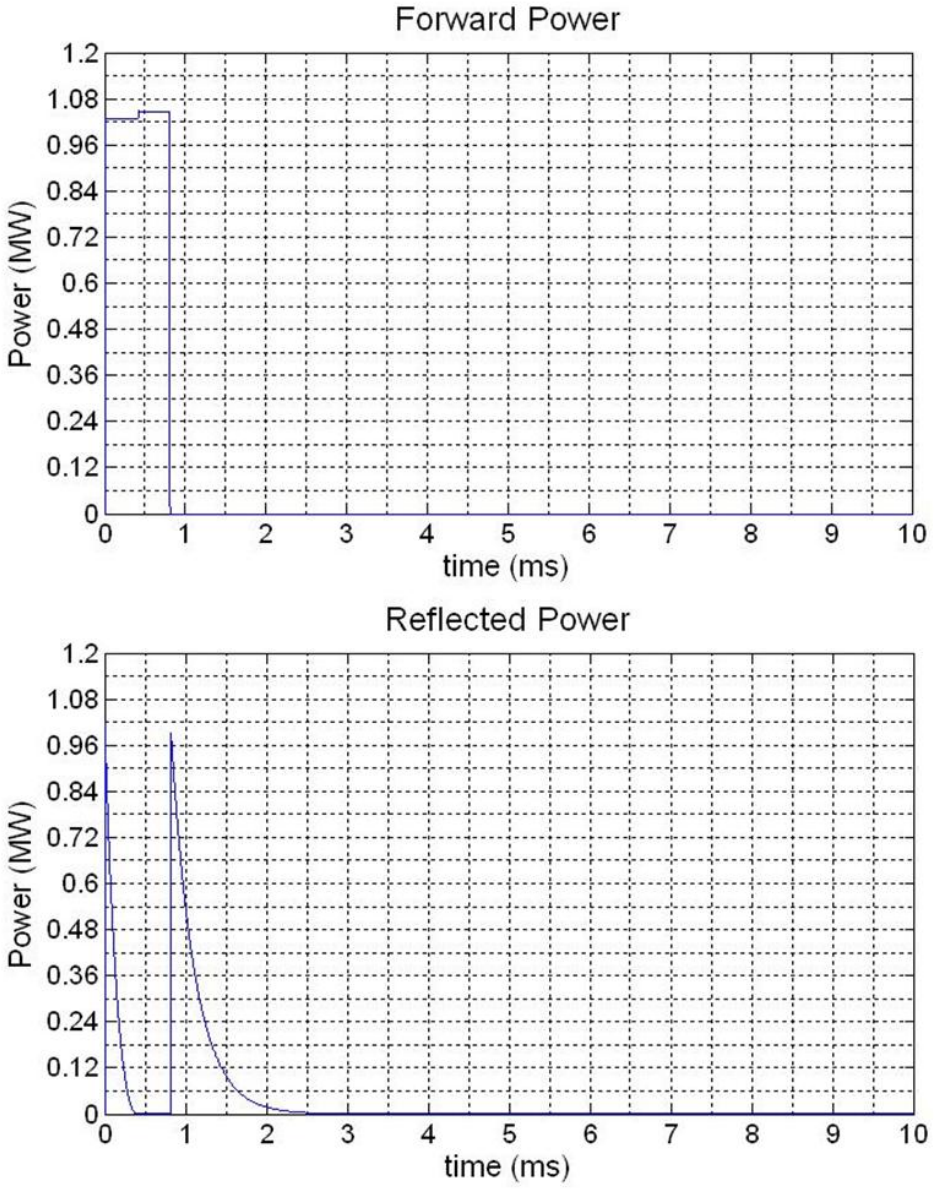

Figure 5.6: Forward and reflected power in closed loop operation

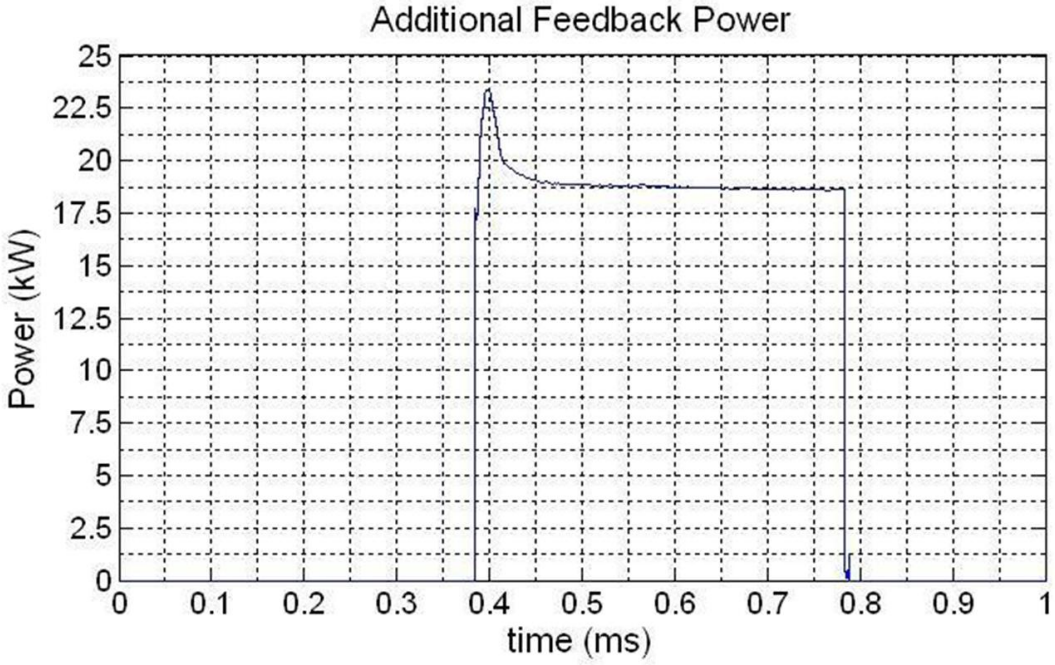

Figure 5.7: Feedback power added

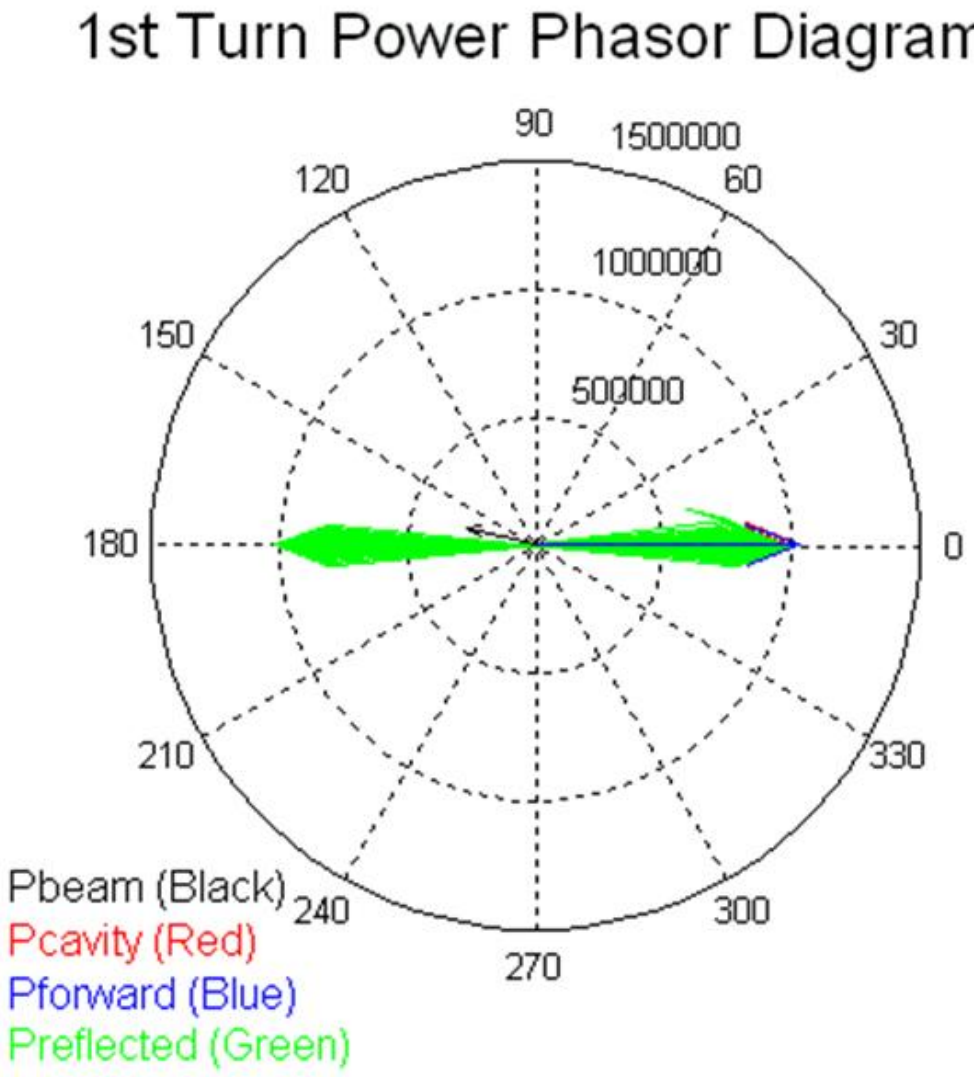

Figure 5.8: Power phasor diagram for closed loop system

5.2 Single Cavity (β=1) with Lorentz Detuning Effects

When a high electric field, and its associated magnetic field, is contained within a resonant cavity, the pressure exerted on the cavity walls due to their magnitudes is known as Lorentz force. Lorentz force can result in the physical deformation of the cavity, which, from the RF point of view, is seen as a damped variation in the resonant frequency of the cavity. This means the cavity is no longer matched to the generator frequency, and this has repercussions on the cavity voltage and power delivered to the cavity, which means it has effects on the total beam acceleration during beam loading. Taking into consideration the stiffness of the cavity and using experimental results from CEA Saclay, the Lorentz detuning coefficient was set to be of -1 Hz/(MV/m)² for the purposes of our model. This results in a time-dependent frequency shift given by a first order differential equation as shown in figure 5.9.

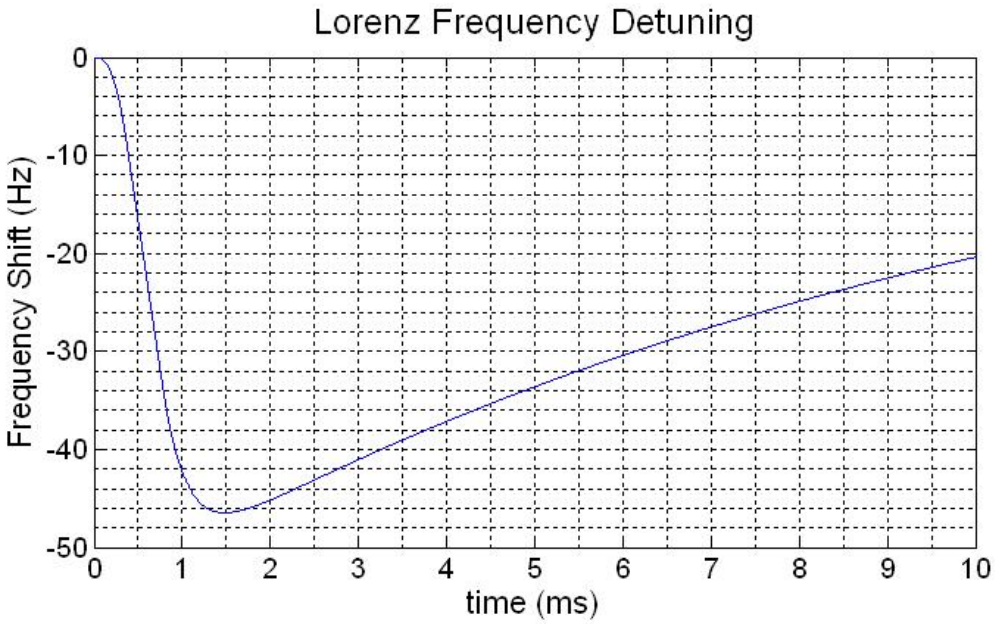

Figure 5.9: Resonant frequency shift due to Lorentz force cavity deformation

$$\frac{d\Delta\omega(t)}{dt} = \frac{1}{\tau}\left(2\pi K E_{acc}^2 + \Delta\omega_T - \Delta\omega(t)\right) \tag{5.1}$$

Thus, a frequency shift of -1 Hz/(MV/m)² results in about a 50 Hz decrease of the cavity's resonant frequency for the given beam + generator pulse time.

5.2.1 Open Loop

The open-loop analysis reveals the effect of Lorentz force detuning on the cavity output, particularly in its output voltage phase. The effect of Lorentz detuning on the cavity voltage magnitude opposes the effect of the beam angle mismatch; now the beam absorbs less power from the generator but due to Lorenz detuning

the generator also delivers less power to the cavity. The Lorentz force (negative coefficient) also opposes the phase shift in the cavity voltage resulting from the beam synchronous angle. After beam loading, however, the cavity is out of tune and the voltage phase will oscillate with a gradient proportional to the detuning. Once again, some reflected power will be observed during beam loading, but it is negligible compared to the filling and dumping of the cavity before and after beam loading.

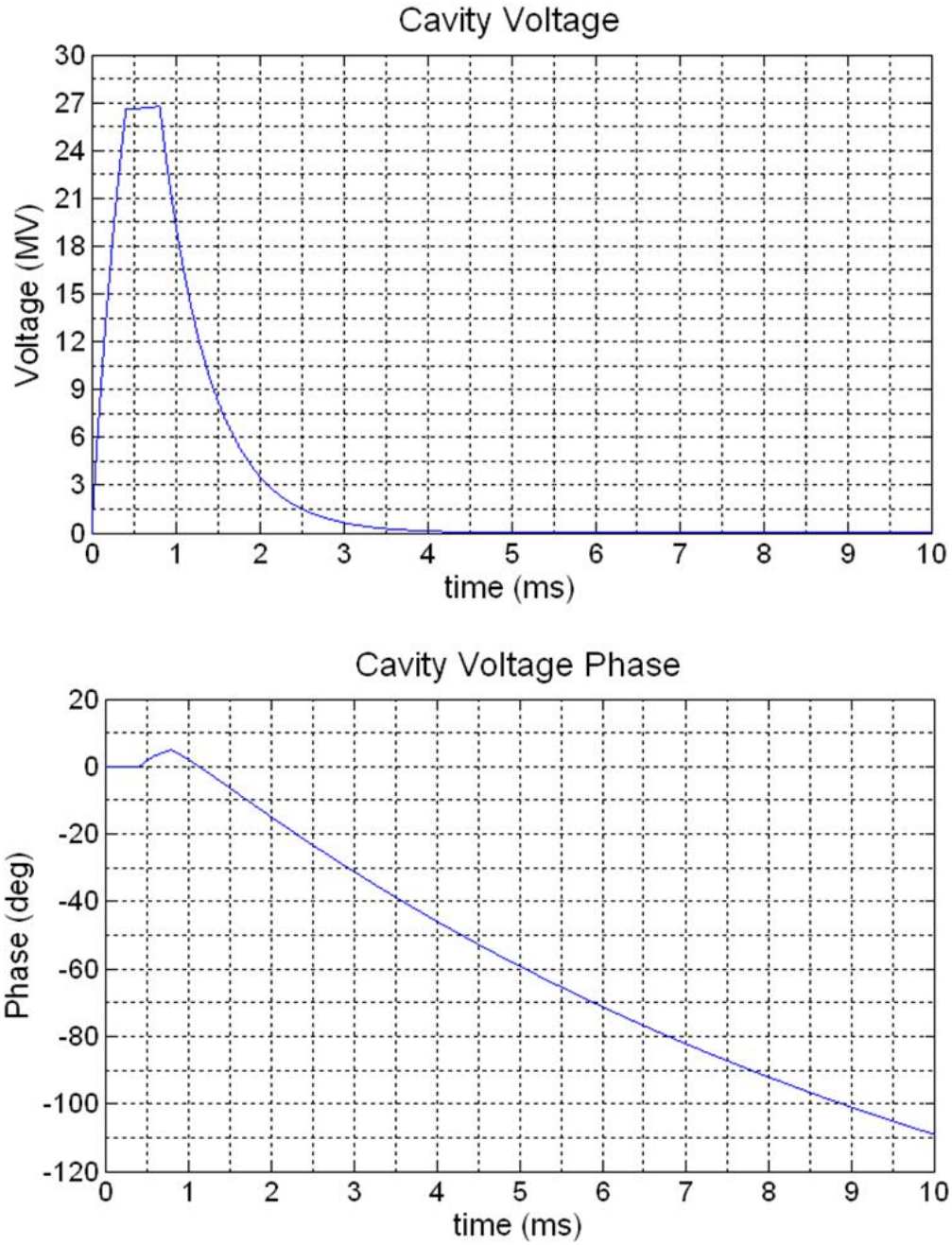

Figure 5.10: Cavity voltage magnitude and phase with Lorentz detuning (Open Loop)

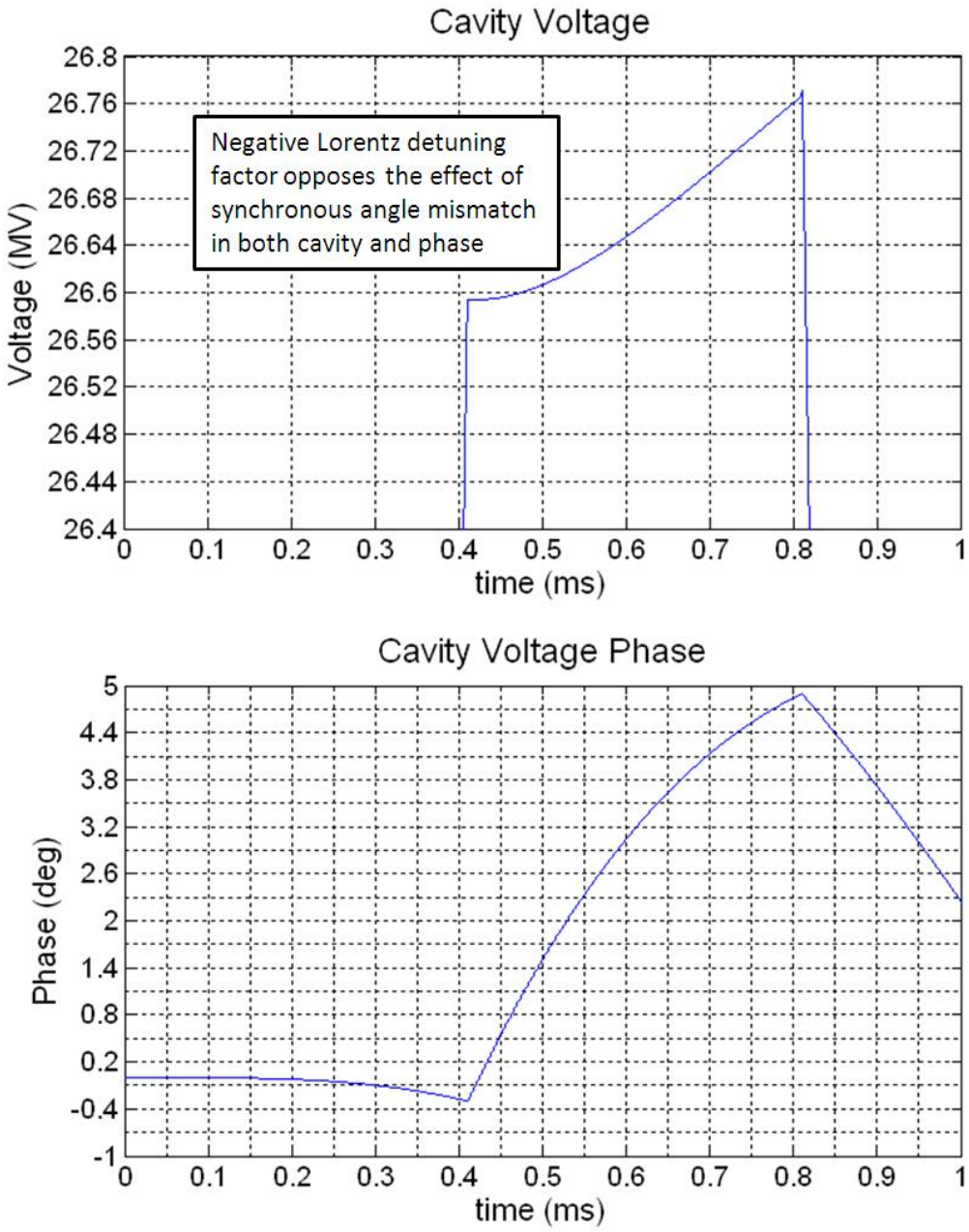

Figure 5.11: Cavity voltage magnitude and phase detail

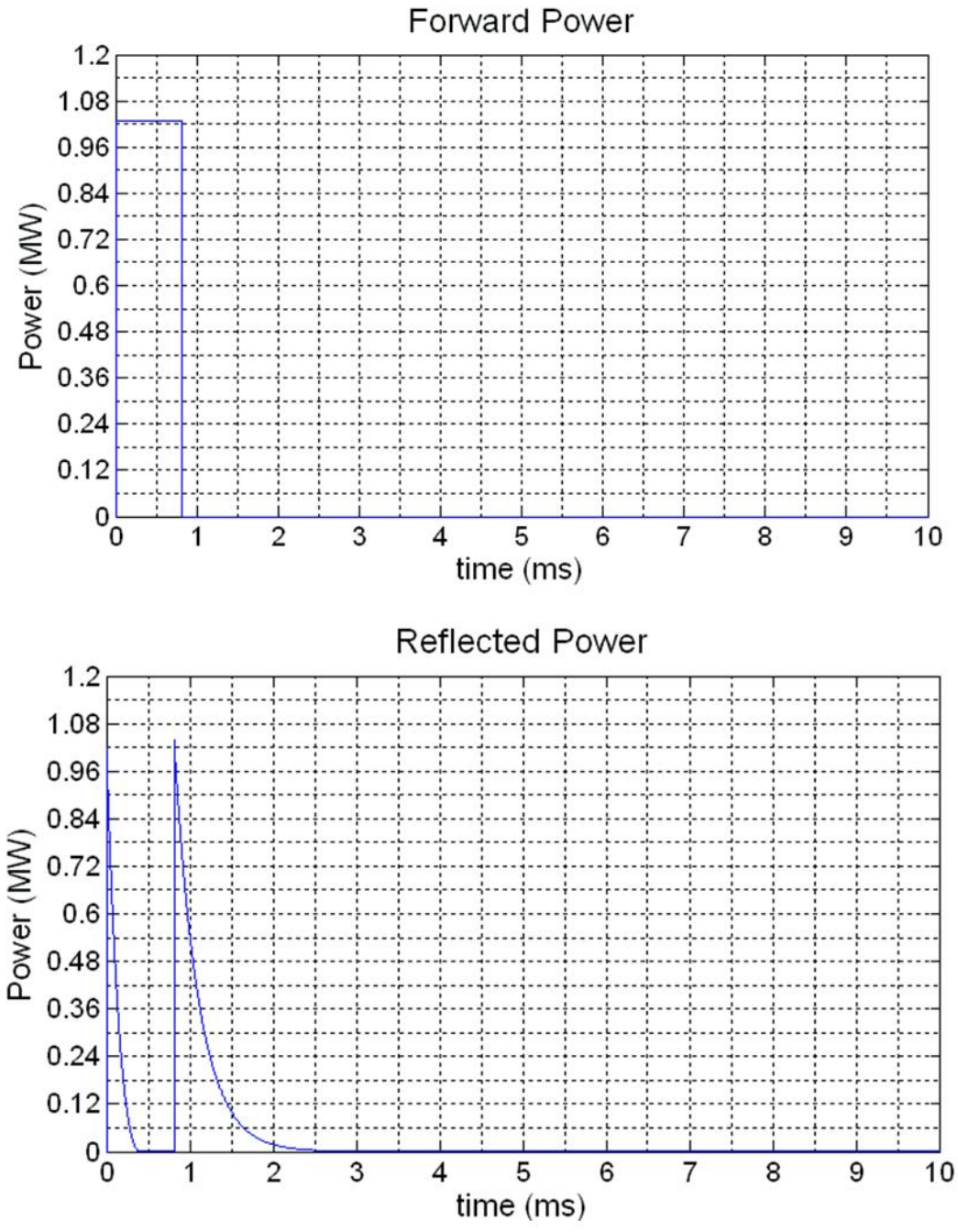

Figure 5.12: Forward and reflected power with Lorentz detuning

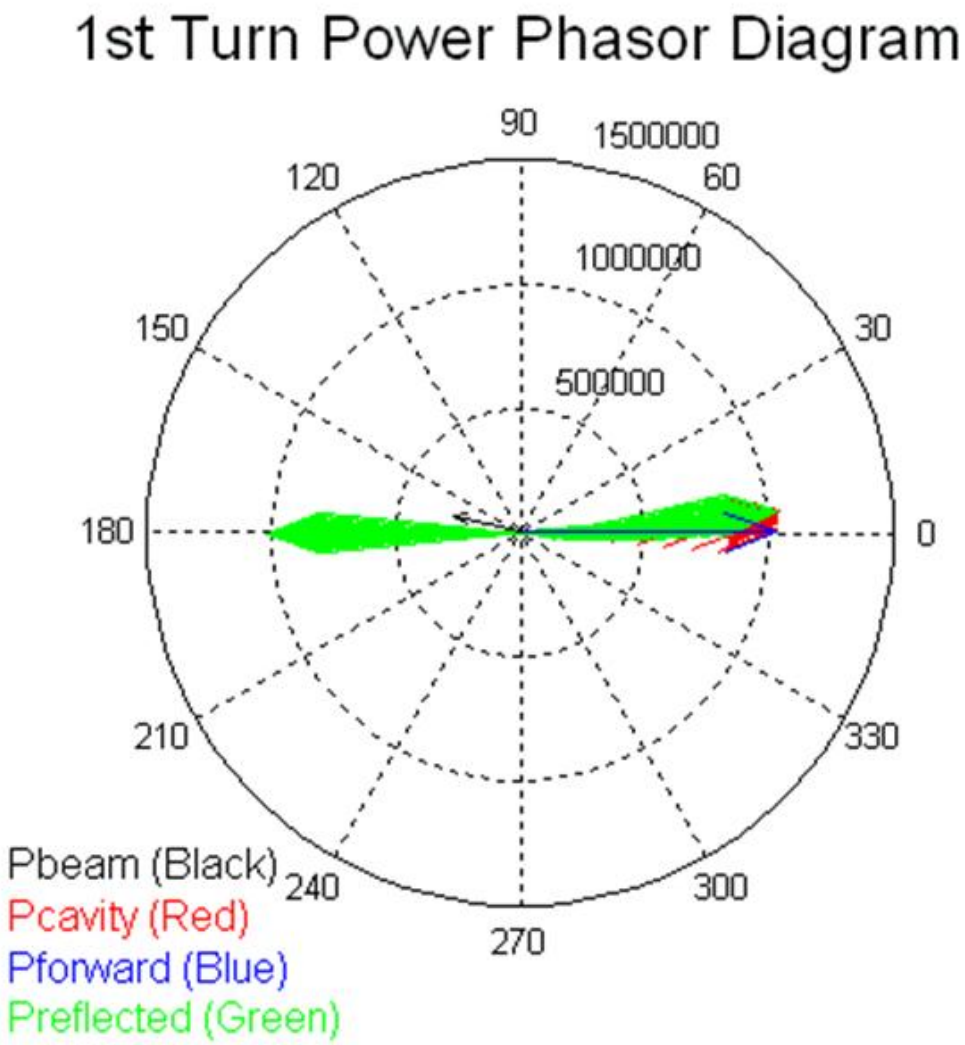

Figure 5.13: Power phasor diagram for open loop system

5.2.2 Closed Loop

It is clear that for the correct operation of the system, the feedback needs to compensate for Lorentz detuning and beam angle effects. Now, as mentioned before, the feedback loop is closed (ON) during beam loading, and open (OFF) right after until the next generator pulse. We can now see that both the cavity voltage magnitude and phase are within design parameters, with the added phase shift when the loop if OFF due to the mismatch between generator frequency and cavity resonant frequency. Due to the fact that negative Lorenz detuning opposes the effect of beam angle mismatch in both the cavity voltage amplitude and phase, the feedback power required is actually lower than for the former case (no Lorentz detuning) as the beam pulse progresses. For the case of a beam passing with a 15 degree synchronous angle through a cavity with a Lorentz coefficient of -1 Hz/(MV/m)^2, driven by a 1.03 MW generator, the maximum feedback power required is of about 20 kW, but it decreases during the beam pulse due to the Lorentz effects.

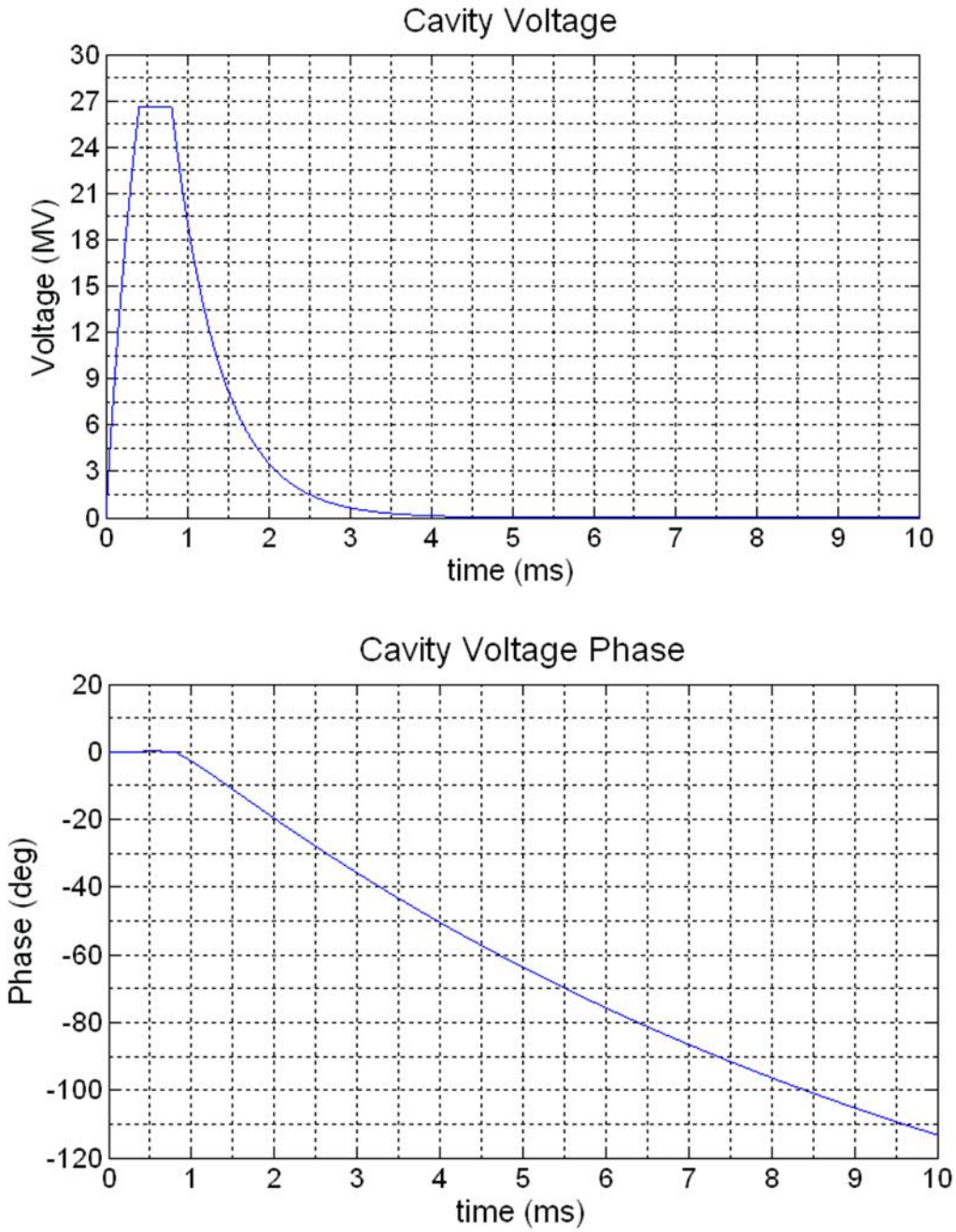

Figure 5.14: Cavity voltage magnitude and phase with Lorentz detuning (Open Loop)

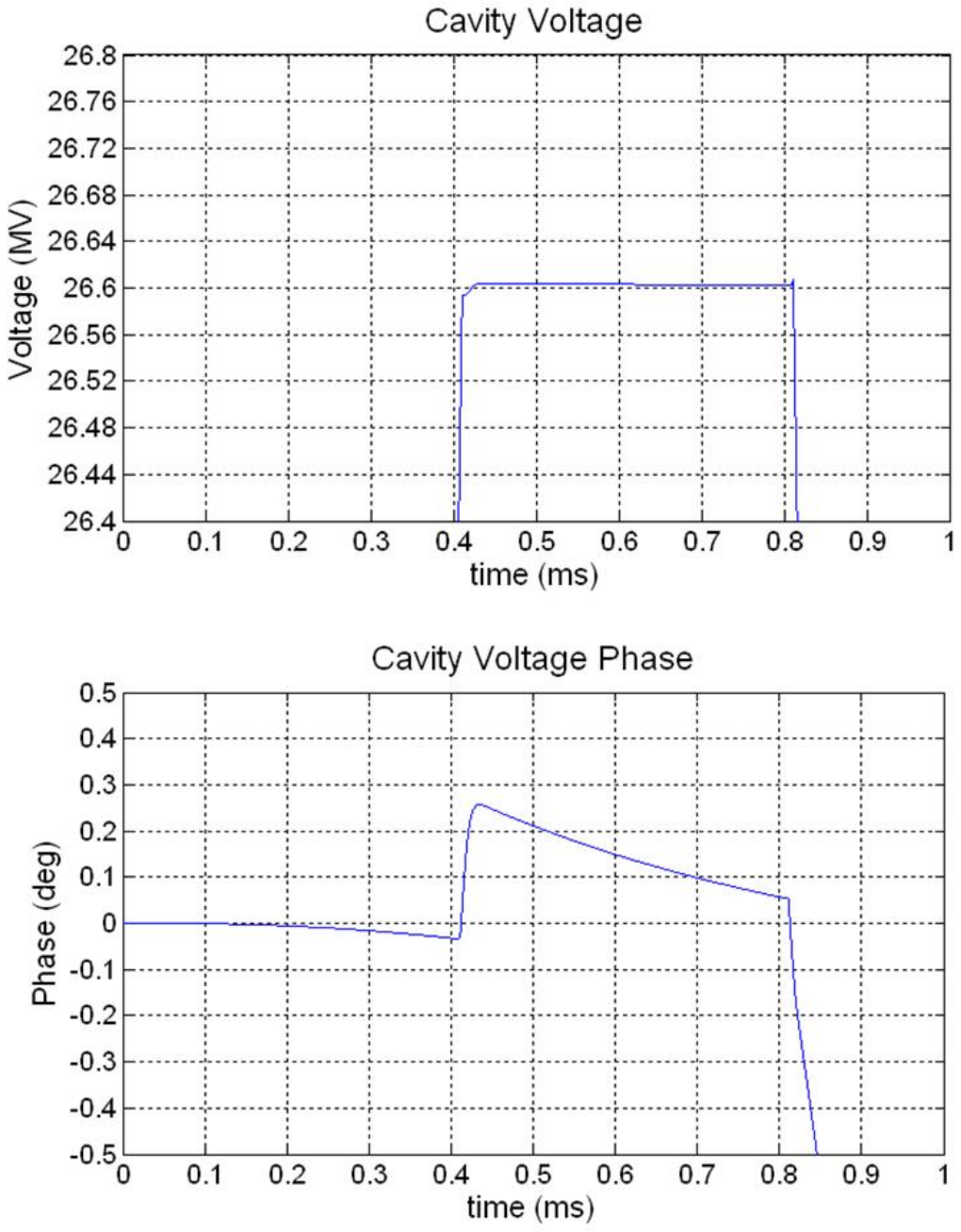

Figure 5.15: Cavity voltage magnitude and phase detail

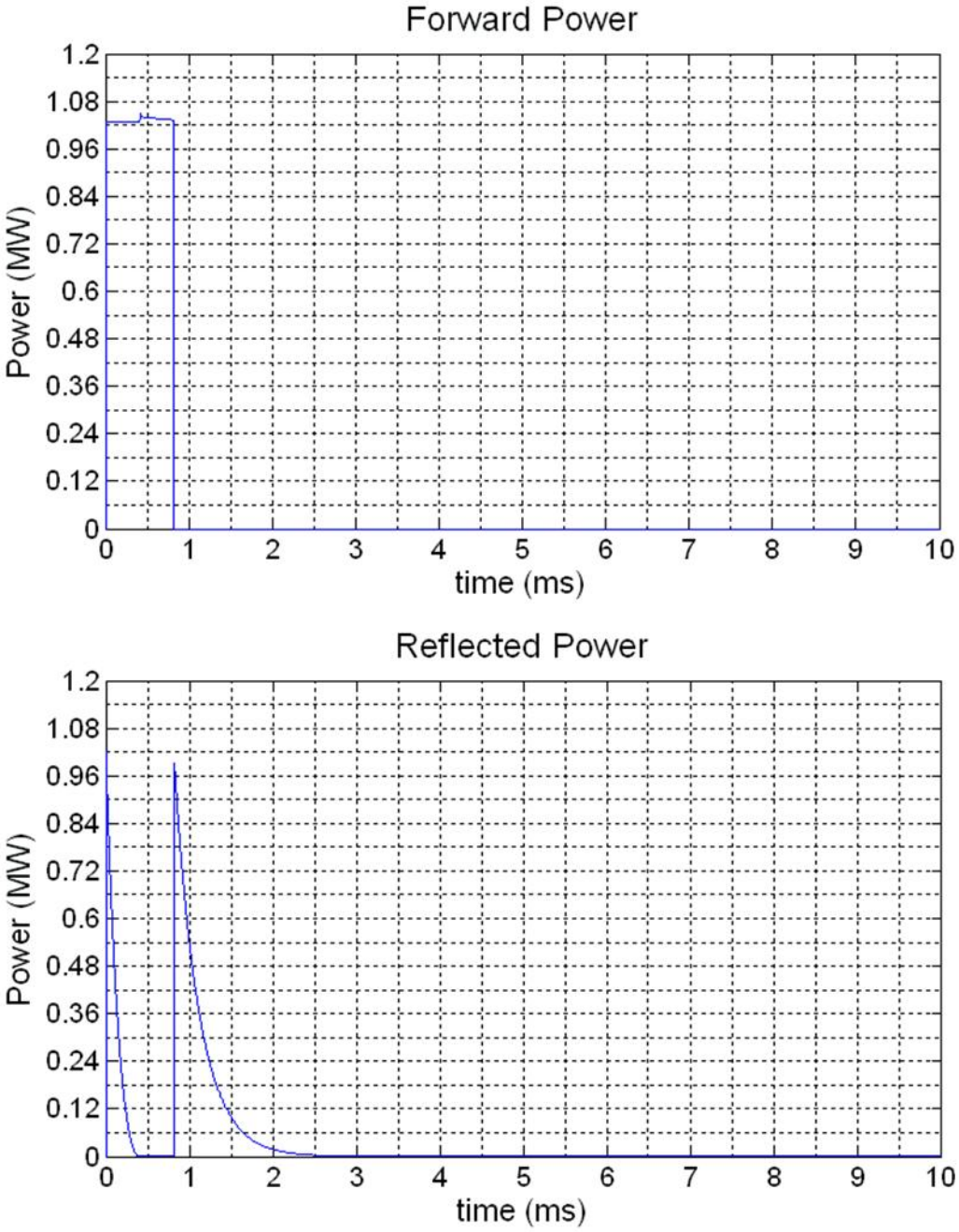

Figure 5.16: Forward and reflected power with Lorentz detuning

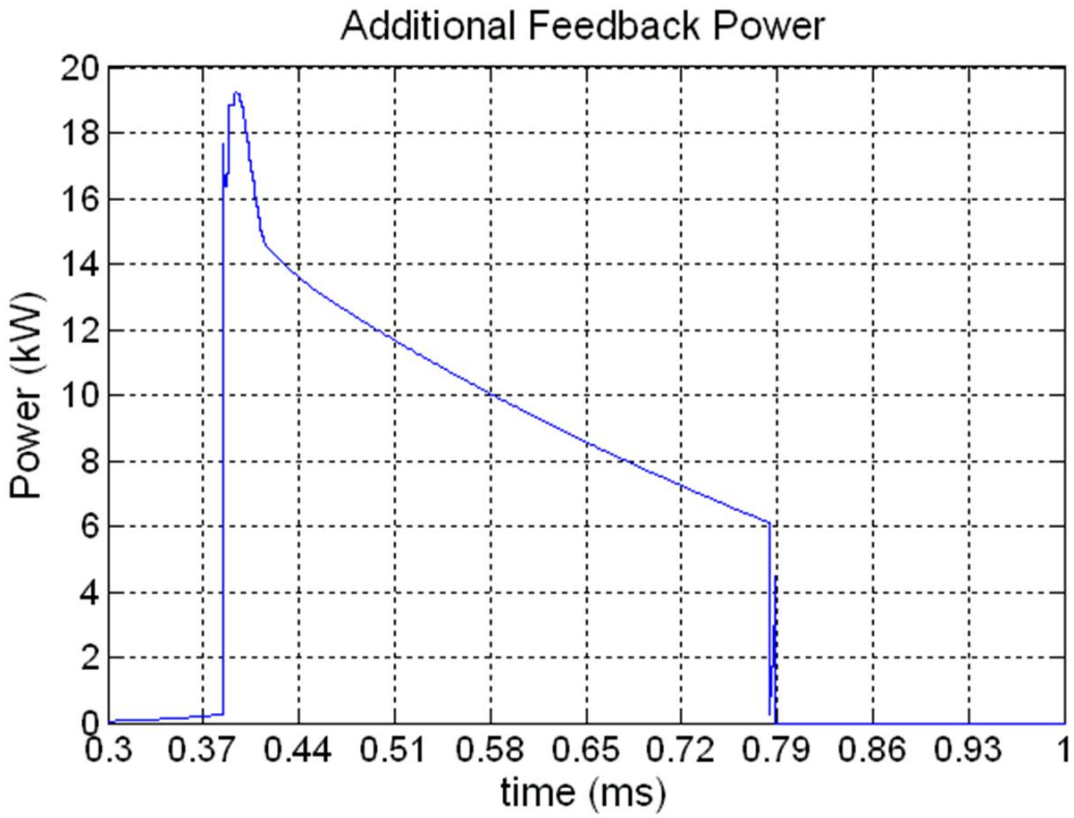

Figure 5.17: Feedback power added

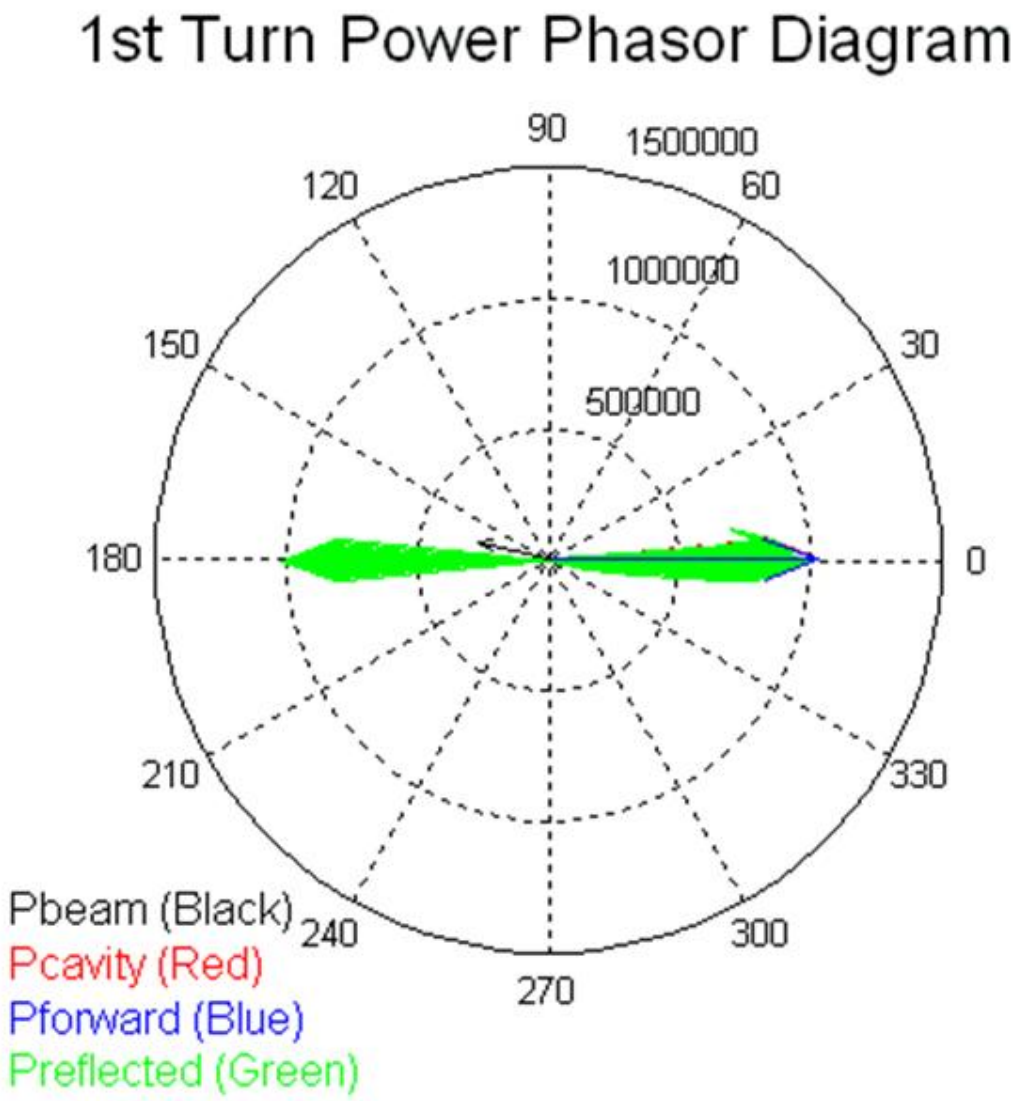

Figure 5.18: Power phasor diagram for closed loop system

5.2.3 Variation of Source Beam Current: Low and High Power SPL Operation

In both high current and low current operation cases for the SPL specifications, the source repetition rate is of 50 Hz. The hydrogen ion source for the LINAC has a specified beam current that can vary within the beam pulse. This variation has been observed to be up to 5% of the nominal beam current. For the purpose of our simulations, we added this variation to ensure that the control loop was adequate. As shown in the following results, the feedback loop has no trouble compensating for the current variations, provided enough power is available. The feedback power requirements were found to be around 30kW/mA for the matched case, and around 20kW/mA for the mismatched (20mA beam current) case. The 20 mA SPL operation has no significant differences with the 40 mA case with respect to cavity voltage phase and magnitude behaviour. It is interesting, however, to note the effects of the power mismatch prior to beam loading and the effects of the mismatched beam on the feedback loop. This would be the case if a lower current beam is sent to an RF system with a loaded quality factor that is optimised for 40 mA operation. This will give us an idea of the power requirements for mismatched operation.

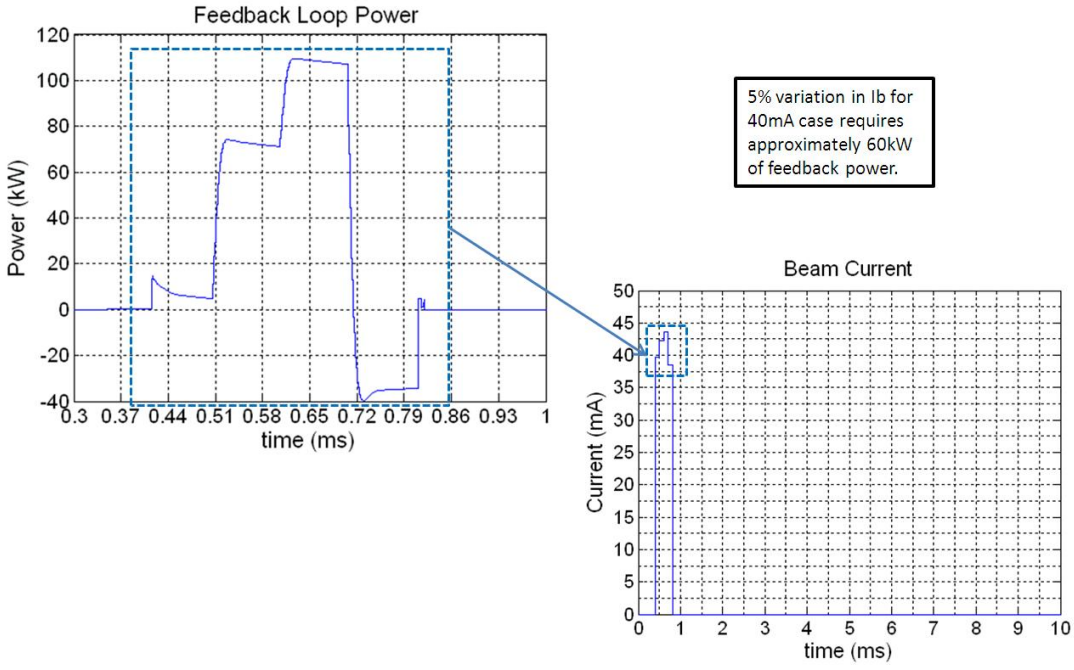

Figure 5.19: Effect of beam current variation on feedback power (matched operation)

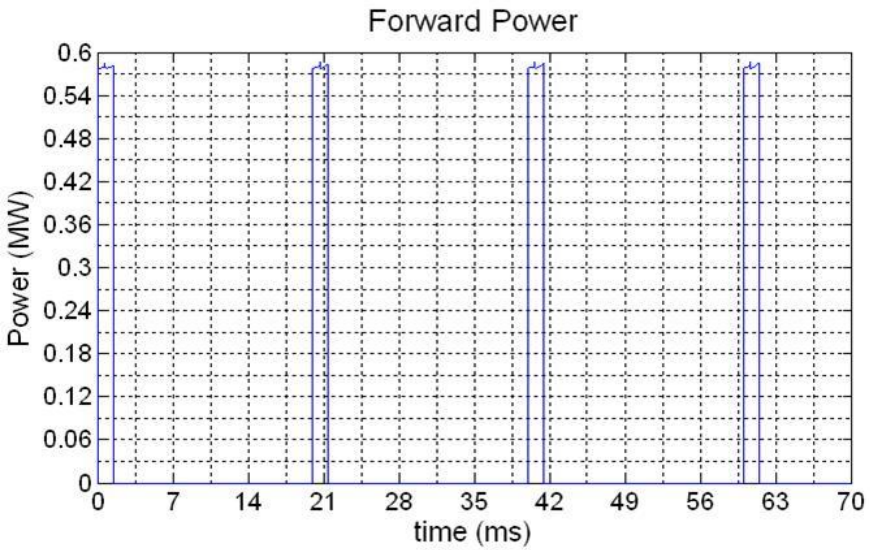

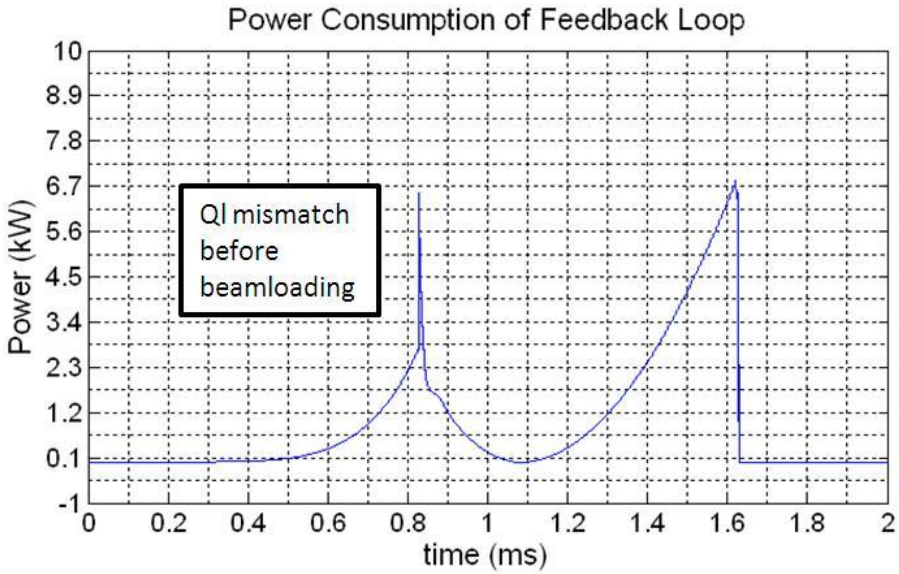

$$I_{\mathrm{b,DC}} \cong 20\ \mathrm{mA}$$

$$P_{\mathrm{b}} = V_{\mathrm{acc}} \times I_{\mathrm{b,DC}} \times \cos(\phi_s) \cong 514\ \mathrm{kW}$$

$$Q_{\mathrm{L,fixed}} = \frac{V_{acc}}{\frac{R}{Q} \times I_{b,40\mathrm{mA}} \times \cos(\phi_s)} \cong 1.3113 \times 10^6$$

$$I_g = \frac{V_{acc}}{R_L} + I_{b,DC}\cos(\phi_s) = 58\ \mathrm{mA}$$

$$\alpha = \frac{I_g}{I_{b,DC}\cos(\phi_s)} = 3$$

$$\tau_{fill} = \frac{2Q_L}{\omega_{RF}} = 0.5926\mathrm{ms}$$

$$t_{inj} = \tau_{fill}\ln(\alpha) = 0.6510\mathrm{ms}$$

$$P_{fwd} = \frac{1}{4}R_L\left|I_g\right|^2 = 578\mathrm{kW}$$

$$t_{pulse} = 0.8\ \mathrm{ms}$$

Figure 5.20: Low-power operation of SPL (power considerations)

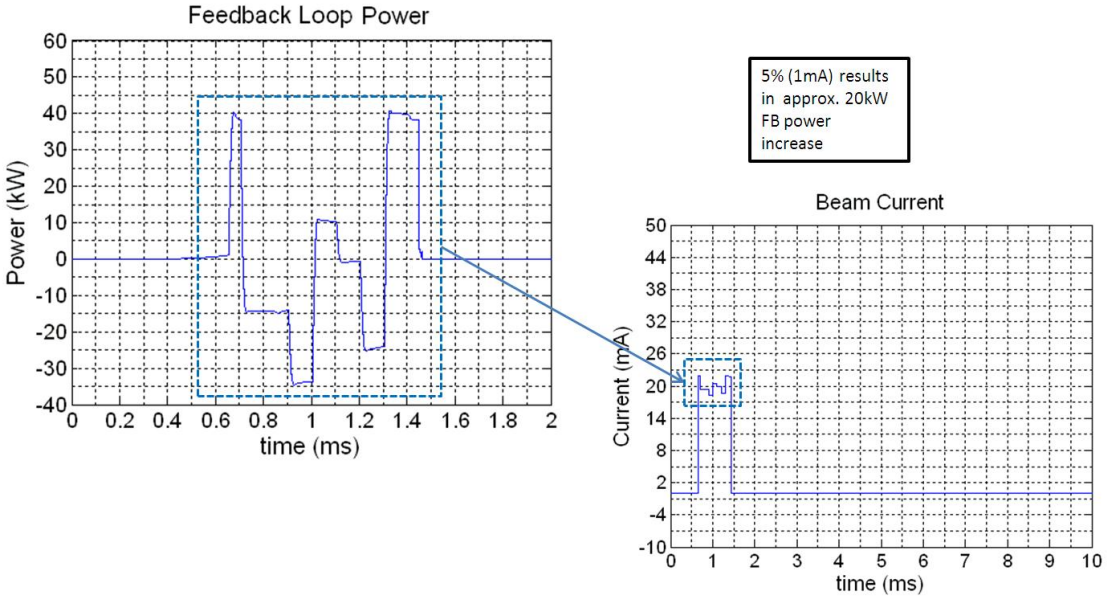

Figure 5.21: Effect of beam current variation on feedback loop power consumption (mismatched operation)

5.3 Beam Speed Effects

In chapter 2, it was explained how a beam arriving at a speed different to the cavity design will affect the voltage inside said cavity. In essence, we know that a beam with a different speed will have a weaker coupling to the cavity field, and this will result on weaker beamloading. In this section we observe the effects of this phenomenon in detail, focusing on the accelerating voltage within both $\beta = 1$ and $\beta = 0.65$ cavities, and possible solutions to unideal behaviour caused by suboptimal beamloading.

5.3.1 β=1 Cavities

As explained before, the effective shunt impedance of a resonant cavity relates the accelerating voltage to the power dissipated. The accelerating voltage "seen" by a beam travelling with a speed of β_x relative to the speed of light is given by

$$V_{acc}(\beta_x) = \left| \int_{gap} \underline{E}_z(z)dz \right| \times T = \left| \int_{gap} \underline{E}_z(z) e^{i\frac{2\pi}{\beta_x c}z} dz \right|$$

where

$$T(\beta_x) = \frac{\left| \int_{gap} \underline{E}_z(z) e^{i\frac{2\pi}{\beta_x c}z} dz \right|}{\left| \int_{gap} \underline{E}_z(z) dz \right|}$$

is the transit-time factor. Thus, the accelerating voltage seen by the ideal beam travelling at $\beta_0 c$ is related to the voltage seen by the unideal beam by

$$\alpha_T = \frac{T(\beta_x)}{T(\beta_0)}$$

and so $V_{acc}(\beta_x) = \alpha_T \times V_{acc}(\beta_0)$.
According to SPL specifications, the beam accelerates from a kinetic energy of about 660 MeV to 5000 MeV in the high-beta section of the machine. This translates into a relativity factor of 0.81 at the beginning of the high-speed section. The following results depict what occurs when the 0.81 beam enters the first cavity in the high-beta section of the SPL.

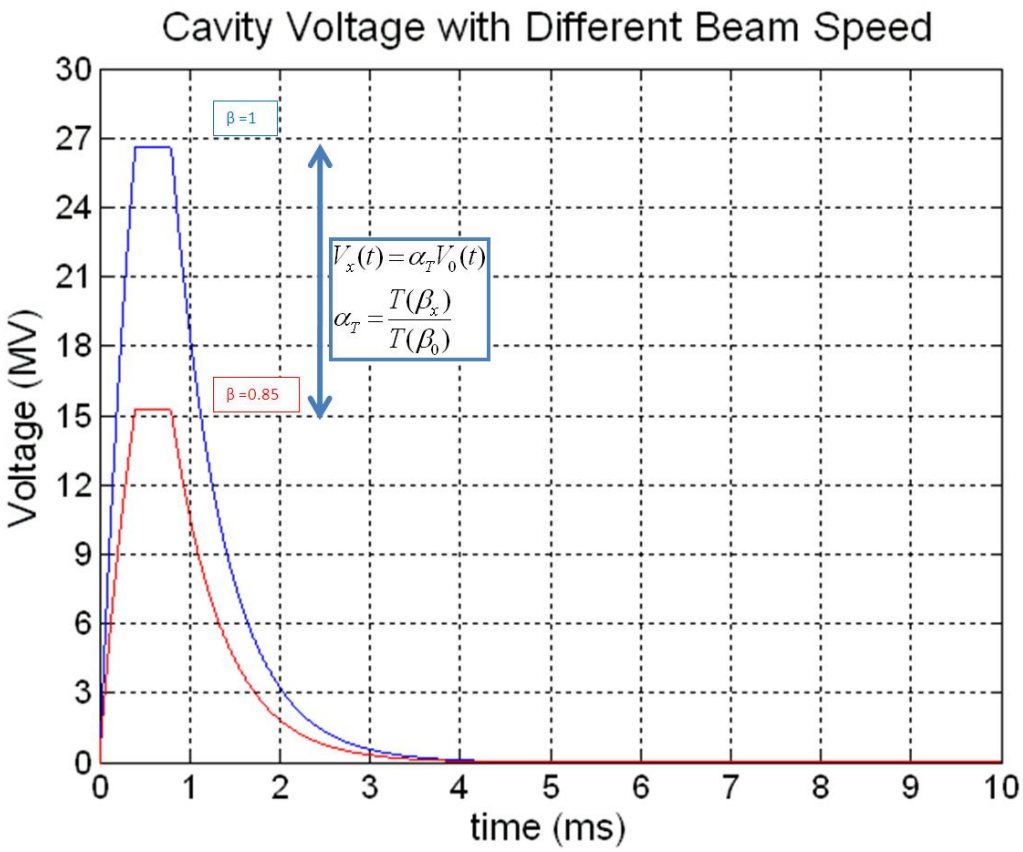

Figure 5.22: Cavity voltage envelope as seem by beams travelling at different speeds relative to the speed of light

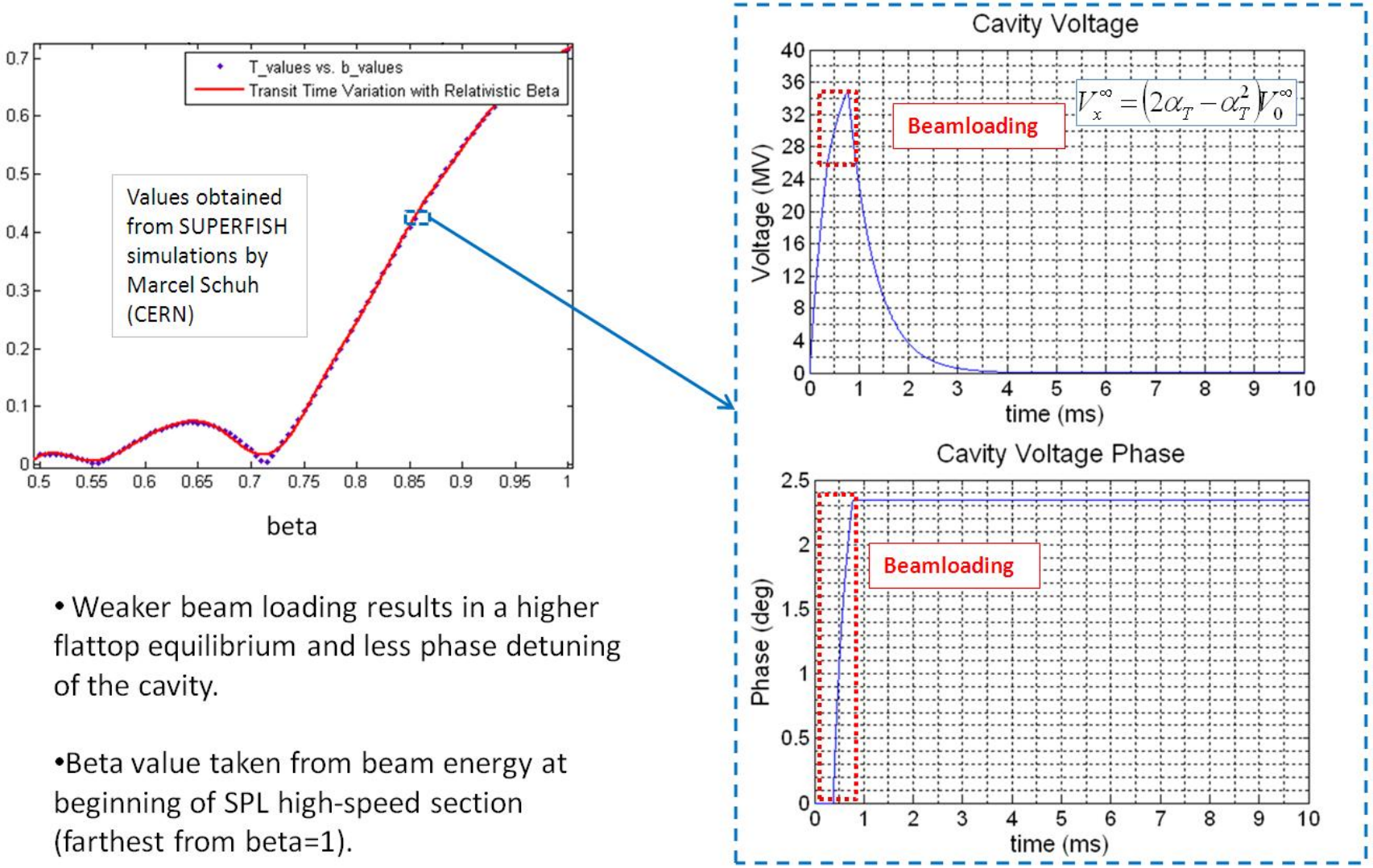

Figure 5.23: Voltage deviation due to suboptimal speed beamloading

Now, how do we maintain the cavity voltage during beamloading without disturbing the original generator pulse in terms of injection and pulse times. It is clear that the beamloading is now weaker than in the optimal case. This is why the voltage deviates from the flattop operation towards higher values as the generator supplies more power to the cavity than the beam is absorbing. A possible solution is, therefore, to change the shape of our generator pulse to drop in power by a calculated amount at the moment the beam arrives. This will result in the same filling and injection times for all cavities as the beam accelerates, with varying drops of forward power at injection time, pre-calculated in a feed-forward control scheme. Figure 5.24 shows in detail the resulting voltage and power signals using this scheme.
The new generator power is found using the same concept explained in chapter 2 to find the new equilibrium voltage. This time, we want to maintain the equilibrium voltage by changing the forward power to complement the effects of weaker beamloading. If we recall

$$\begin{aligned} Ig^{(0)} &= \frac{V_0^{(0)}}{(R/Q)_0 Q_L} + I^* \\ Ig^{(x)} &= \frac{V_x^{(x)}}{(R/Q)_x Q_L} + I^* \end{aligned} \tag{5.2}$$

Where $I^* = I_{b,DC}\cos\phi_s$. We need to find the new (virtual) generator current such that $V_0^{(0)} = V_x^{(0)} = \frac{V_x^{(x)}}{\alpha_T}$. Equating the voltages:

$$\begin{aligned} \big(Ig^{(0)} - I^*\big)(R/Q)_0 Q_L &= \frac{\big(Ig^{x} - I^*\big)(R/Q)_x Q_L}{\alpha_T} \\ \big(Ig^{(0)} - I^*\big) &= \alpha_T \big(Ig^{(x)} - I^*\big) \end{aligned}$$

and so finally, the new virtual current becomes

$$Ig^{(x)} = \frac{Ig^{(0)} + I^*(\alpha_T - 1)}{\alpha_T} \tag{5.3}$$

and the new power, which is absolute. is therefore given by

$$P_g = \frac{1}{4}(R/Q)_x Q_L \left| \frac{Ig^{(0)} + I^*(\alpha_T - 1)}{\alpha_T} \right|^2 \tag{5.4}$$

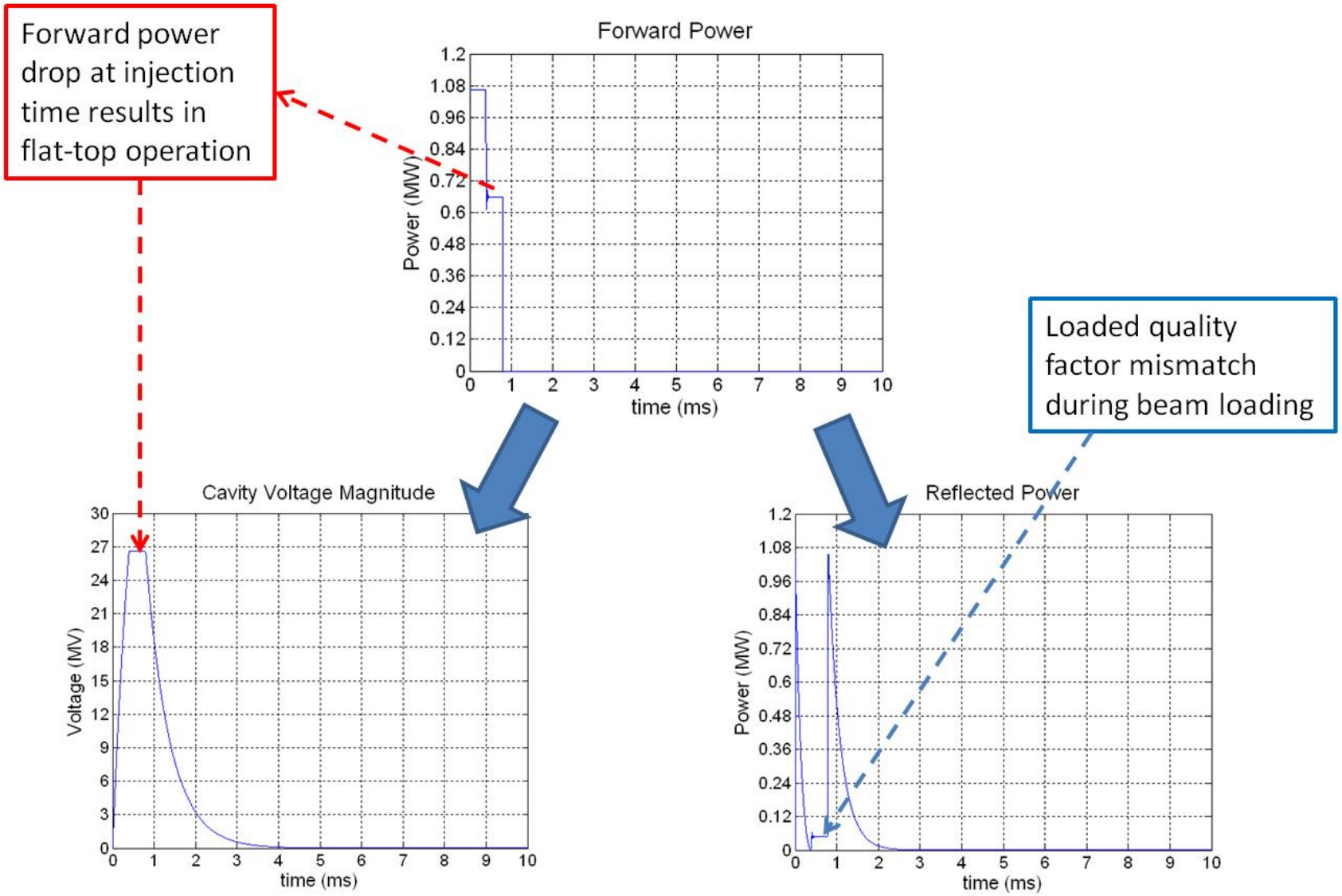

Figure 5.24: Suboptimal beam speed solution using feed-forward power drop at beam arrival

5.3.2 β=0.65 Cavities

The SPL low-beta cavities have different specifications from their counterparts in the high-speed section of the LINAC. In principle, however, there are no momentous differences between cavities with different geometric relativistic factors except in the ratio of their electric fields to accelerating voltage experienced by a certain beam. This means the following results will follow those before. The electric field gradient for the $\beta = 0.65$ section of the SPL was specified to $E_{acc} = 19.3$ MV/m, which results in an accelerating voltage of about $V_{acc} = 13.348$ MV. The forward power is accordingly lower. The results below show the nominal operation of the low-beta cavities under the effects of Lorentz detuning.

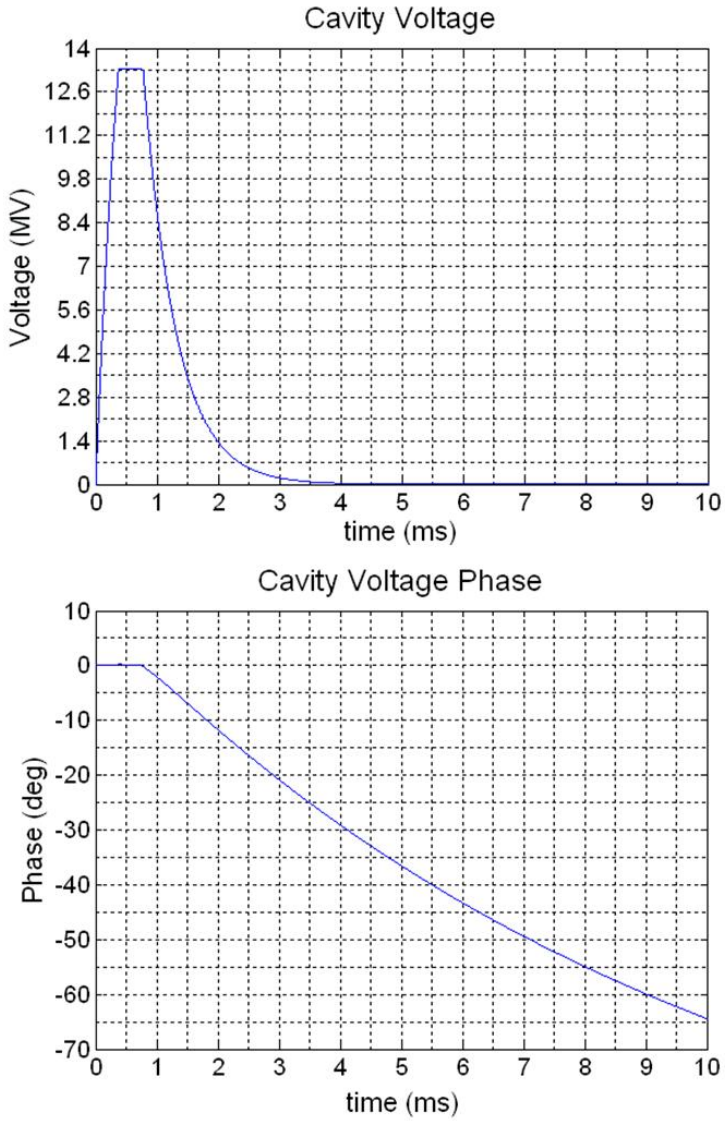

Figure 5.25: Cavity voltage magnitude and phase for correct β=0.65 cavity operation

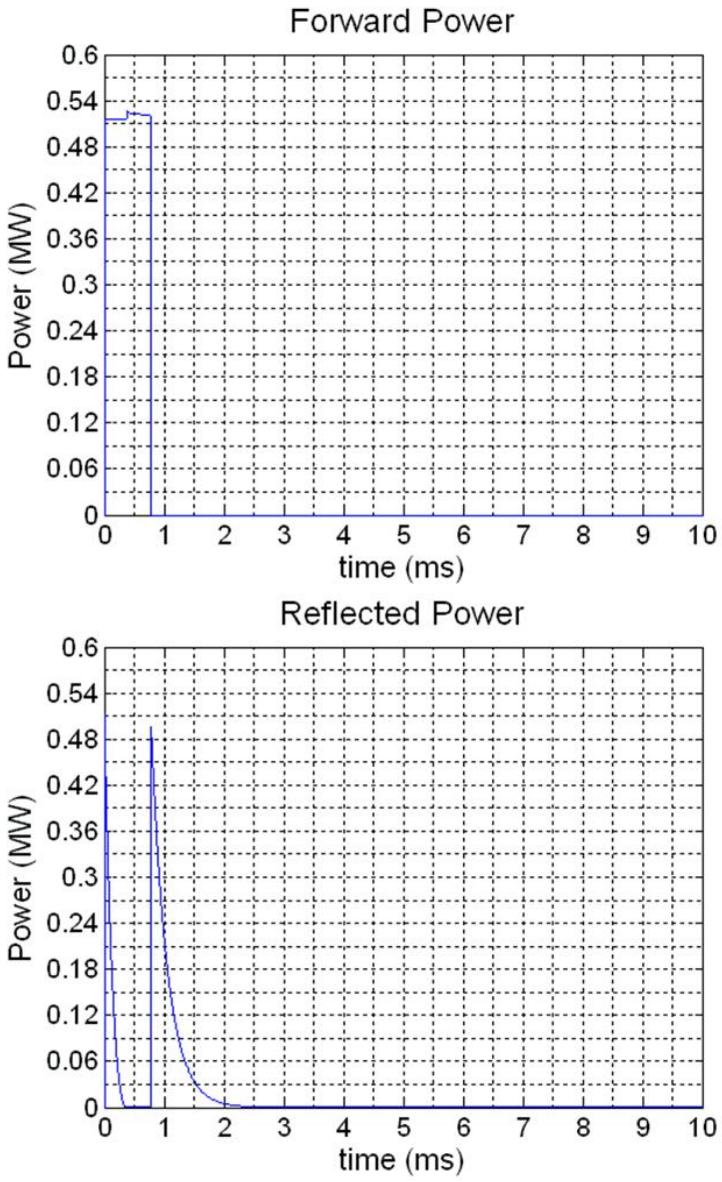

Figure 5.26: Forward and reflected power for correct β=0.65 cavity operation

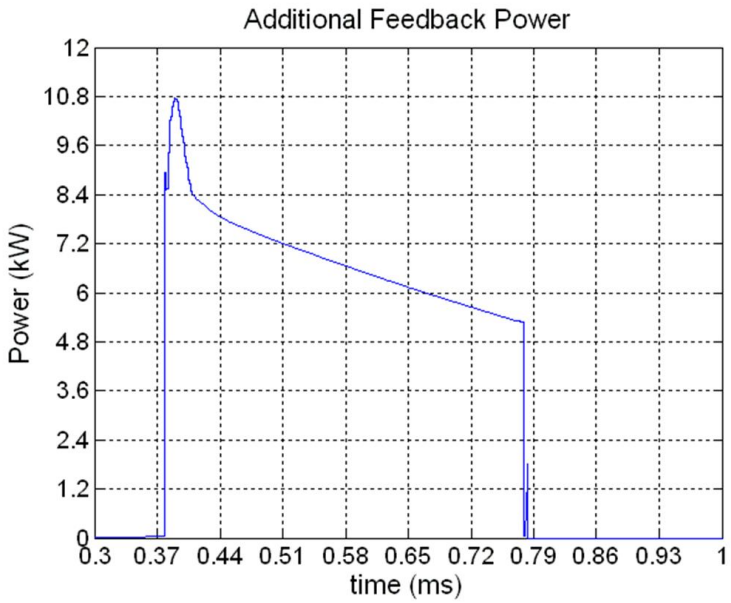

Figure 5.27: Additional power due to feedback correction

Now we investigate the effects of suboptimal beamloading on the cavity voltage. Of particular interest regarding to the low-beta cavities, is the fact that the design range of beam speeds for this section of the SPL is higher as this is the initial instance of beam acceleration. In the low-speed section of the LINAC, the beam accelerates from a kinetic energy of around 165 MeV to 660 MeV, which corresponds to relativity factors of 0.53 and 0.81 at the beginning and end of the machine respectively. The optimal acceleration occurs somewhere in the middle, the ideal energy being approximately 296 MeV. The solution is as displayed for the high-speed case.

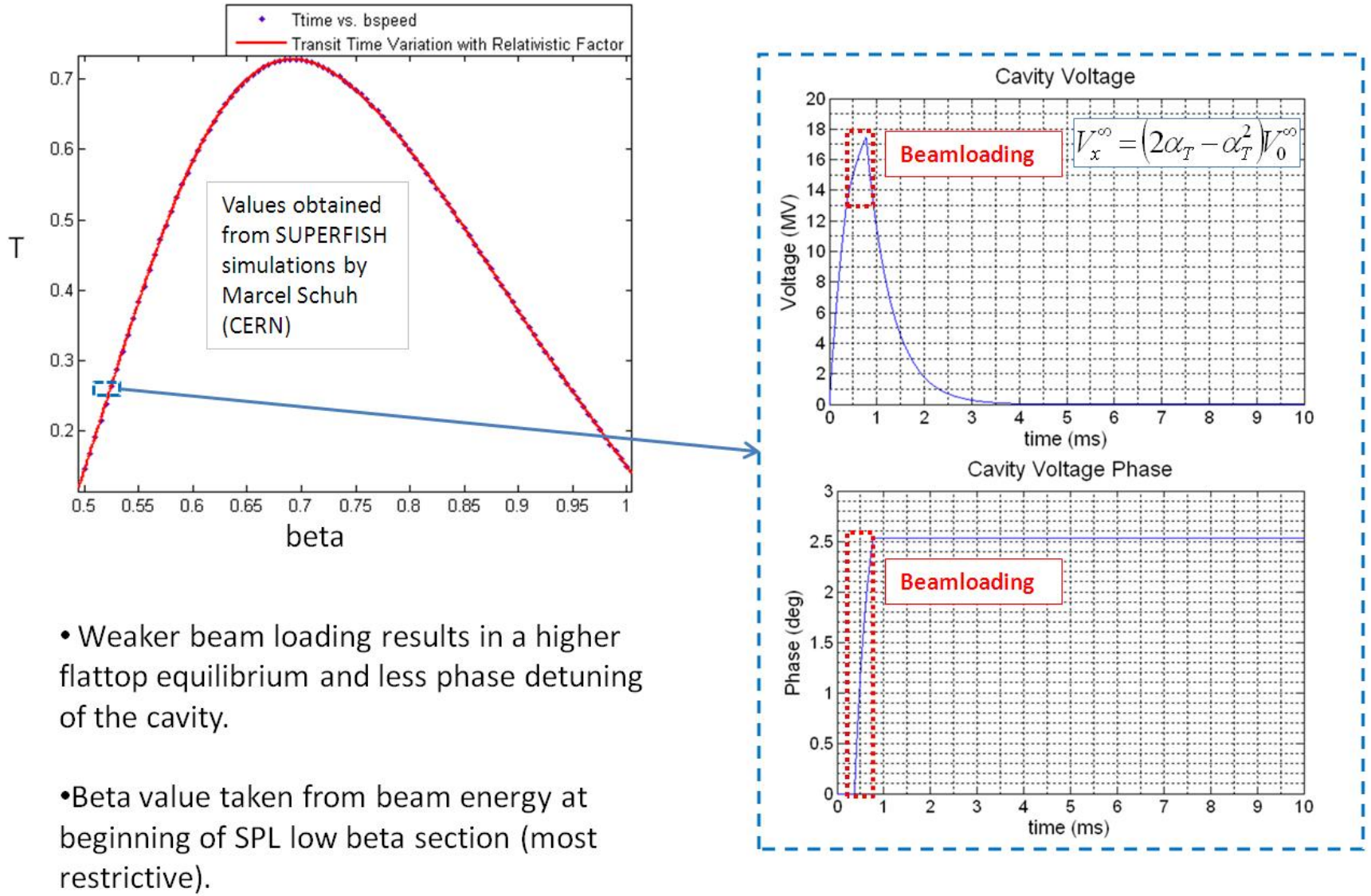

Figure 5.28: Voltage deviation due to suboptimal speed beamloading

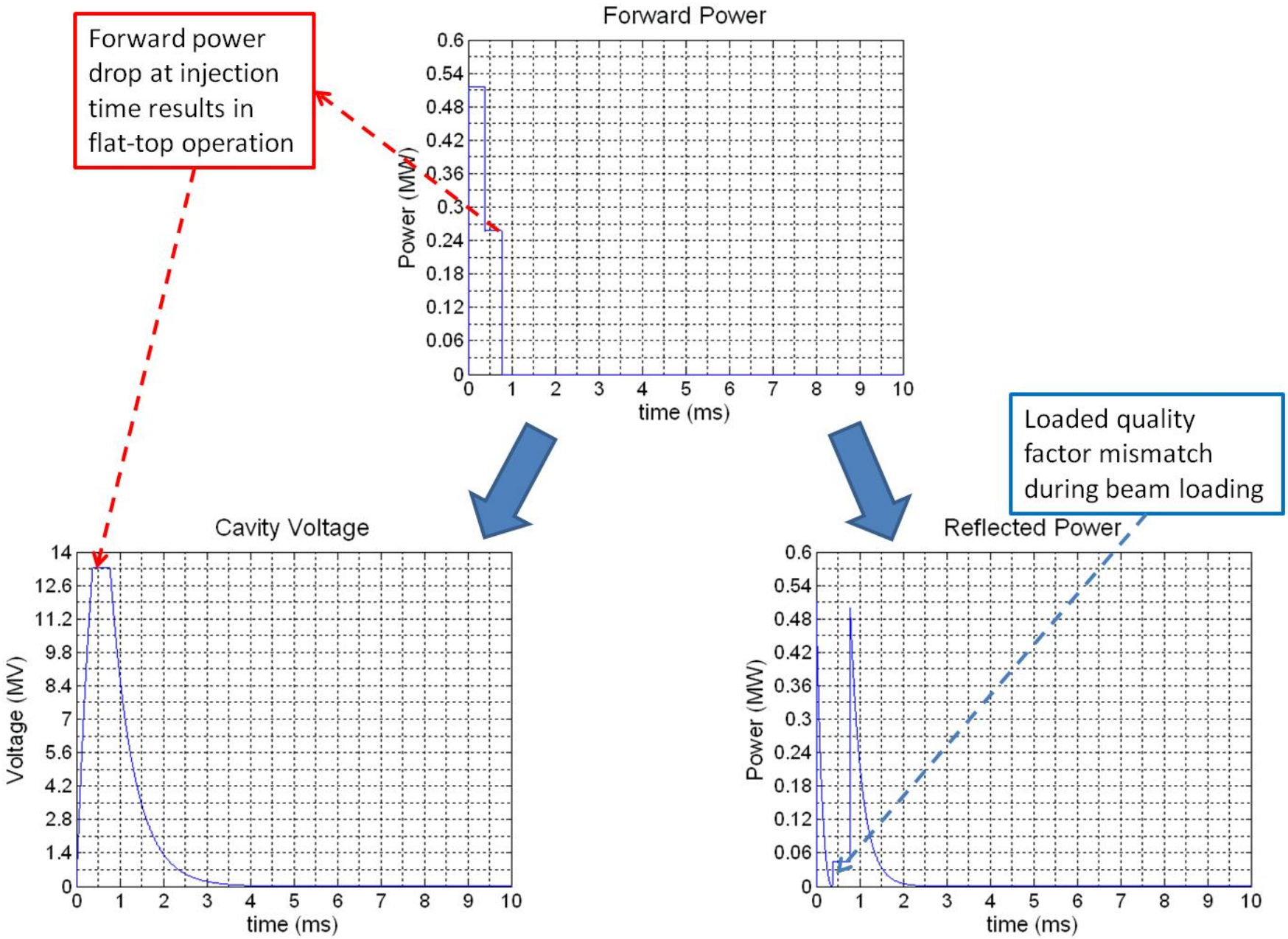

Figure 5.29: Suboptimal beam speed solution using feed-forward power drop at beam arrival

5.4 Dual-Cavity Case

5.4.1 The Need for Feed-Forward

In context with the superconducting SPL project, there are a few possible schemes to use as a solution for power requirements and design constraints. Until this point, this report has dealt with the case of one 1.6 MW Klystron driving a single cavity to accelerate a 40mA or 20mA beam, the following results deal with a different possible scheme in which a single Klystron will be used to supply two cavities, and the model is capable of dealing with a quad-cavity scheme driven by a single Klystron. As the results for the 4-cavity case do not reveal new information on the operation of the feedback and feed-forward loops, or on power requirements, the results are not displayed in this report. They are observable, however, using the graphical user interface. Figures 5.30, 5.31, and 5.32 below show the cavity voltage of both cavities separately and of their vector sum. The cavities are identical but for their Lorentz detuning coefficient (-1 and -0.5 $Hz/(MV/m)^2$ respectively). If we are able to control only the vector sum output of two cavities, it is possible, as the figures suggest, to observe a vector sum within specifications resulting from two cavities whose phases are well outside the acceptance range of 0.5 degrees. The cavity voltage magnitude is controlled acceptably for both cavities but, if the individual phase of each cavity is critical, the necessity for the addition of feed-forward becomes quite clear.

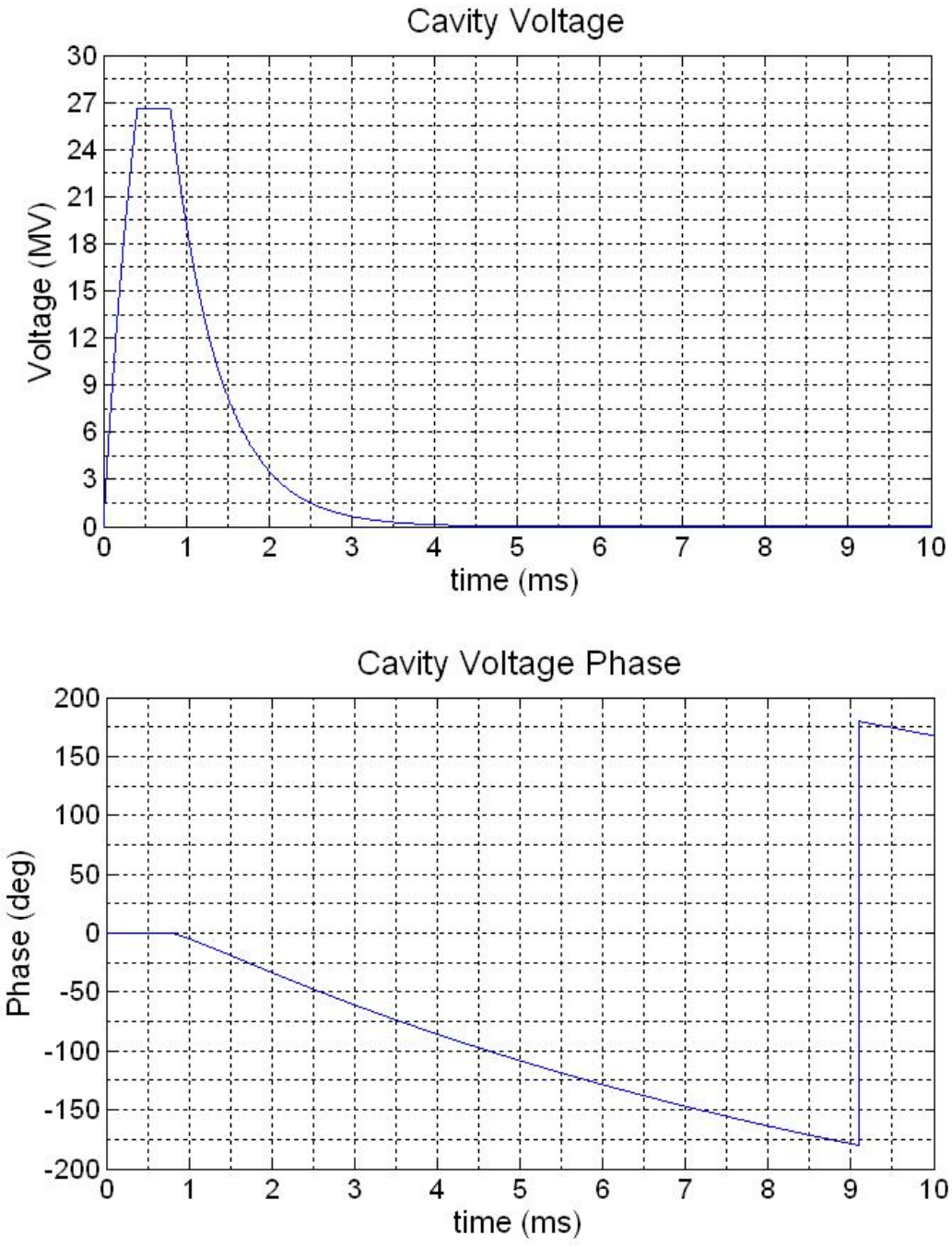

Figure 5.30: Cavity voltage magnitude and phase of vector sum output, feedback loop is ON

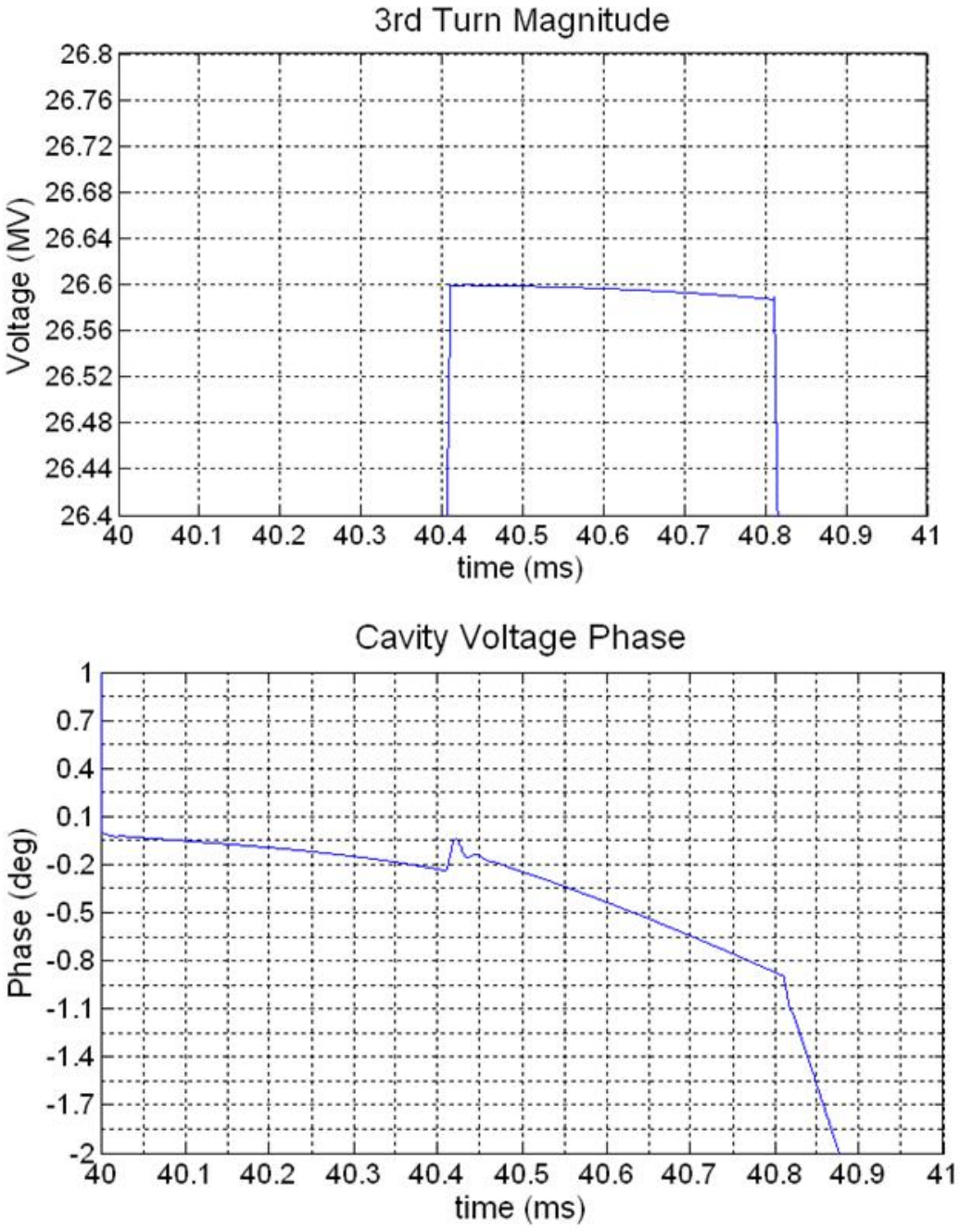

Figure 5.31: Cavity voltage magnitude and phase for cavity 1

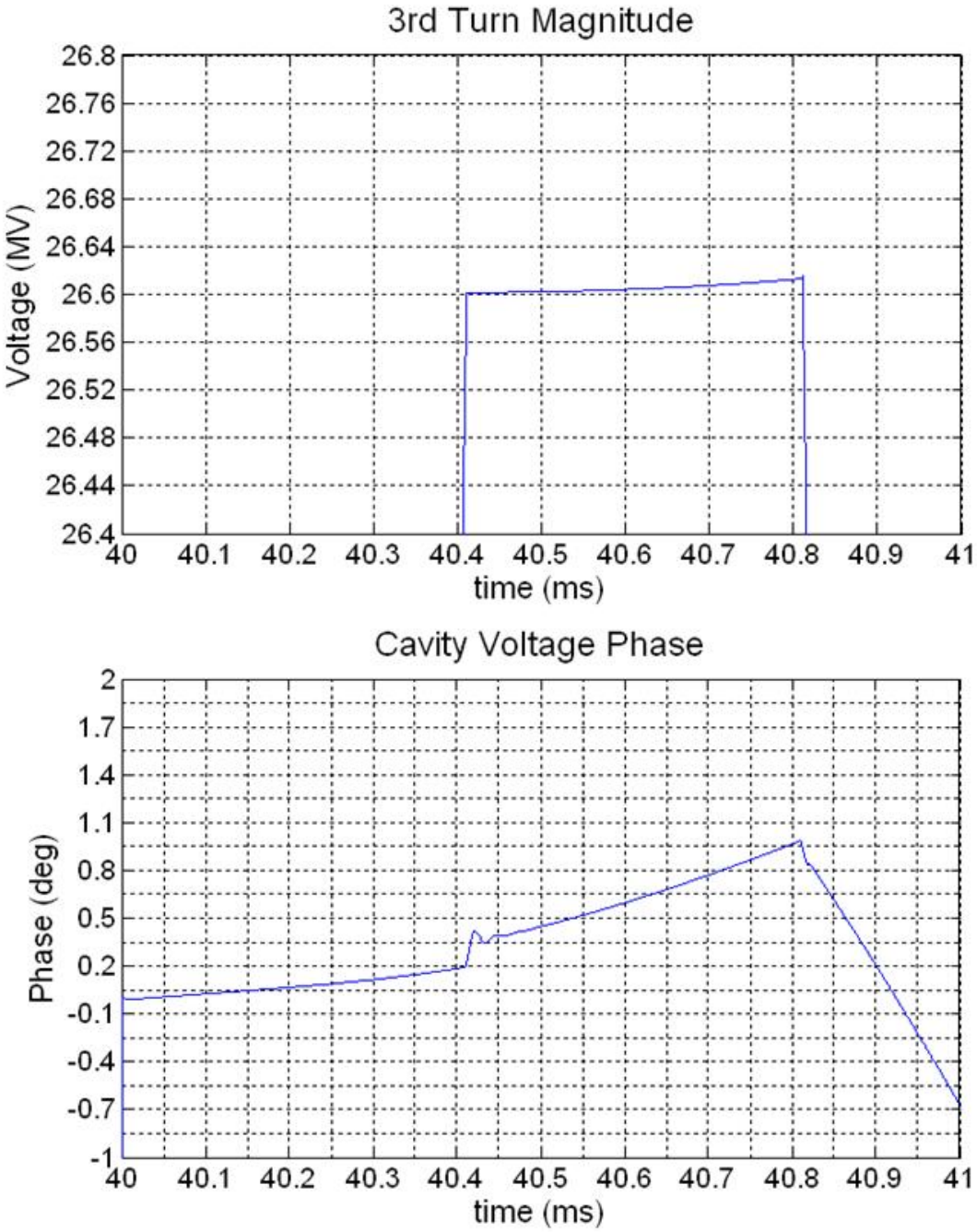

Figure 5.32: Cavity voltage magnitude and phase for cavity 2

5.4.2 Dual Cavity with Feed-Forward

The following results show the output of the cavity when using feed-forward. The model uses a piezo-electric tuner that acts on a measured cavity frequency deviation obtained from the forward voltage and cavity pickup voltage waveforms. The idea is to measure the frequency deviation during a given beam pulse and act on the next pulse, recursively calibrating the input to the piezo-electric system in order to obtain the best possible cavity tune for a given sampling rate and quantization. In the model, the measured frequency shift is directly subtracted from the actual detuning (also modelled) in an effort to imitate the effects of a similar waveform produced by the piezoelectric circuitry installed in the real cavities. There are a couple of shortcomings with this model that can be foreseen; first of all the piezo control has an additive recursion that can result in the addition of high-frequency errors (from the derivative part of the mathematical manipulation in the DSP board) and in addition there is the need for transfer function characteristics and power consumption of the piezoelectric circuit to really model the actual performance.

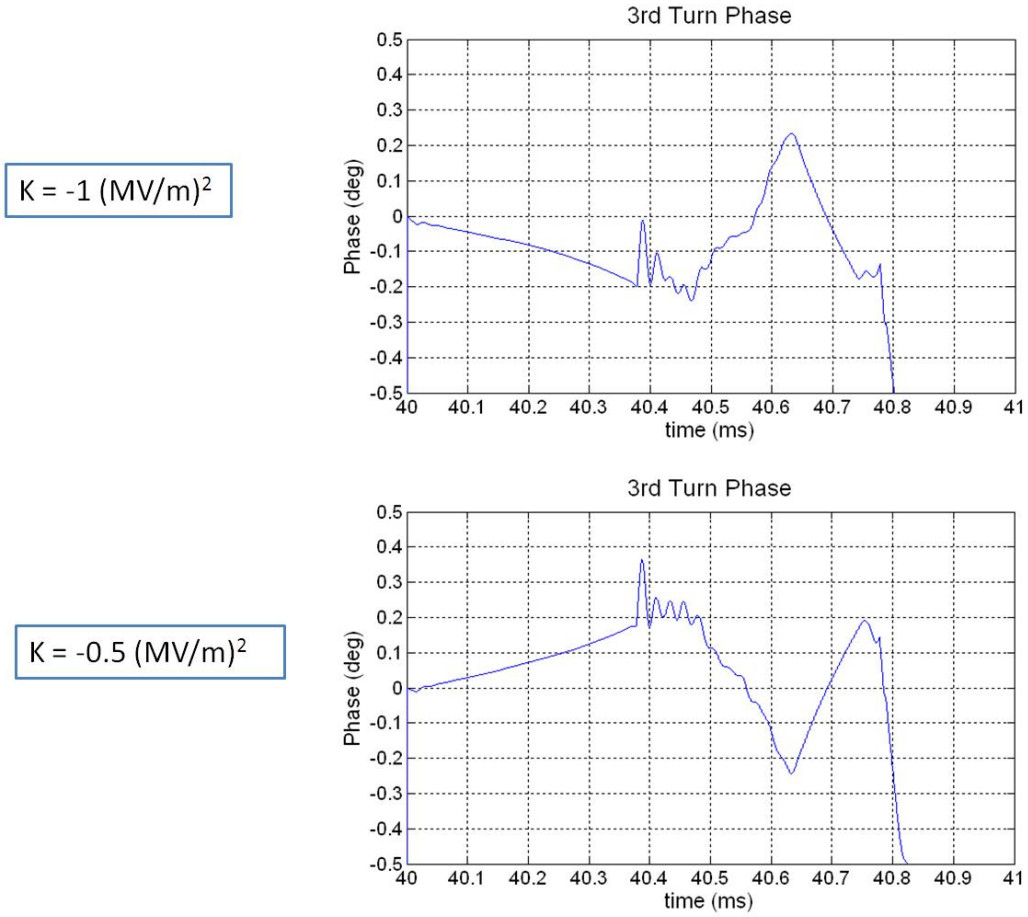

Figure 5.33: Cavity phase for cavities controlled by a single loop, feed-forward correction is applied

As can be seen in figure 5.34, the measured frequency corrections have increasing noise on each pulse. This is due to the fact that errors of this nature will be added

to the next correction effort as part of the measured frequency deviation. It might be necessary for prolonged operation of the system (which will most certainly be the case) to use some sort of average of the correction waveform or a high-performance filter.

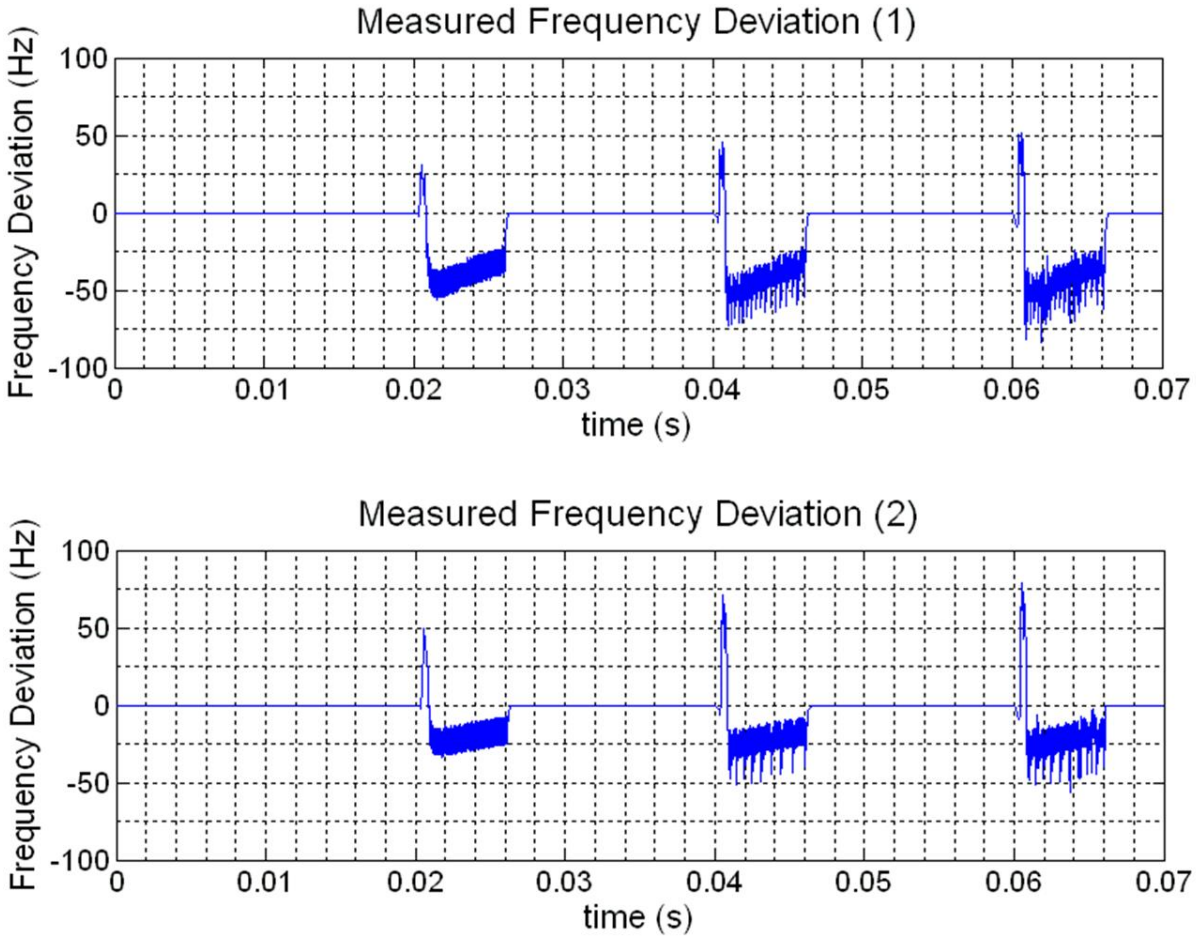

Figure 5.34: Recursively measured frequency corrections

5.4.3 Loaded Quality Factor Mismatch

As previously mentioned; when feeding multiple cavities using a single Klystron, it is not possible to control each cavity output individually, but rather the vector sum of each voltage. This means that there is nothing we can do with the control loop to compensate for variations within the individual cavities in loaded quality factor. The control loop will optimise the vector sum while the individual cavities might diverge from the specifications of SPL operation. According to modelling results, for the deviation constraints for the cavity voltage magnitude of +-0.5% of the total ($26.6 \times 10^6 MV$), we find that the limit of Q_L difference lies around 1.5% difference in value between both cavities, where the optimum value is 1.2078×10^6.

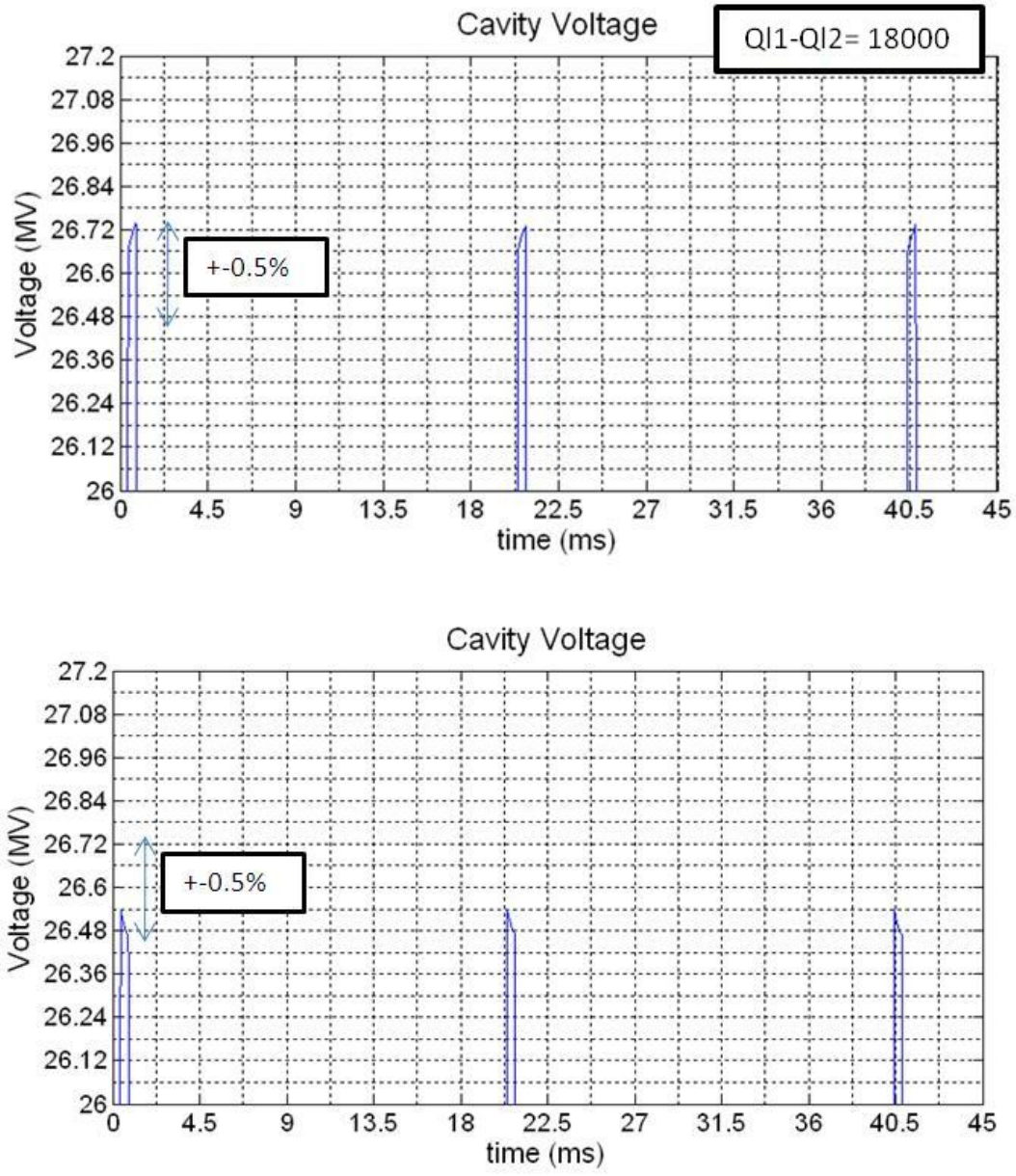

Figure 5.35: Effect of 18k (1.5%) difference between loaded quality factors of resonant cavities

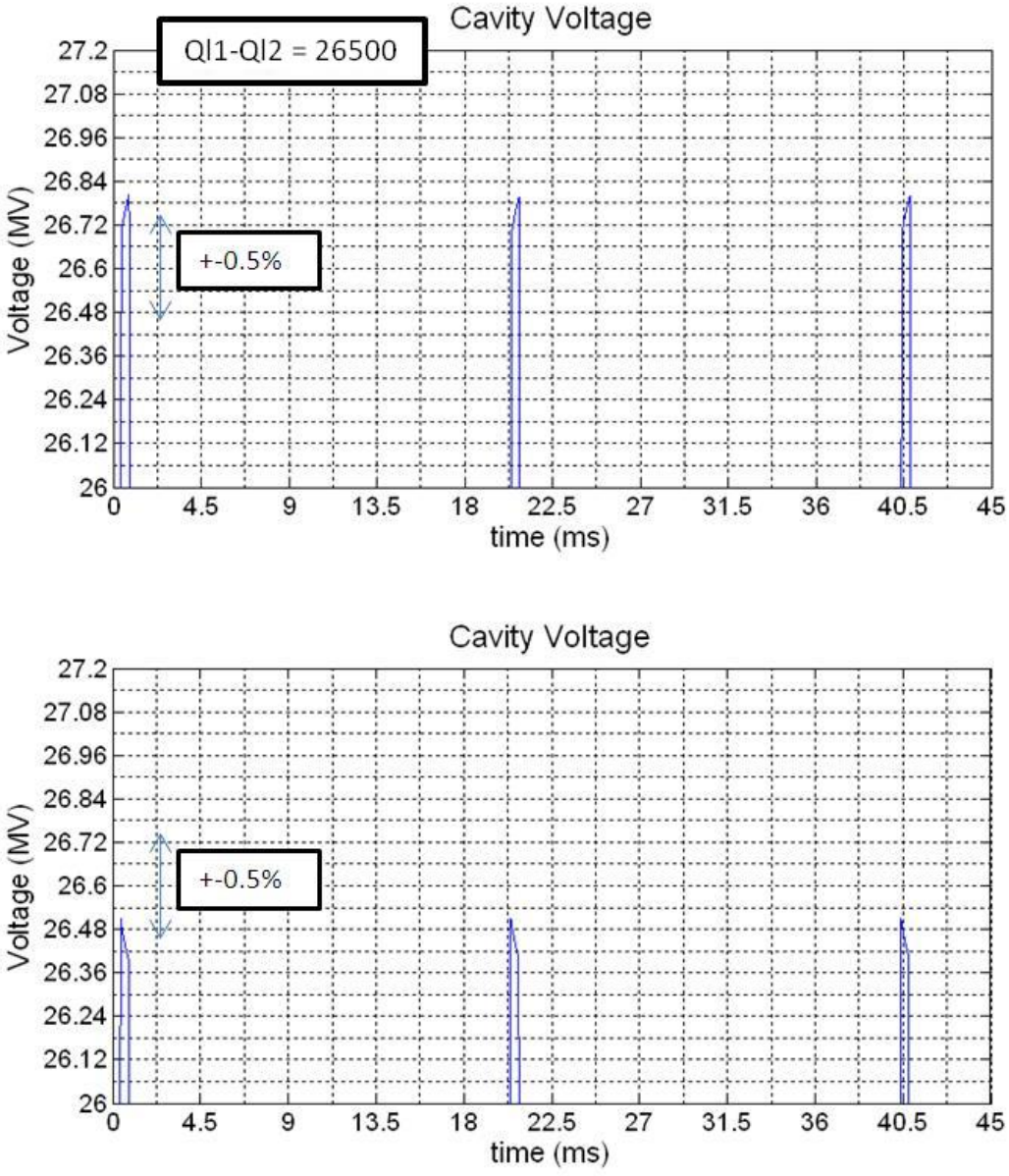

Figure 5.36: Effect of 26.5k (2.2%) difference between loaded quality factors of resonant cavities

At its most restrictive, the output specifications for the SPL in terms of energy jitter is of a maximum of 10 MeV peak to peak. Simulations of output jitter with different cavity voltage errors in magnitude and phase were carried out at CERN by Piero Posocco [20].
The figure below shows the probabilistic distribution of the beam jitter at the output of the SPL with different errors in cavity voltage magnitude and phase along its high-beta section. The first 5 curves (ranging from 0.5% to 5.0%) correspond to coupled magnitude deviations in cavity voltages, the next 3 (2.0% corr. to 5.0% corr.) refer to the same situation with an equal correction applied to the phase of each cavity to account for the cavity voltage magnitude deviation's effect on the beam synchronous angle at the beginning of the cavities. The next two observe the effects of Lorentz force detuning effects and the original constraints for completeness. All simulation results include the effects of input jitter (from LINAC4) and the low-beta section cavity voltage bounds of 0.5% in magnitude and 0.5 degrees in phase uncorrelated. If we take a probabilistic bound of 99% percent reliability of the output beam, it is clear that the maximum coupled magnitude deviation of the cavity voltage for the 2-cavity per feedback loop operation is of about 1.5% for the uncorrected phase operation (5 MeV taken as ideal bound), and in its best case 3%. This corresponds of a maximum deviation in loaded quality factor between adjacent cavities of around 5% and 10% respectively.

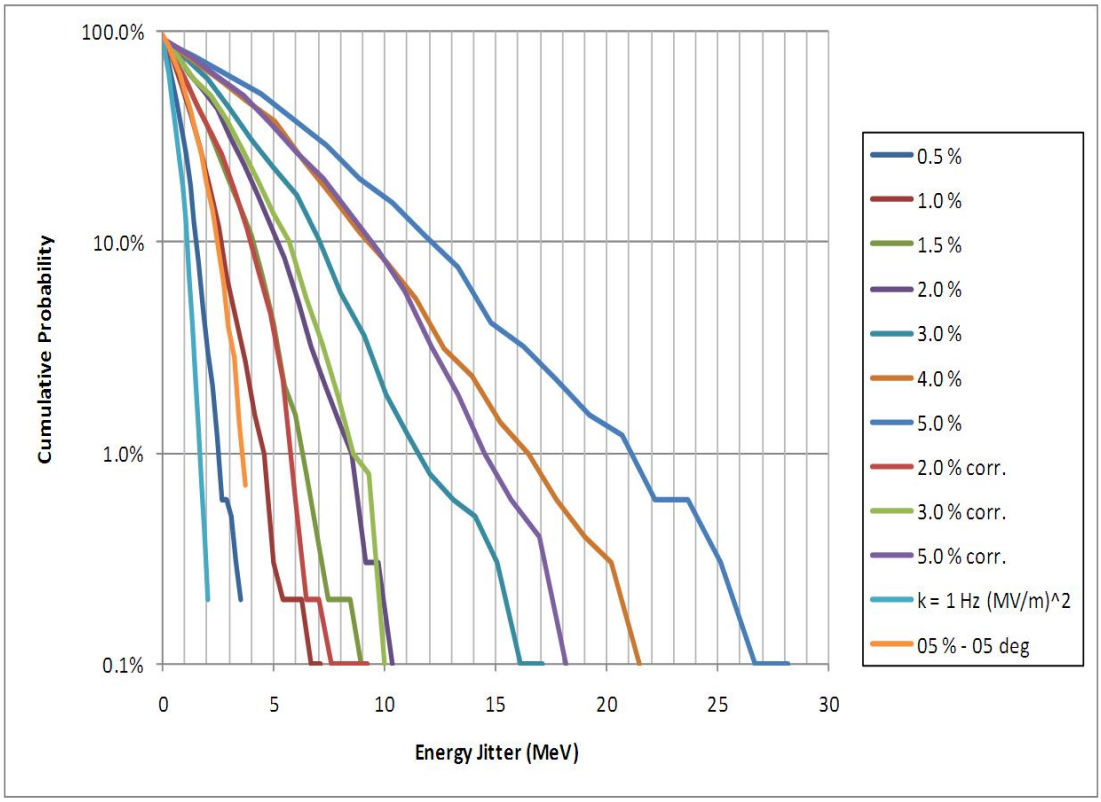

Figure 5.37: Probability distribution of energy jitter for different cavity voltage errors along SPL (figure taken from report by Piero Antonio Posocco at CERN) [20]

5.5 Full SPL Simulation Results

When a beam passes through a resonant cavity with a certain field inside, it creates an excitation on the system. This excitation is then corrected by the feedback loop, but a small spike still exists due to the feedback effort response to the change in setpoint of the system. This fact leads to believe that in every single cavity that the beam passes through, it will experience a small variation in effective voltage phase that will almost negligibly deteriorate the head of the beam pulse with respect to the majority of the bunches in the pulse. This effect, however, can accumulate over the 254 cavities in the LINAC and will result in an unacceptable deviation in terms of kinetic energy at the SPL output and time of flight (TOF) of the affected particles. The results below show the variation in relativistic factor along the beam pipe for a proton travelling with nominal acceleration as opposed to that which is affected by a 0.3 degree spike in synchronous angle. The cumulative effect clearly becomes unacceptable. The energy specifications at the output of the SPL allow for a maximum 0.1% variation from the nominal, which is of about 5 MeV.
In order to compensate for this effect, the simplest solution is to add a slow feed-forward excitation to the cavity before the arrival of the beam. The idea is to detune the voltage from its nominal offset to have a phase of -0.3 at the point of beam arrival. This results in the opposite experience of the beam to the normal feedback transient deviation. If we intersperse the feed-forward cleverly along the SPL, we can correct the beam deviation to minimal deviations from nominal which are within the required tolerances. The following results show the correction using intermittent feedback. It is interesting to note that matching the positive/negative phase arrangement to the cryostat layout of the SPL can significantly increase the correcting effect of this feed-forward scheme.

• The SPL is comprised of 254 cavities with RF phases that are designed to fit the acceleration of the hydrogen ion beam as it traverses its length.

• The cumulative effect of a 0.3 degree phase deviation on each cavity at beam arrival can result in merging of beam bunches and a deterioration in the output energy of particles.

•The difference in "time of flight" (ToF) for a single charge that receives full acceleration as opposed to that which experiences a 0.3 degree deviation at arrival on each SPL cavity, is two orders of magnitude higher than the bunch separation.

•The kinetic energy variation from nominal at SPL output is higher than 0.1%

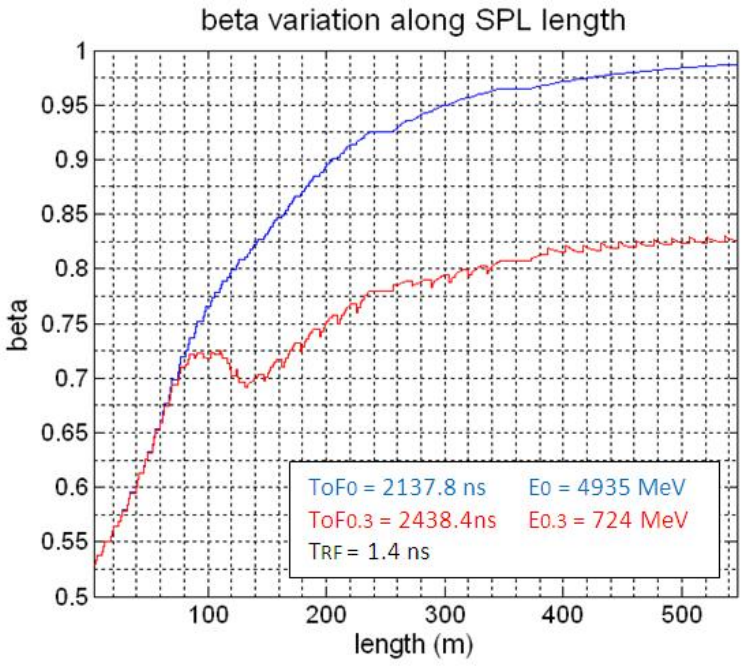

$ToF_{0.3} - ToF_0 >> T_{RF}$

$dE_{0.3deg} >> 0.1\% E_o$

Figure 5.38: Beam deterioration due to cumulative effect of accelerating voltage phase deviation

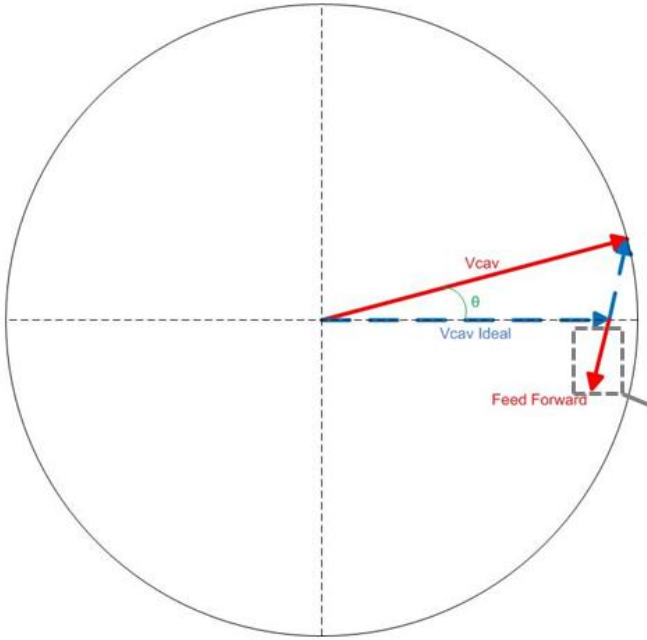

• We measure the vector deviation of the cavity voltage from its ideal and add an excitation to the power source feeding the cavity that nullifies it.

• The excitation to the power source (generator current) is dependent on the transient relationship between cavity and generator.

$$V_{cav}(t) = R_L I_g \left(1 - e^{\frac{-t}{t_{fill}}}\right)$$

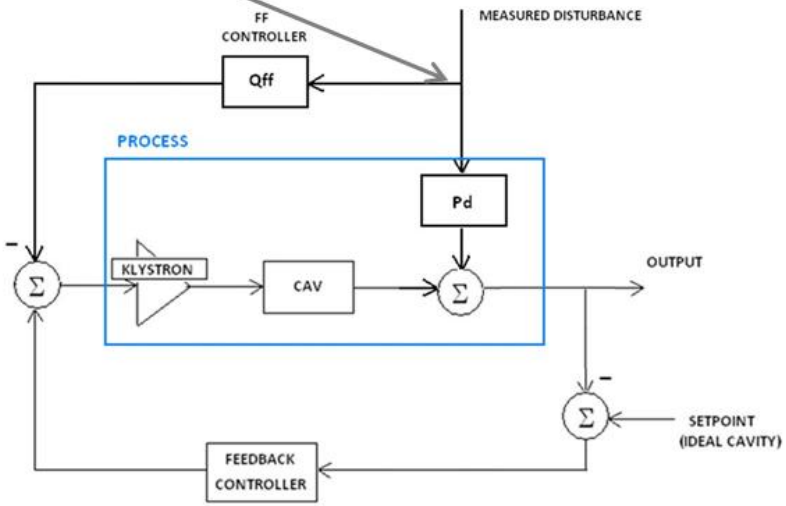

Figure 5.39: Slow feed-forward scheme using small excitation

• Easiest solution is to intersperse slow feed-forward so that each SPL cavity will have the opposite error from the preceding one along the accelerator.

• In this way, particles travelling along the LINAC will not experience an accumulated deviation.

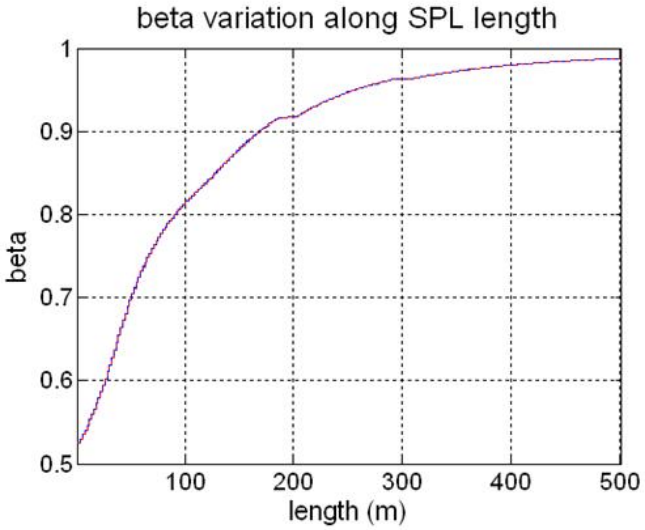

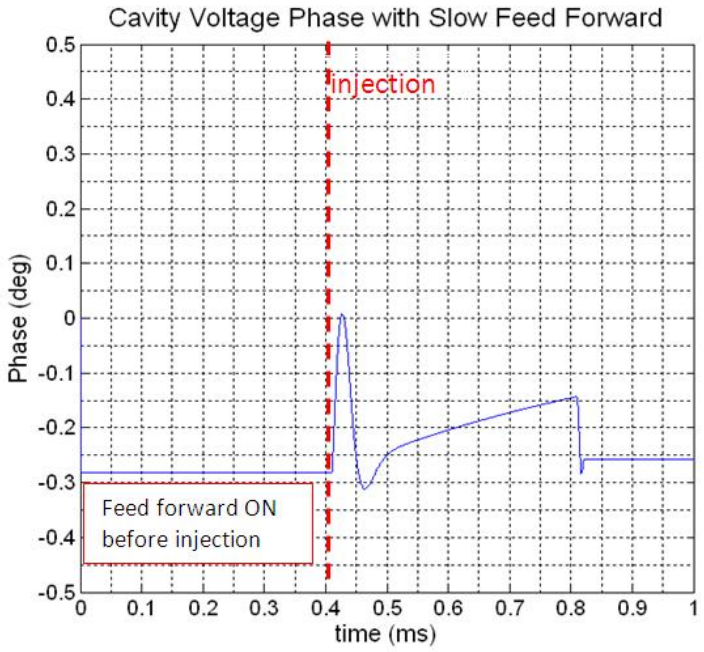

$ToF_{0.3} - ToF_0 < T_{RF}$

$dE < 0.1\%\ Eo$

Figure 5.40: Beam deterioration solution: randomising cumulative phase effects

5.6 Further Analysis and Stability Considerations

Until this point in the report, we have shown the versatility of the model with regard to the stabilisation of the electric field within superconducting RF resonant cavities with the specifications needed to build the SPL. However, no analysis is full without pointing out some of the limitations of the system. As shown in the last chapter, a >1.5% difference in the cavities' quality factor can result in a deviation on cavity voltage magnitude that cannot be resolved using feedback or feed-forward when more than a single cavity is driven by one Klystron. The feedback loop compensates the vector sum of the cavity voltages, keeping it within specifications (0.5% magnitude and 0.5° phase deviations), but that does not mean that each cavity separately is also exhibiting the same behaviour. The cavity voltage magnitudes vary with the difference in the loaded quality factors and their magnitudes and phases vary with the difference in their Lorentz detuning coefficients. To observe the extent of these variations, a simulation "sweep" was carried out, recording the voltage magnitude difference at the output, as well as the phase difference (voltage of cavity 1 minus voltage of cavity 2). For both the loaded quality factor (Q_L) and Lorentz detuning coefficient sweeps (K), it was found that fitting a curve based on the results was more suited than an analytic approach. With this curve, an exhaustive analysis using a model for the whole SPL length can be developed as a parallel project, to observe if the beam cannot ultimately tolerate the single cavity variations even though their overall effect (vector sum) might appear within specifications. The results are as follows:

Cavity voltage difference between two cavities with different loaded quality factors

$Q_{L\_optimal} = 1.2078 \times 10^6$

Measurements of the voltage difference between both cavities were taken with feedback control on their vector sum. As the quality factor of the cavities has no impact on their voltage phases, the analysis is restricted to cavity voltage magnitudes. The sweep was done using values for Q_{L1} and Q_{L2} (for cavities 1 and 2 respectively) from 1e6 to 1.5e6 at 1e4 intervals resulting in 51 different values of Q_L and 51*51=2601 different Q_{L1}, Q_{L2} combinations minus redundant values. Thus, the obtained $V_{diff} = f(Q_{L1}, Q_{L2})$ curve was fitted using 1326 points. The polynomial equation relating the voltage output difference to the individual loaded quality factors of the cavities was found to be of the form

$$V_{diff}(x, y) = p00 + p10x + p01y + p20x^2 + p11xy + p02y^2 \tag{5.5}$$

where $x = Q_{L1}$ and $y = Q_{L2}$, with coefficients:

$p00 = 1.742 \times 10^6$
$p10 = 34.63$
$p01 = -37.44$

$p20 = -8.286 \times 10^{-6}$
$p11 = 1.477 \times 10^{-7}$
$p02 = 9.261 \times 10^{-6}$

Figure 5.40 below shows the curve fit. The blue points are given by model experimental results, while the continuous plane is given by the equation above. The individual cavity voltages can be reproduced as $V_{cav1} = V_{acc} + \frac{V_{diff}}{2}$ and $V_{cav2} = V_{acc} - \frac{V_{diff}}{2}$, where the low voltage corresponds to the cavity with lower Q_L.

Cavity voltage difference between two cavities with different Lorentz detuning coefficients

K_optimal= 0 Hz/(MV/m)²

As before, measurements were taken in closed-loop operation with no feed-forward. In this case, however, both the cavity voltage magnitude and phase are affected by varying Lorentz detuning coefficients. Two curves are therefore fitted, with values of K from -1 Hz/(MV/m)² to 0 Hz/(MV/m)² using 0.01 Hz/(MV/m)² intervals (5151 points). Figures 5.41 and 5.42 show the fitted surfaces for magnitude and phase difference respectively. The respective polynomials for the voltage magnitude and phase difference were found to be:

$$V_{diff}(x, y) = p00 + p10x + p01y + p20x^2 + p11xy + p02y^2 \tag{5.6}$$

with coefficients:

$p00 = -8.644$
$p10 = -3.062 \times 10^{14}$
$p01 = 2.988 \times 10^{14}$
$p20 = -3.061 \times 10^{28}$
$p11 = 2.37 \times 10^{26}$
$p02 = 3.037 \times 10^{28}$

and:

$$V_{diff}(x, y) = p00 + p10x + p01y \tag{5.7}$$

with coefficients:

$p00 = 6.801 \times 10^{-4}$
$p10 = 3.5 \times 10^{12}$
$p01 = -3.498 \times 10^{12}$

where x=K1 and y=K2.

Once again, the individual cavity voltage magnitudes can be found using the aforementioned formula centered at Vacc. The phase equation is centered at 0°.

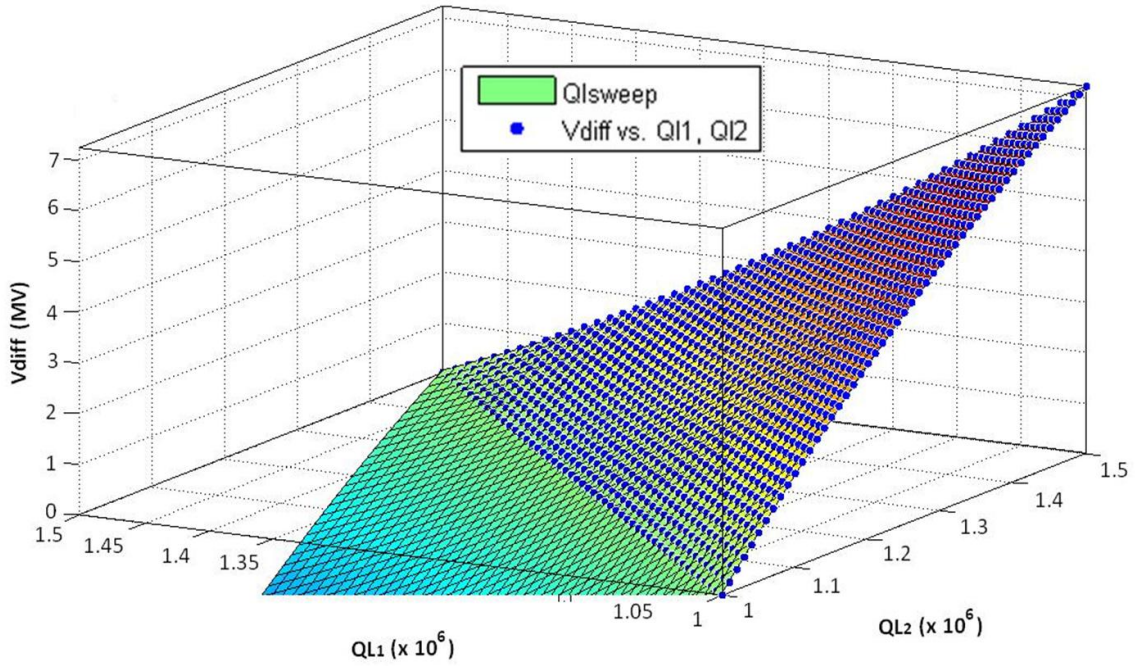

Figure 5.41: Curve fit for cavity voltage difference with varying loaded quality factor

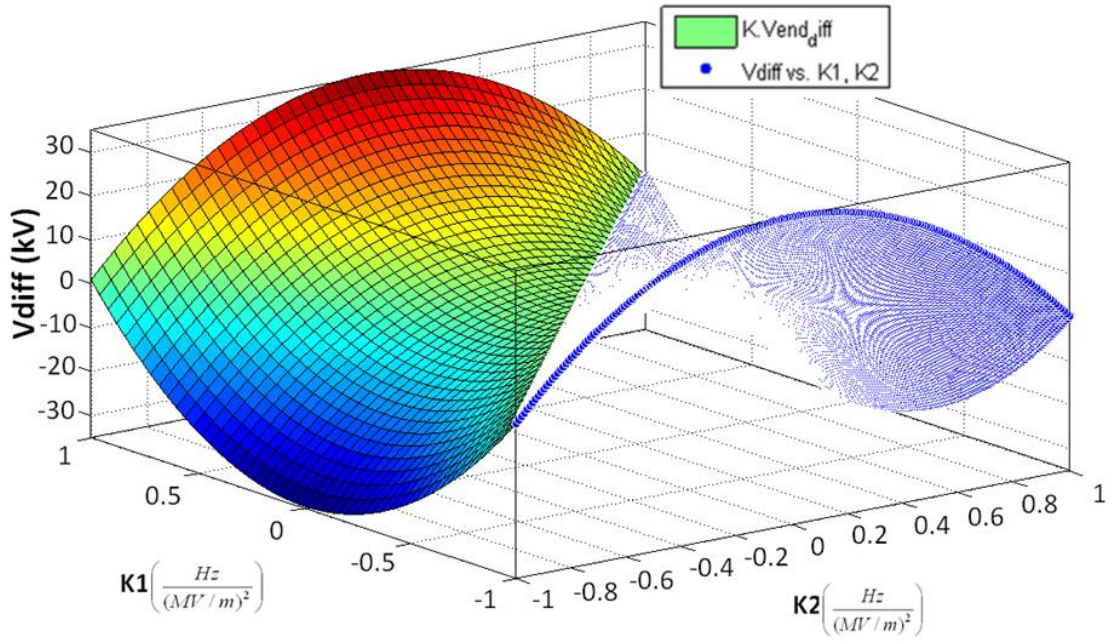

Figure 5.42: Curve fit for cavity voltage magnitude difference with varying Lorentz force detuning

All system configurations described are part of an analysis whose goal is to prove the viability of a superconducting, high-power proton LINAC from the point of view of

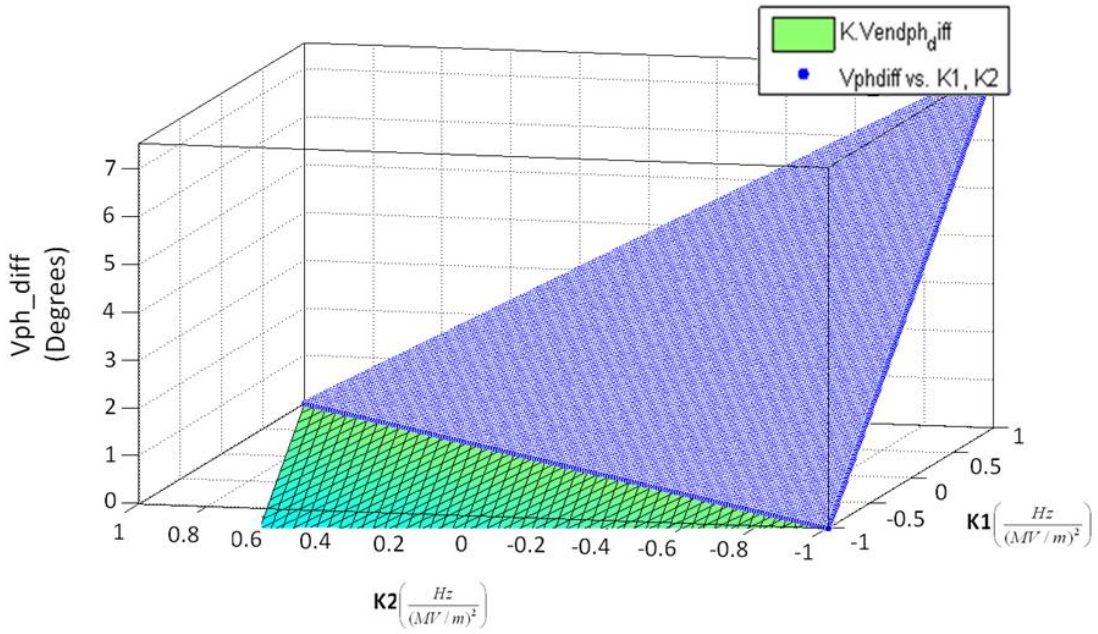

Figure 5.43: Curve fit for cavity voltage phase difference with varying Lorentz force detuning

the RF systems. The SPL is not only a challenge because of the energies and bunch densities involved, but the fact that the underground cavities are driven by pulsed klystrons operating from the surface adds complexity to the situation. The time delay of the feedback loop becomes an issue when the connectors are of considerable length, and the operating frequency of the system is of the order of hundreds of megahertz. In addition to this effect, pulsed generators introduce transients to the system with components in the whole frequency spectrum. A feedback delay of 5 us is included in the model, and stability analysis was carried out using low-pass filters to model the feedback loop and generator frequency responses. Finally, the proportional feedback gain was set to ensure that the system is stable [21] [22]. The open-loop transfer function is given by:

$$H_{SPL}(s) = H_{FB}(s)H_{Kly}(s)H_{Cav}(s)H_{Delay}(s)H_{probe}(s) \tag{5.8}$$

where

$$H_{FB}(s) = \frac{G_{FB}}{\frac{s}{2\pi f_{cFB}} + 1} \qquad H_{Kly}(s) = \frac{G_{FB}}{\frac{s}{2\pi f_{cKly}} + 1} \tag{5.9}$$

$$H_{probe}(s) = G_{probe} \qquad H_{Delay}(s) = e^{-s\tau} \tag{5.10}$$

$$H_{Cav} = \begin{bmatrix} H_s(s) & -H_c(s) \\ H_c(s) & H_s(s) \end{bmatrix} \tag{5.11}$$

The cavity self and cross-coupled transfer functions are given by

$$
\begin{aligned}
H_s(s) &= \sigma R \left[\frac{s + \sigma\left(1 - \frac{\Delta\omega}{\omega_R}\right)}{(s+\sigma)^2 + (\Delta\omega)^2} \right] \\
H_c(s) &= \frac{\sigma^2 R}{\omega_R} \left[\frac{s + \left(\sigma + \frac{\omega_R \Delta\omega}{\sigma}\right)}{(s+\sigma)^2 + (\Delta\omega)^2} \right]
\end{aligned}
\tag{5.12}
$$

where

$$\sigma = \frac{\omega_R}{2Q_L}$$

ω_R is the resonant frequency of the cavity, and $\Delta\omega = \omega_R - \omega_0$ is the frequency deviation between RF source and resonant frequency of the system. The value was chosen as the maximum value observed in simulations.

We find that the problem of observing the characteristics of the system transfer function is not as straightforward as expected, as the behaviour of the model is the result of a coupled action between in-phase and quadrature signal components. The output of the system can be expressed using the following coupled equations:

$$
\begin{aligned}
Y_I(s) &= H_K(s)H_s(s)X_I(s) - H_K(s)H_c(s)X_Q(s) \\
Y_Q(s) &= H_K(s)H_s(s)X_Q(s) + H_K(s)H_c(s)X_I(s)
\end{aligned}
\tag{5.13}
$$

where

$$H_K(s) = H_{FB}(s)H_{Kly}(s)(s)H_{Delay}(s)H_{probe}(s)$$

I/Q refer to inphase and quadrature components, and s/c refer to the self and cross-coupled components of the cavity transfer function respectively. X and Y are inputs and outputs to the system. If we assume a purely inphase unit step input to the system to begin with, the system equations simplify to yield

$$
\begin{aligned}
Y_I(s) &= H_K(s)H_s(s)X_I(s) \\
Y_Q(s) &= H_K(s)H_c(s)X_I(s)
\end{aligned}
\tag{5.14}
$$

and so we can investigate the stability behaviour of the system by analyzing the transfer function given by

$$H_K(s)\big(H_s(s) + iH_c(s)\big)$$

in both magnitude and phase.
We want to find G_{FB} such that the open-loop transfer function is such that the closed-loop system is stable. For a feedback loop with a 100 kHz bandwidth and a 1 MHz bandwidth klystron driving an SPL cavity at its resonant frequency of 704.4 MHz, we find a gain margin of about 43 dB (x150) as shown in figure 5.43.

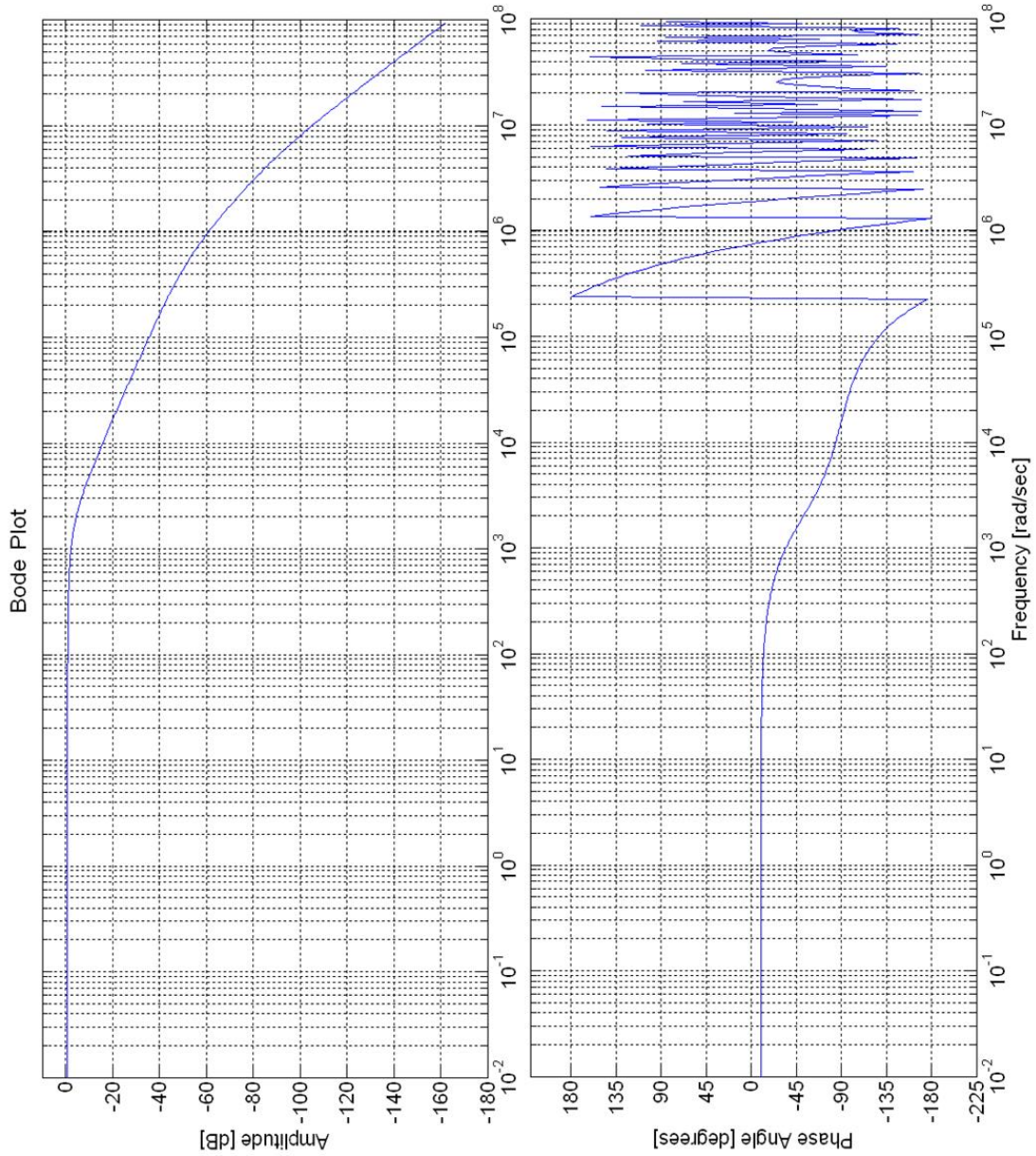

Figure 5.44: Bode plot of open-loop system

Chapter 6

Conclusion and Outlook

Through the course of this report, a detailed analysis of a model for controlling the beam acceleration along the superconducting proton linear accelerator has been described. The system consists of 254 accelerating structures with individual control loops ensuring rigorous beam specifications in terms of output energy and time-structure. At its most restrictive of configurations, the SPL low speed section will consist of 54 $\beta = 0.65$ resonant cavities accelerating a 40 mA beam with a time-structure of 0.4 ms pulses repeating every 20 ms with an accelerating field strength close to 19 MV/m, while the high speed 200 $\beta = 1$ cavities will reach electric fields of 25 MV/m. The challenges arise from the fast-pulsing H^- source and the high fields within the thin walled niobium cavities, where Lorentz force effects induce a deformation in shape, resulting in a detuning in resonant frequency. The control for the low-speed section includes dedicated RF loops acting on a single klystron per cavity scheme whereas the high-speed section favours a 2 cavity per klystron configuration with control loops acting on the vector average of the cavity voltages in terms of magnitude and phase. This gives rise to problems in dealing with slightly mismatched cavities in terms of Lorentz detuning factor and loaded quality factors. A piezo-electric system is in place to oppose the effects of Lorentz deformations and full SPL simulation reveal a best case of just under 10% loaded quality factor mismatch between adjacent cavities from ideal value. Fast RF feedback and slow feed-forward are intended for compensating synchronous angle effects and cumulative phase errors, as well as other non-foreseeable or uncharacterised errors.
From the RF control point of view, there is strong evidence to support the development of an I/Q system that can be successful in dealing with the foreseeable drawbacks that arise when attempting an engineering feat of this magnitude.

Bibliography

[1] R. Garoby *et al.*, "**Project Periodic Report**," tech. rep., sLHC-PP Project, CERN, Geneva, Switzerland, May 2010.

[2] J. Le Duff, "**High Frequency Non-Ferrite Cavities**," in *Cern Accelerator School Proceedings*, Seeheim, Germany, May 2000. Edited by J. Miles, CERN-2005-003, p. 47.

[3] T. Weiland, M. Krasilnikov, R. Schuhmann, A. Skarlatos, and M. Wilke, "**Review of Theory (I, II, III)**," in *Cern Accelerator School Proceedings*, Seeheim, Germany, May 2000. Edited by J. Miles, CERN-2005-003, p. 1.

[4] T. Schilcher, ***Vector Sum Control of Pulsed Accelerating Fields in Lorentz Force Detuned Superconducting Cavities***. PhD thesis, Hamburg University, Hamburg, Germany, April 1998. TESLA-98-20.

[5] J. Tuckmantel, "**Cavity-Beam-Transmitter Interaction Formula Collection with Derivation**." Internal Note, CERN-ATS-NOTE-2011-002 TECH.

[6] P. B. Wilson, "**Transient Beam Loading In Electron - Positron Storage Rings**," Preprint, CERN-ISR-TH-78-23-rev.

[7] D. Boussard, "**Beam Loading**," Preprint, CERN-SPS-86-10-ARF.

[8] F. Gerigk, "**SPL Web**." `https://twiki.cern.ch/twiki/bin/view/SPL/SplWeb`.

[9] F. Gerigk, "**SPL parameter table**." `https://twiki.cern.ch/twiki/bin/view/SPL/SPLparameterList`.

[10] W. Hofle, "**SPL LLRF Simulations Feasibility and Constraints for Operation with more than one Cavity per Klystron Power Overhead**," in *3rd SPL Collaboration Meeting*, Geneva, Switzerland, November 2009. `https://indico.cern.ch/materialDisplay.py?contribId=80&sessionId=11&materialId=slides&confId=63935`.

[11] M. Luong and O. Piquet, "**RF Control System Modeling**," in *IP-EUROTRANS / DM1 / WP1.3*, June 2007.

[12] "**PID controller**." `http://en.wikipedia.org/wiki/PID_controller`.

[13] K. J. Astrom and R. M. Murray, ***Feedback Systems***. (Princeton University Press, New Jersey, Oxfordshire, 2008), Electronic Edition Version 2.10c, Chap. 10. `http://www.cds.caltech.edu/~murray/amwiki`.

[14] C. Brosilow and B. Joseph, ***Techniques of Model-Based Control***. (Prentice Hall, New Jersey 2002), Chap. 9. `www.bgu.ac.il/chem_eng/pages/Courses/oren%20courses/Chapter_9.pdf`.

[15] M. Hoffman, "**Digital Signal Processing Mathematics**," in *Cern Accelerator School Proceedings, Sigtuna, Sweden*, May-June 2007. Edited by D. Brandt, CERN-2008-003, p. 10.

[16] P. S. Maybeck, ***Stochastic Models, Estimation, and Control***. (Academic Press, New York, San Francisco, London, 1979), Vol.1, Chap. 1.

[17] P. S. Maybeck, ***Stochastic Models, Estimation, and Control***. (Academic Press, New York, San Francisco, London 1979), Vol.1, Chap. 3.

[18] G. Welch and G. Bishop, "**An Introduction to The Kalman Filter**," tech. rep., TR 95-041, University of North Carolina at Chapel Hill, Department of Computer Science, Chapel Hill, NC, USA, July 2006.

[19] J. Holma, "**The Model and Simulations of the LHC 400 MHz Cavity Controller**," Internal Note, CERN-AB-Note-2007-012.

[20] P. A. Posocco, "**Longitudinal Error Studies Description**." CERN, Geneva, 2011 (unpublished).

[21] R. Garoby, "**Low-Level RF and Feedback**," in *Joint US-CERN-Japan Accelerator School on Frontiers of Accelerator Technology Proceedings*, Tsukuba, Japan, September 1996. Edited by S. Kurokawa, M. Month, and S. Turner, p. 455, Article CERN-PS-97-034-RF.

[22] W. Hofle, "**Cavity-Laplace**." CERN, Geneva, 2009 (unpublished).